2(mix)

NATIONAL AERONAUTICS AND SPACE ADMINISTRATION

Technical Memorandum 33-583

Volume I

Solar Electric Propulsion System Integration Technology (SEPSIT) Final Report

Technical Summary

J. A. Gardner

JET PROPULSION LABORATORY
CALIFORNIA INSTITUTE OF TECHNOLOGY
PASADENA, CALIFORNIA

November 15, 1972

208

NATIONAL AERONAUTICS AND SPACE ADMINISTRATION

Technical Memorandum 33-583

Volume I

Solar Electric Propulsion System Integration Technology (SEPSIT) Final Report

Technical Summary

J. A. Gardner

JET PROPULSION LABORATORY
CALIFORNIA INSTITUTE OF TECHNOLOGY
PASADENA, CALIFORNIA

November 15, 1972

Prepared Under Contract No. NAS 7-100
National Aeronautics and Space Administration

PREFACE

The work described in this report was performed by the Project Engineering Division and the technical divisions of the Jet Propulsion Laboratory under the cognizance of the office of Research and Advanced Development.

ACKNOWLEDGEMENTS

The cooperation and contributions of the people who supported the Solar Electric Propulsion Systems Integration Technology study are greatly appreciated. The following people were primarily responsible for the technical analyses: G. L. Anenberg, J. C. Arnett, K. L. Atkins, M. H. Bantell, Jr., A. Bratenahl, E. R. Bunker, Jr., P. O. Chelson, E. N. Costogue, R. H. Dawe, J. A. Gardner, H. H. Gernandt, E. Greenberg, R. W. Gulizia, W. Irace, R. A. Jacobson, D. J. Kerrisk, D. B. Kubly, T. W. Macie, M. L. MacMedan, E. L. Marsh, R. A. McCreary, J. P. McDanell, M. J. Olsasky, E. V. Pawlik, R. A. Proud, R. G. Ross, D. B. Smith, W. J. Weber III, J. R. Womack, C. W. Yen, B. Zeldin and, for documentation, L. Pottage.

CONTENTS

CONTENTS (Contd)

CONTENTS (Contd)

TABLES

FIGURES

CONTENTS (Contd)

FIGURES

CONTENTS (Contd)

FIGURES

ABSTRACT

The use of solar electric propulsion as a means of exploring space beyond the reach of ballistic missions was investigated in 1972. The method used was to study the application of this new propulsion technology to a future flight project. A 1980 Encke rendezvous mission was chosen because a design successful for Encke could be used for less difficult, but scientifically rewarding, missions. Design points for the mission and for the thrust subsystem were specified. The baseline-vehicle design was defined. A preliminary functional description document for the thrust subsystem was originated. Analyses were performed in support of the design point selection for the SEP-module thrust subsystem to specify parameters, to clarify and optimize the interface requirements, and to assure feasibility of some of the more critical technological aspects of SEP application. This final report is published in three volumes: Volume I, Technical Summary; Volume II, Encke Rendezvous Mission and Space Vehicle Functional Description; and Volume III, Supporting Analyses.

SECTION I

INTRODUCTION

Spacecraft employing solar-electric propulsion offer a number of potential advantages when compared to their ballistic counterparts, including reduction of flight times to the outer planets and the capability of performing high-energy missions, such as comet rendezvous, with moderate-sized launch vehicles.

The main goal of the solar electric propulsion (SEP) study at the Jet Propulsion Laboratory, under the direction of NASA/OAST Office of Space Propulsion and Power Division, was to enhance the potential value of this promising new technology by applying it to a representative future flight project.

The method used was to place the technology in a mission-oriented environment so that mission factors would dictate SEP parameters, emphasize the technology, and reveal the design tradeoffs.

A. OBJECTIVE

The overall objective of the program was to obtain the required technical information needed to identify and define the interface and functional requirements of a SEP thrust subsystem.

The specific objectives during FY 1972 were to:

(1) Select a SEP mission design point.
(2) Define a baseline-vehicle design to which the thrust subsystem should be integrated.
(3) Specify a thrust-subsystem design point.

(4) Originate a functional description document for a preliminary thrust subsystem.

The purpose in selecting a single mission-design point was to narrow the total number of applicable SEP missions to a mission or range of missions in which the basic thrust-subsystem design requirements could be emphasized, and yet the mission set would not be too broad to satisfy the overall program objectives.

To understand the impact of SEP technology upon other interfacing subsystems which may be incorporated on a SEP vehicle, it is necessary to define a baseline design comprised of those subsystems which, at the least, satisfy the basic mission requirements.

The selection of the thrust-subsystem design point was made to facilitate the identification of those characteristics of the thrust subsystem which would or could influence the operation, design, or performance of the other space-vehicle subsystems affected.

Upon completion of the three objectives described above, it is then possible to determine the interfaces between subsystems and levy functional requirements and constraints upon the thrust subsystem.

B. TECHNICAL APPROACH

Because the purpose of this program was to answer the technological questions relating to the thrust subsystem in a flight application environment, a study team with the technical expertise in those subsystem areas believed to be influenced the most by a thrust subsystem was established. This study team was responsible for performing the necessary tradeoff studies and supporting analyses required to develop the functional requirements and constraints for a thrust-subsystem design. The tradeoff studies and supporting analyses, which cover many technical areas, are summarized in this volume. A complete description of the studies is presented in Volume III.

In addition to the above studies, the study team developed a SEP-baseline mission and vehicle definition. The concept of a SEP module was selected because a baseline design close to that required for a flight application could then be established. The SEP module concept is analogous to the propulsion module approach used successfully in the Mariner 9 spacecraft design for a flight application of chemical propulsion. A complete description of the SEP module concept is presented later in this volume, and functional descriptions of the spacecraft and thrust subsystem are presented in Volume II.

SECTION II

MISSION STUDIES

The selection of a mission or range of missions for the application of SEP technology is extremely subjective, in the final analysis. This is especially true when such a mission or missions may have several opportunities and a selection-time extending over a 10-yr period between the latter 1970s or early 1980s. However, the selection is simplified, when it is based upon the desire to stress further development of the SEP technology.

A. MISSION SELECTION RATIONALE

Several technical/scientific discussions were held to develop criteria for selecting a mission set. The criteria derived from these discussions are that:

(1) Spacecraft and science would be acceptable to NASA/OSSA.
(2) SEP technology would be acceptable to NASA/OAST.
(3) Spacecraft and exploration would be acceptable to JPL.
(4) The design would be based upon existing spacecraft: the Mariner Venus-Mercury 73 (MVM 73), Viking, or the Thermoelectric Outer Planet Spacecraft (TOPS).
(5) Science and technology objectives would be combined.
(6) The spacecraft would be launched in the latter 1970s or 1980s.
(7) The mission would be scientifically interesting over the next 5 to 10 years.
(8) The mission would be enhanced by, or would require, SEP and thus would prove the desirability and feasibility of a SEP follow-on mission.

Additional criteria were derived for two alternatives:

(1) SEP would not be required for the initial science goals, i.e., two targets, two encounters, etc. Additional science objectives rely

primarily on the use of SEP. (This criterion is beneficial because it increases the probability of attaining part of the science objectives in the event of a failure in the new system.)

(2) SEP is required to achieve all of the science goals.

From the mission selection criteria, a set of possible missions was determined as shown in Table II-A-1. The selection criteria for the mission set are divided into the two alternative groupings, as defined above. Because the basic rationale behind this program is the application and development of SEP technology, rather than mission/spacecraft design and compatibility studies, a single mission was selected from the set. This mission, the 1980 Encke rendezvous with a 1978 launch, was chosen because it requires development of the SEP technology to a performance level sufficient for most of the missions possible during the decade considered. Power requirements and SEP operational flight time also influenced the final selection.

Table II-A-1. Mission Selection Set

Launch Opportunity	Mission Description	Selection Criteria Alternatives	Power Requirement
1976	d'Arrest-Geographos Flyby	I	Low (5 kW)
1977	Grigg-Skjellerup-Asteroid (?) Flyby	I	Low
1978	Encke Rendezvous	II	High (20 kW)
1978-80	Encke Flyby (0 to 35 km/sec)	II	High to Low
1981	Kopff Rendezvous	II	High
1983	Kopff-Asteroid (?) Flyby	I	Low
198(?)	Jupiter Orbiter	II	High
198(?)	Saturn Orbiter	II	High
1981, 2, 3	Saturn-Uranus-Neptune Flyby, Probe	II	High

B. BASEPOINT MISSION DESCRIPTION SUMMARY

The trajectory options for the 1980 Encke rendezvous mission were investigated to determine a desirable path for use in hardware analyses and tradeoff studies. Primary considerations included launch date, flight time, and arrival date. The objectives were to have

(1) Sufficient capability for a vehicle of 1200 to 1300 kg (dry mass).
(2) Reasonably fast transfer to the comet.
(3) Early arrival at the comet to provide flexibility for exploration strategies.
(4) Achievement of these objectives with a 16-kW (20-kW installed) power allowance for the thrust subsystem. The nominal thrust subsystem was assumed to be capable of a fixed 3,000 sec I_{sp} at an efficiency of 0.62.

Trajectories were developed with an adjusted solar-power profile as a function of solar distance (see Volume II, Section II-C-1) to provide an auxiliary power allowance of $\Delta P/P_o \approx 0.02$. No adjustments were included to account for making the solar-array orientation angle discrete for normal sun incidence. The predicted capability for orientation of hardware should allow a close approximation of the power profile.

Figure II-B-1 illustrates flight time tradeoff data for direct trajectories (transfer angles less than 360 deg). Although indirect trajectories were also considered, the characteristic flight times begin at about 1100 to 1200 days. Selection of an indirect trajectory was undesirable because of the longer times, plus the feature of initial passage inside the earth's orbit, although the mass capability is increased. As shown in Fig. II-B-1, direct missions in the 950-to 1000-day range appear to provide sufficient mass capability with an arrival in the vicinity of the comet 50 days before its perihelion passage.

Launch period alternatives were examined for several criteria including planned coasts for performance contingency. Whereas optimally placed coasts

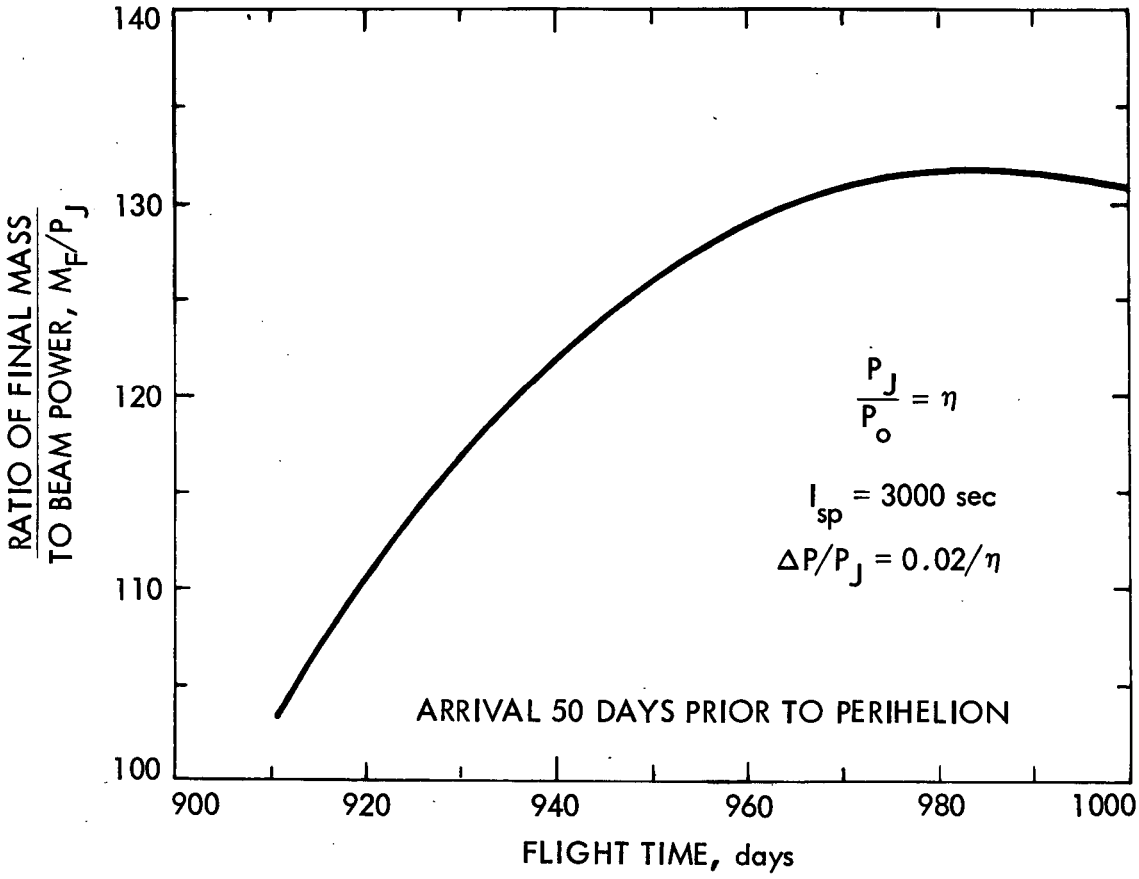

Fig. II-B-1. Flight Time and Performance Tradeoff Data for Direct Rendezvous Trajectories to Encke (1980 Perihelion)

could have been included in the desired trajectory, and, in fact, were considered in individual tradeoff studies, the path selected was without coasts to provide stringent requirements for hardware designs. This approach stressed "worst-case" conditions, and, therefore, the selected trajectory described here and in Volume II is preliminary and must be updated as detailed mission design progresses. However, the final trajectory will not be vastly different in overall geometry.

Generally, the trajectories of interest correspond to launch dates from mid-February to slightly past mid-March in 1978. The trajectory selected for use in the hardware implementation analysis, risk evaluation, and navigation studies begins on March 16, 1978. The normal transfer time is 950 days. The arrival date is October 21, 1980, 47 days before the comet's perihelion passage on December 6, 1980. The ecliptic projection of the trajectory is given in Fig. II-B-2, which shows the positions of the earth and the space vehicle every 100 days.

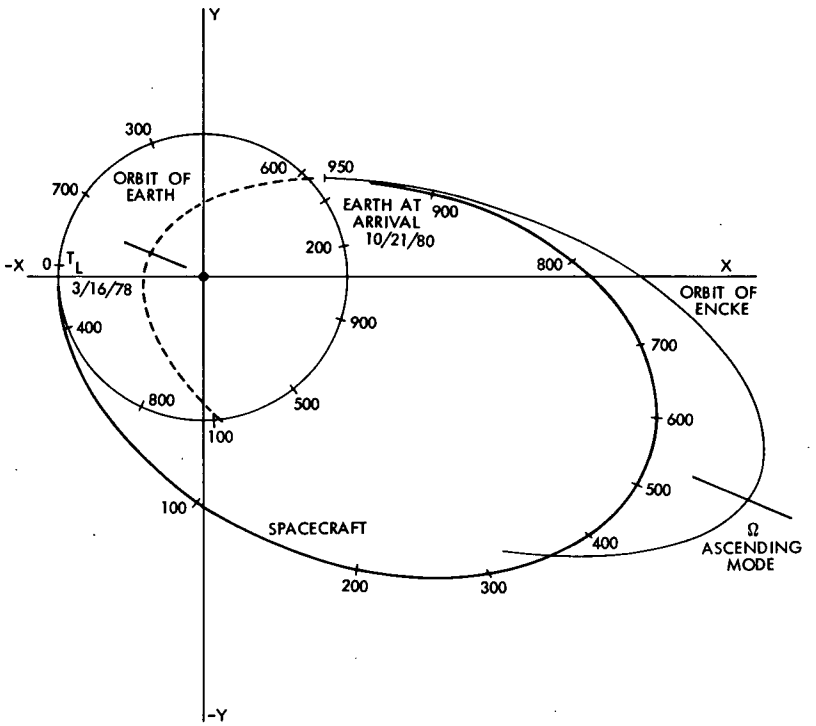

Fig. II-B-2. Ecliptic Projection of Selected Trajectory, Encke Rendezvous 1980

The selected trajectory begins with an injection energy of about 54 km^2/sec^2. This value for the Encke rendezvous is typical of the range from 20 to 100 km^2/sec^2, over which the SEP performance is relatively insensitive to injection energy. The selection point in this range is therefore not critical and is to be based primarily on the requirement that the initial injected mass be such that the ratio of P_o to M_o gives the proper initial electric-thrust acceleration for the selected path.

For an adequate description of this trajectory, an explanation of the time-varying thrust profiles common to solar electric missions is needed. The principal thrust component applied in the orbital plane must initially be along the path to increase the aphelion radius. Subsequently, as the vehicle reaches aphelion, the in-plane component must be directed retrograde to decrease the perihelion radius. To reach Encke's small perihelion radius (0.34 AU), a large total retro-impulse must be applied near aphelion, where the solar electric power available is only 10 to 20% of its value near earth. This fact explains the large, initial power requirement for the Encke rendezvous mission. After aphelion, the component is again directed posigrade to further increase aphelion until the orbit of the comet is matched.

Out-of-plane thrusting is also required to match Encke's 12-deg orbital inclination. The most effective use of this component is near the line of nodes between the departure plane (ecliptic) and Encke's orbit. The ascending node of Encke's orbit lies near its aphelion, as shown in Fig. II-B-2. The thrust subsystem is starved for power as the transfer trajectory nears the line of nodes outbound, reinforcing the requirement for large, initial power supplies on this mission.

To facilitate analysis of time-varying pointing requirements for the thrust vector, a body-fixed, vehicle-centered coordinate system was adopted. Such a system is needed because of the continuous change in thrust pointing with respect to the sun. This changing thrust program causes reference stars, the earth, and the sun to change location in the vehicle coordinate system and makes look-angles difficult to define in terms of inertially fixed coordinate

systems. Pointing angles in the body-fixed system are denoted as co-elevation and azimuth. Definitions of these angles are detailed in Volume II, Section II-C-1.

Figure II-B-3 is typical of the data compendium in Volume II,

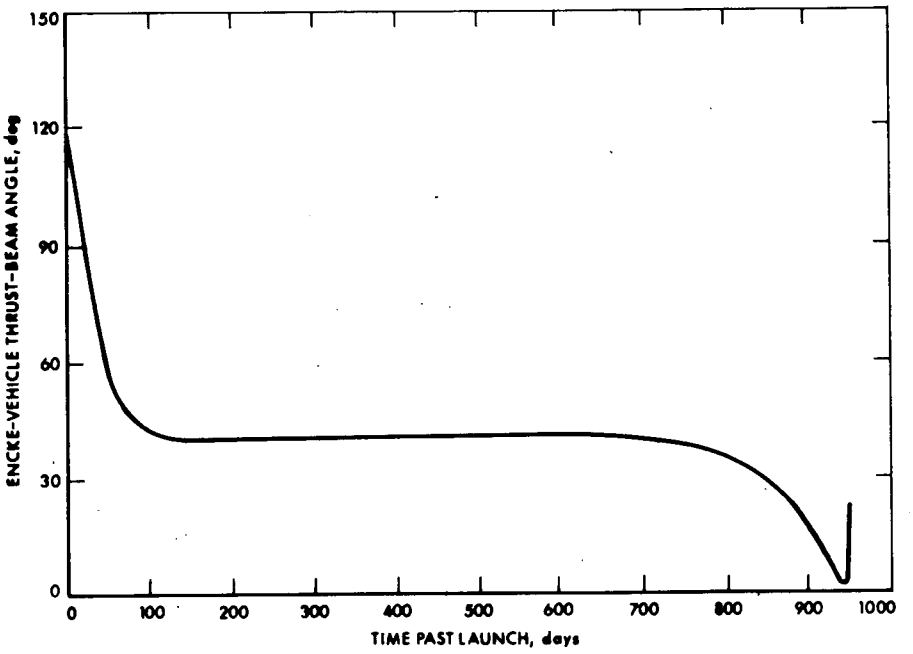

Fig. II-B-3. Encke/Space-vehicle Thrust Beam Angle

Section II-C-1, which describes the time history of important parameters during the mission. Included are object locations, ranges, range rates, and various angles, shown in Fig. II-B-3 above. This data provided mission constraints for hardware design and analyses.

The most important mission phase for the normal path is the final 100 or so days before encounter. Up to this point, the vehicle is primarily in a cruise configuration, navigating within the earth-based uncertainty of the comet's expected position. During the cruise, navigational updating once a week should be sufficient. However, as encounter nears, the knowledge of the comet's position will quickly improve after it is acquired by on-board optical sensors.

A desirable linear terminal maneuver strategy was devised, based on an initial uncertainty of about 30,000 km in Encke's position, as described in Volume III, Section II-B. It was determined that optical onboard recovery of the comet occurs some 60 days before rendezvous. Navigation must begin prior to 40 days before encounter. Figure II-B-4 shows the desired approach path in comet-centered coordinates. A successful rendezvous concluding this path is defined as a state within 1000 km of the nucleus with a relative speed of less than 4.0 m/sec. This definition was chosen to provide a stringent test of proposed terminal-maneuver strategies and navigational techniques. A relaxation of the rendezvous definition will ease implementation constraints but must be done in relation to scientific objectives, whose definition was beyond the scope of the FY 1972 work.

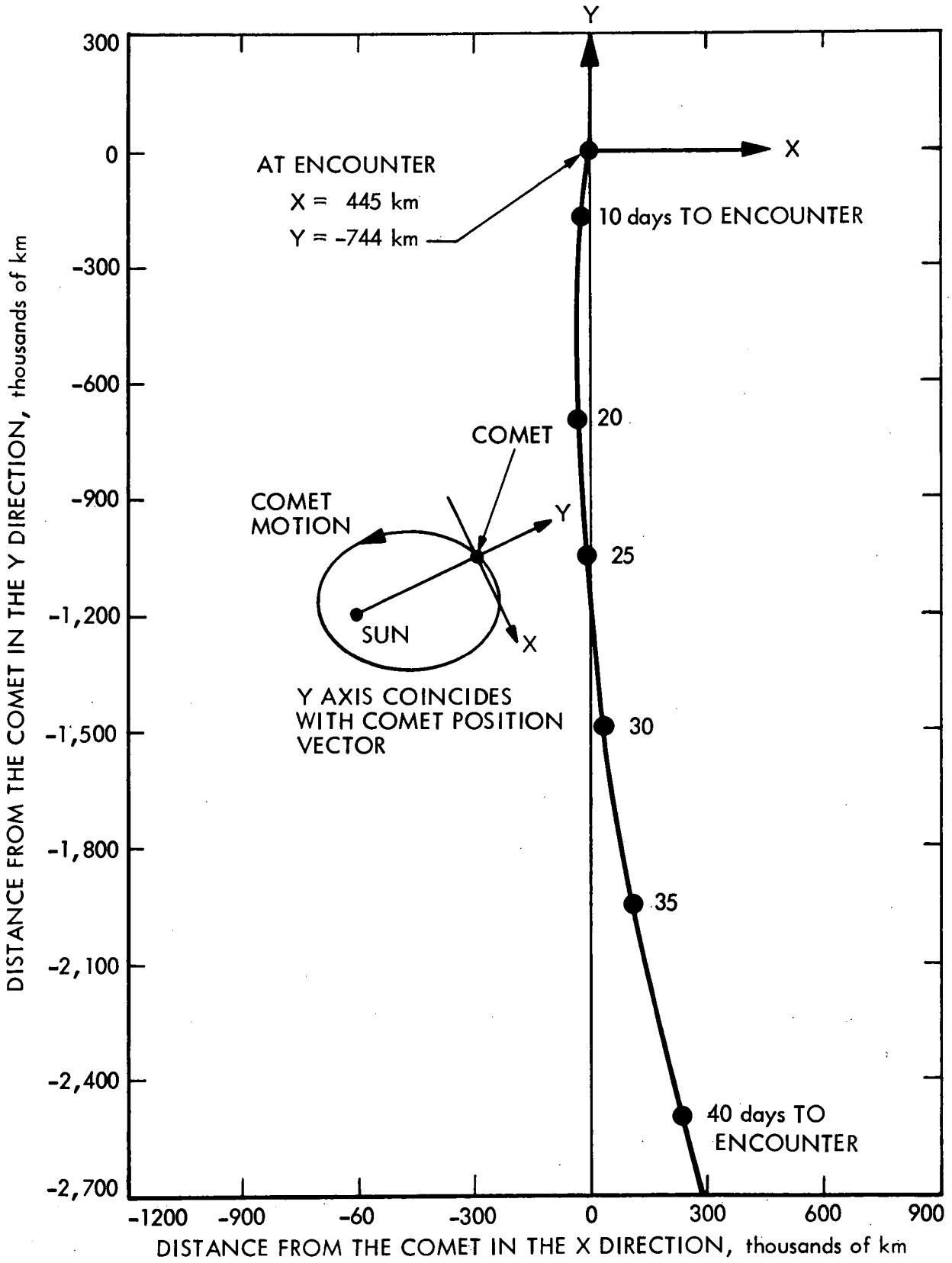

Fig. II-B-4. Curved Approach Trajectory

C. BASEPOINT MISSION SEQUENCE OF EVENTS

The date of launching the space vehicle is assumed to be March 16, 1978. The sequence of events describes major events occurring from launch until Encke rendezvous, in chronological order, as shown in Fig. II-C-1. The five phases are:

1. Launch Phase

The launch phase starts with liftoff and continues through sun and star acquisitions until the cruise phase begins two days later with thruster turn-on. Events related to the launch vehicle are not included because a specific launch vehicle has not been chosen. Either a Titan III D-Centaur or a space shuttle/Centaur launch vehicle are possible choices.

2. Cruise Phase

The cruise phase begins with a period of continuous tracking to evaluate thrust-subsystem performance in a space environment. Some 11 days later, tracking is performed only as often as necessary to determine the orbit and make the required changes to the thrust vector. This is approximately one pass per week with one 64-m net station. Changes in reference stars and changing thrust levels are made necessary because of changing solar-array output and thrust vector during the long cruise period, as discussed in this section. Thruster sequencing and usage is shown in Fig. II-C-2.

Two communication blackouts occur when the sun-earth-space vehicle angle becomes less than five degrees. These blackouts occur about 320 and 750 days from launch.

3. Calibration Phase

A calibration phase permits the television camera and scan control subsystem to be calibrated together using known star clusters for the approach

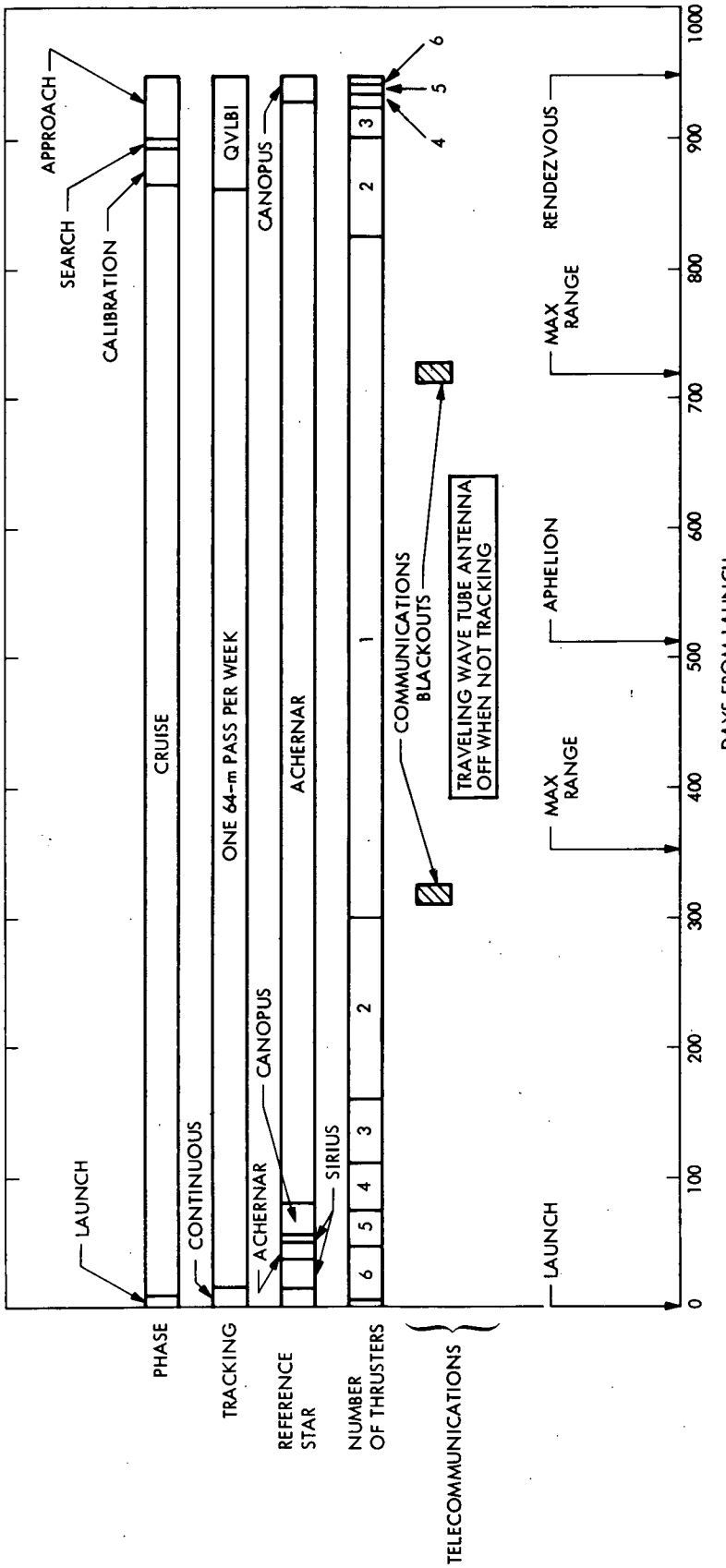

Fig. II-C-1. Major Mission Events, Space Vehicle, Encke Rendezvous 1980

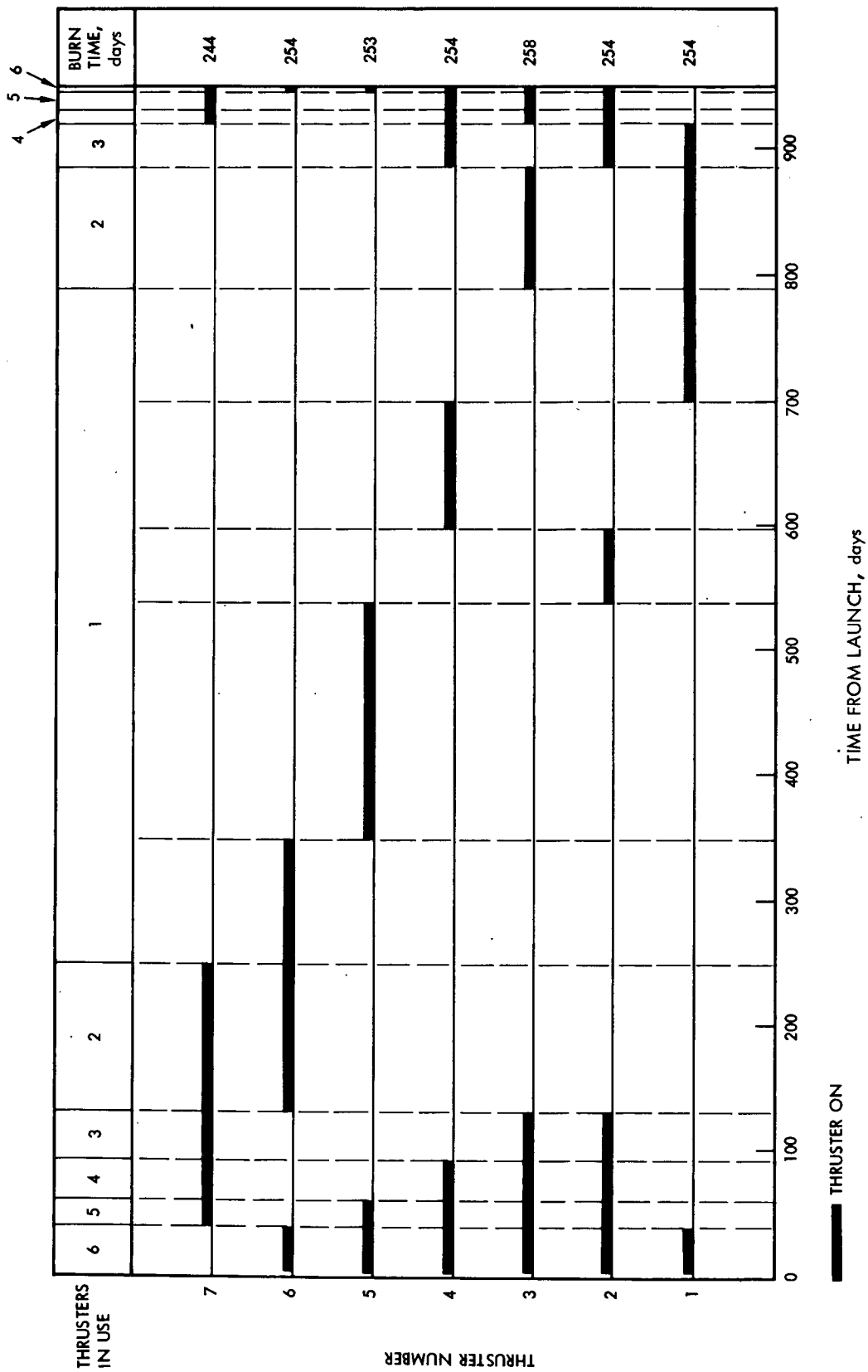

Fig. II-C-2. Thruster Sequencing for an Equal-burn Policy

guidance activities to follow. In-space calibration allows the gravity effects present during ground testing to be removed, significantly improving the pointing knowledge of the instruments. At this time, 8 kbps telecommunications performance becomes available.

Quasi very long baseline interferometry (QVLBI) tracking with two 64-m ground stations begins in this phase and continues until rendezvous to improve orbit determination accuracy at this time.

4. Search Phase

In the search phase, an attempt is made to take pictures of Encke while maintaining a trajectory representing the best guess from earth-based data.

5. Approach Phase

Once the comet is acquired by the spacecraft television camera, the approach guidance system derives the information necessary to ascertain the true cometary trajectory and the resultant changes to the trajectory of the space vehicle to effect a rendezvous.

Pictures of the comet's position are made daily, and thrust vector changes are made as needed. A 16-kbps data rate can be sustained in this phase for visual imaging data. Rendezvous occurs when the space vehicle is within 1000 km of the nucleus at a relative rate of 4 m/sec or less. This should normally take place at launch + 950 days.

SECTION III

SPACECRAFT STUDIES

A. GUIDELINES FOR THE SEP MODULE

A "final" conceptual design for the SEP spacecraft which would meet the SEPSIT program objectives under the criteria previously discussed (Sections I and II of this volume) was defined. The approach to the conceptual design definition was to identify various configurations which would technically satisfy the mission requirements under the constraint of one of the following three optional guidelines:

1. Option 1

The SEP module consists of the thrust subsystem, power subsystem, and all other supporting subsystems which would be required, when an MVM 73 spacecraft is used. All MVM 73 capabilities and subsystems which are presently defined will remain unchanged, with three exceptions:

(a) Spacecraft subsystems/hardware, which were MVM 73 mission-dependent and are no longer required by a SEP mission, will be removed.

(b) Changes in cable subsystem are permissible as long as the connectors for other spacecraft subsystems remain unchanged.

(c) Minor changes may be made to spacecraft structure to accommodate adapters to accept/attach the SEP module.

2. Option 2

The SEP module is identical to that in option 1, except that basic changes in the MVM 73 spacecraft bus are acceptable.

3. Option 3

The SEP module is a combination of options 1 or 2 with the additional flexibility of utilizing Viking subsystems as long as they remain in themselves unchanged.

The definition of the "final" design concept selected is believed to be the most adaptable technically to:

(a) SEP requirements and constraints.
(b) Sound spacecraft design practices.
(c) A 1980 Encke rendezvous mission with possible extension to other SEP mission applications.

The final design definition is described in Section III-D of this report.

B. REQUIREMENTS AND CONSTRAINTS

The following basic mission requirements and constraints were levied upon the spacecraft studies:

(1) An Encke rendezvous mission will be performed with a SEP module attached to an MVM 73-and/or a Viking-derived spacecraft.

(2) Modifications to the MVM 73 and/or Viking spacecraft subsystems should be minimized.

(3) The SEP module should provide for all functions required by the SEP which can not be provided by the MVM 73 and/or the Viking.

(4) The SEP thrust-subsystem must be jettisonable, leaving a viable cruise-configured spacecraft after the propulsion phase of the mission.

(5) Science requirements will not be considered, although a typical comet science package will be included in mass estimates.

(6) Rendezvous is defined as 1000 km in position and 4.0 m/sec in velocity relative to Encke. Post-rendezvous operations were not considered.

(7) Rendezvous must be achieved prior to 40 days before Encke's 1980 perihelion.

(8) Sufficient command margins on spacecraft omni antenna with the DSN 64-m (210-ft) antenna should be maintained throughout the mission.

(9) Telemetry and data-system performance will be sufficient to support engineering and approach-navigation requirements throughout the mission.

(10) The spacecraft will be configured so that it is compatible with the space-shuttle/Centaur launch system and with the Titan III D-Centaur with a 4.27-m (14-ft) shroud.

Because a spacecraft/space vehicle configuration is an iterative process, it is necessary to refine and make the general requirements and constraints listed in the previous section more specific so that possible design options or flexibilities can be identified.

These specific requirements and constraints, translated into design assumptions for the space vehicle system and SEP module subsystems, are:

1. Space Vehicle System

(a) The SEP module need not necessarily be detachable for an Encke mission; however, for future mission and design flexibility, it is highly desirable.

(b) Command and telemetry reception capability via the Deep Space Net will be maintained continuously throughout the mission. (This statement, however, does not imply that this capability will be exercised continuously.)

(c) The target, Encke, will be within the field of view of the science scan platform at least 60 days prior to and during rendezvous.

(d) Post encounter (post rendezvous) view-angle geometry need not be considered at this time in the design.

(e) Space-vehicle thermal requirements will include the environment from launch up to and including rendezvous and extending to 0.7 AU. No special thermal protection beyond that provided by MVM 73 technology, will be provided to assure survival nearer than 0.7 AU at this time in the design.

(f) The spacecraft portion of the space vehicle will receive all of its electrical power from the SEP module primary power bus.

(g) Solar arrays must be oriented normal to the sun line at all times, from deployment after launch until completion of rendezvous.

2. Thrust Subsystem

(a) Seven 30-cm thrusters will be mounted on the travelling-gimballing TVC mechanism.

(b) The structure will support the PC units.

(c) Power switching will be provided to switch PCs to different thrusters.

(d) The mercury propellant tankage will be capable of handling 480 kg of mercury.

3. Module Power Subsystem

(a) The SEP module will support two GE rollout arrays, 66 W/kg (30 W/lb), capable of supplying a total power of 20 kW at 1 AU.

(b) A maximum power point detector will be provided.

(c) Regulated power will be supplied to all module support subsystems and pre-regulated power, to the spacecraft power subsystem.

4. Module Data Handling, Command and Control

(a) All ground and system commands required by the SEP module will be handled by and/or through the spacecraft. All SEP module telemetry required by the ground will be handled by and through the spacecraft.

(b) Data-handling subsystems or units may be added to the SEP module, depending upon the mode of implementation and the needs of the SEP module and/or thrust subsystem.

C. CONFIGURATION STUDIES

Consistent with the SEP-module guidelines described in Section III-A, and the requirements, constraints, and design assumptions in Section III-B, several configuration concepts were developed in FY 1972. The purpose of these configuration-concept studies was to select a space-vehicle conceptual design as a baseline for the SEP vehicle design.

1. Option 1

The option 1 configuration study under the option 1 guidelines utilized the MVM 73 spacecraft bus as the basic building block for the space-vehicle concept. The primary objective of the study was to ascertain the capability of the MVM 73 subsystems to fulfill the functional requirements of a SEP vehicle.

Figure III-C-1 is an orthographic projection of the option 1 space-vehicle concept, which depicts the configuration of the vehicle in a flight mode as well as in a launch mode. Several section views are included to show where individual equipments and subsystems are located on the vehicle.

Figure III-C-2 is an isometric drawing of the option 1 space vehicle viewed from the anti-sun side. The MVM 73 spacecraft is attached to an open truss structure, which supports all of the equipment considered as part of the SEP module: the rollout solar array, power conditioners (PCs) electric thruster array, and power subsystem.

Early in the option 1 study, it was determined that electronic-bay volume requirements would exceed the eight bays available in the MVM 73 spacecraft. For example, the CCS subsystem was found to have insufficient storage capacity for all the functions required by a SEP vehicle. The MVM 73 CCS has a limited storage capacity of 512 words of 22 bits and a slow processing capability at a 2.4-kHz bit rate. Preliminary analysis showed the word requirement to be about 4000 to 5000 words. Similarly other electronic subsystems needed more bay volume to accommodate the growth in the hardware to meet SEP electrical interface requirements. It therefore became necessary to find more space to allow for the needed growth of the electronic subsystems. Because the MVM 73 can hold only eight bays of electronics and from 12 to 15 bays would be needed, five additional bays were designed into the SEP module structure. These supplemental Mariner-size bays are shown in sections B-B and C-C of

Page intentionally left blank

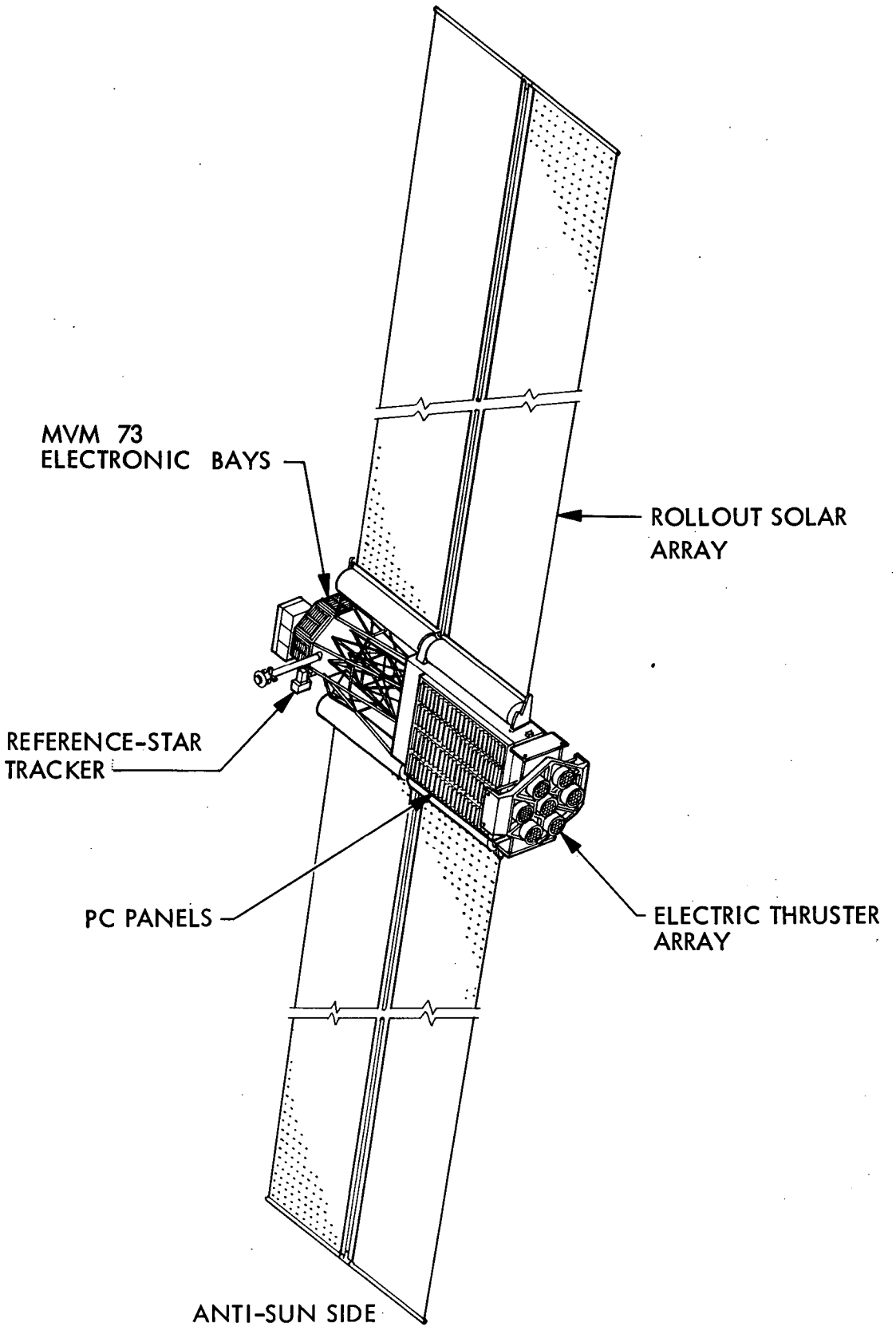

Fig. III-C-2. SEP Module with MVM 73 Bus

Fig. III-C-1. The space vehicle could now accommodate thirteen bays of electronic subsystems, which was deemed sufficient at this time in the study.

The option 1 space-vehicle configuration was completed in enough detail to allow critiques from the various technical disciplines. At first, the increased number of bays was considered as a serious violation of the constraints. However, later in the study, it was determined that all three options would require a minimum of 12 bays of electronics to meet SEP requirements; it was therefore decided not to consider this a serious violation of option 1 guidelines.

However, three serious disadvantages of the option 1 configuration were perceived during the study. Specifically, electronic packaging considerations relative to electromagnetic interference (EMI), noise levels, line drops, and thermal control had significant impact on any SEP vehicle configuration under this option.

a. Thermal Control

Study of the configuration revealed that serious problems can be encountered in maintaining the required temperature environment for the electronic subsystems in the supplemental bays (Fig. III-C-1, Section B-B) and in the Mariner spacecraft, when they are exposed to direct solar flux during flight. As many as six bays will be exposed to direct solar flux because of the variable thrust-vector pointing requirements of the Encke, and other similar missions (Fig. II-B-2). At solar distances of 1.2 AU or less, the state-of-the-art temperature-control techniques are not adequate to maintain subsystem temperature requirements. Use of fluid loop or optical solar reflectors was considered too costly or unreliable at this point in the study.

b. Structure

Adapting the MVM 73 bus to the SEP module is not difficult technically, although the SEP module dwarfs the MVM 73 in both size and weight (Figs. III-C-1, launch mode). Analysis showed that the "overturning"

moment caused by lateral launch loads would exceed the capability of the MVM 73 bus. The bus might be able to withstand the launch loads of the Titan III D-1A booster only if major structural modifications were made. This course of action was not pursued because major redesign of the MVM 73 bus was against option 1 guidelines.

c. Science Scan-platform Pointing

The position of the science scan platform beneath the bus was inherited as part of the MVM 73 design. From this position, the science platform is not able to view Encke at various times prior to rendezvous because of the location of the bus or other spacecraft structures. Relocation of the science platform would violate the option 1 constraints.

Because of these above outlined disadvantages, the option 1 configuration study was discontinued, and a study under option 2 guidelines was initiated.

2. Option 2

The only difference between option 1 and 2 guidelines is that a MVM 73 bus will not be used as the basic structural building block and housing for the electronic subsystems. Thus, a rectangular, rather than octagonal, configuration can be used. In this study, the entire primary structure of the space vehicle was made on an open truss, rectangular box. To overcome the disadvantages and problems of the option 1 concept, the equipment with thermal control problems and viewing difficulties were reconfigured and relocated. The evolution of this option 2 configuration is shown in Figs. III-C-3, 4, and 5. The position on the vehicle of the major equipment and subsystems can be seen in the exploded view shown in Fig. III-C-5.

Temperature control requirements played an important role in shaping the configuration and integration of electronic assemblies for the option 2 space vehicle. The primary thermal consideration was the wide variation in solar irradiance, which would be encountered during an Encke

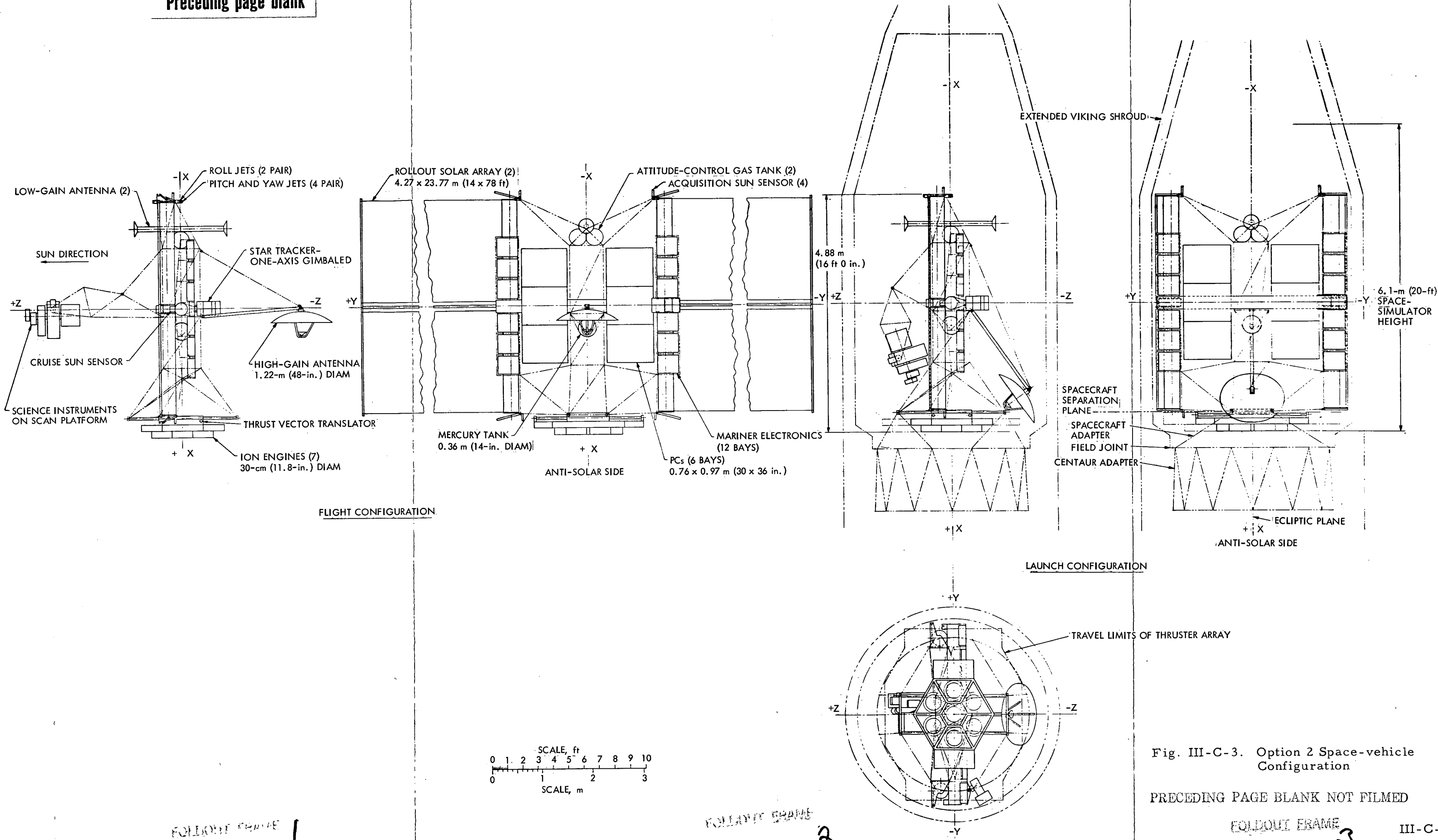

Fig. III-C-3. Option 2 Space-vehicle Configuration

PRECEDING PAGE BLANK NOT FILMED

FOLDOUT FRAME 1

FOLDOUT FRAME 2

FOLDOUT FRAME 3

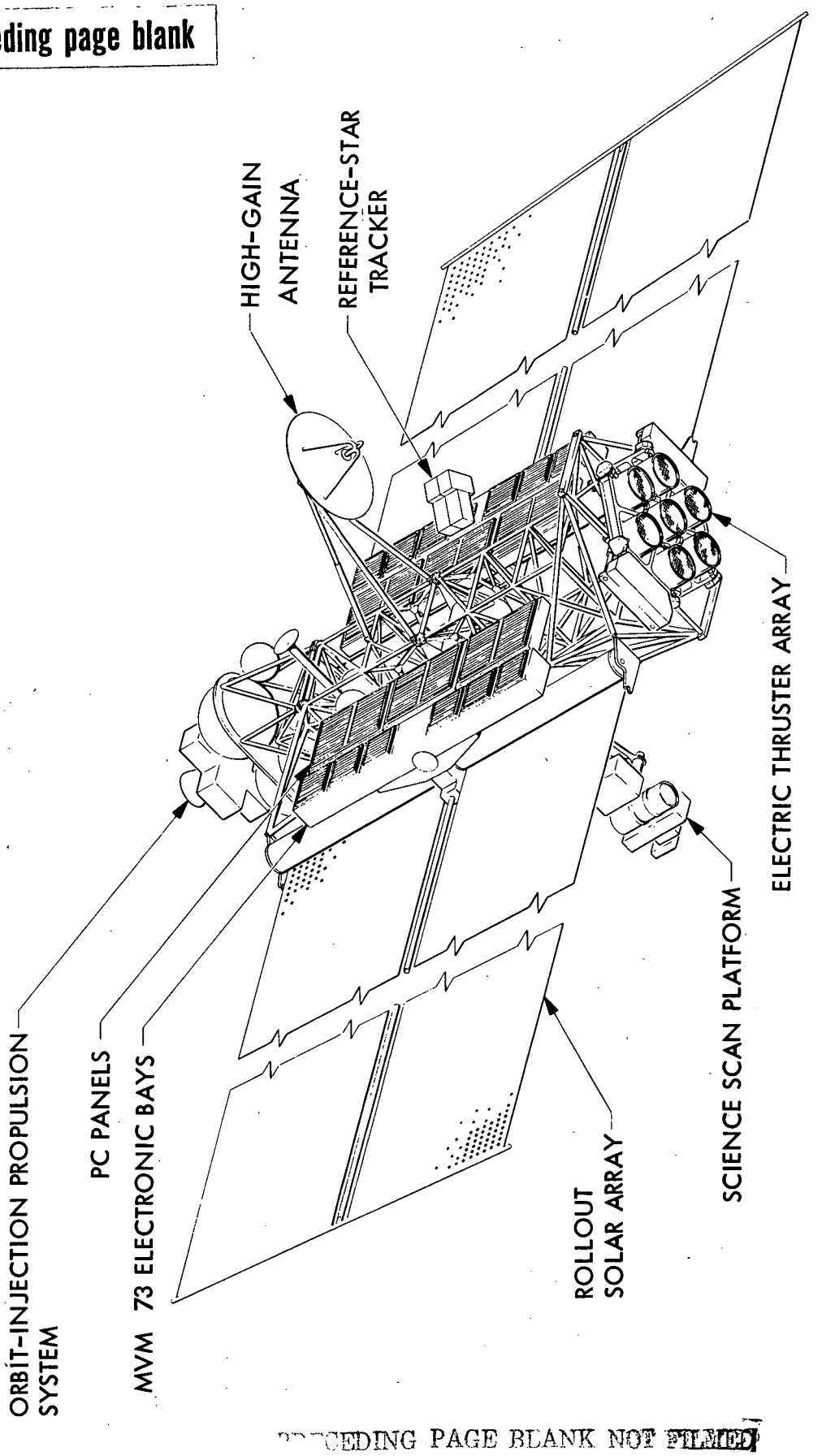

Fig. III-C-4. Option 2 Space-vehicle Configuration, Isometric

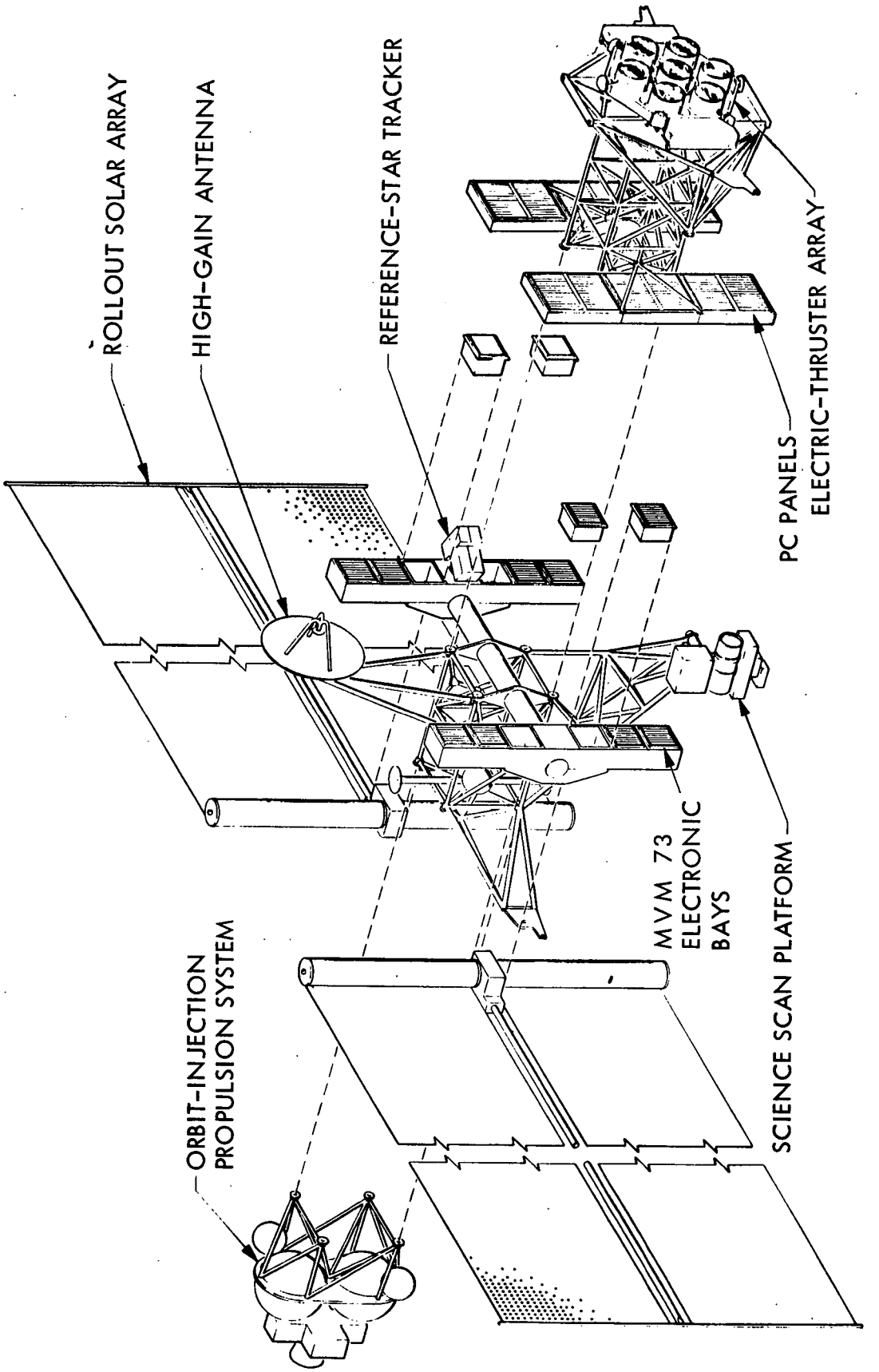

Fig. III-C-5. Option 2 Space-vehicle Configuration, Exploded View

rendezvous mission from about 110 W/m^2 at aphelion (3.5 AU) to about 12,000 W/m^2 at perihelion (.34 AU). Because of this wide variation, a design guideline was established which stated that the PC radiator surface must never be illuminated by the sun. This constraint can be met by mounting the PC shearplate, which was designated as the thermal radiator surface, on a non-illuminated side of the SEP module. The two mounting surfaces considered were:

(a) The anti-sun side of the vehicle.
(b) The side (or sides) which are normal to the solar-array axis of rotation (y-y axis on Fig. III-C-3).

Mounting on the anti-sun side has the advantage of minimizing the radiant coupling between the electronic assemblies, PCs, and the solar arrays. (The arrays re-radiate, in all directions, the majority of the solar energy they collect.) However, this mounting scheme places a restriction on the thrust-beam pointing direction (thrust vector). Furthermore, it places the shearplates directly in the path of micrometeoroid travel during the flight through the asteroid belt.

These two objections are eliminated when the PC shearplates are mounted normal to the solar-array axis of rotation. Radiant coupling between PCs, electronic assemblies, and the solar array requires further study in FY 1973. However, two sides of the space vehicle can be used for the mounting of all electronic assemblies, which has several advantages:

(a) A significant reduction in overall space-vehicle dimensions.
(b) A well-placed center of gravity.
(c) Efficient utilization of the inherent load-carrying capability of the PCs, leading to a lighter overall structure.
(d) Strong radiative coupling between PCs, which is highly desirable.

On this basis, the second mounting scheme was selected, and the back-to-back configuration shown in Fig. III-C-6 was derived. Variable-emittance louvers were added to the PC shearplates to eliminate the need for heater power, when all but one PC is inoperative. In addition, the louvers can also be used as micrometeoroid shields.

This view shows the MVM 73 electronic bays and the PCs attached to the primary structure and located directly behind the solar arrays. Figure III-C-4 shows the composite assembly of these equipments and the relationship of the PC and electronic bay to the solar arrays. This equipment is on the anti-sun side of the solar arrays. Shading this equipment with the solar array and rotating the equipment synchronously with the rotation of the array makes it easier to control the temperature of the electronic bays, but does not solve the problem of re-radiation from the arrays.

Two heavy actuators must be added to rotate this equipment, which presents a potential reliability problem not associated with the option 1 configuration. Moreover, preliminary analysis indicated that the weight and the added stiffening of the primary structure necessary to support the electronic bays and PCs would be approximately one and one-half to two times the weight of the option 1 primary structure. Thus, in relieving the thermal problem of the electronic bays, significant structural weight was added.

As shown in Fig. III-C-4, the primary structure of the SEP module is an open truss box structure rather than an octagon. The structure will be designed to support the electric-thruster array, the PCs, electronic bays, solar arrays, science platform, high-gain antenna, and other external equipment. The Mariner bays housing the electronic subsystems are shown in Figs. III-C-4 and 5 as two long, rectangular-box frames capable of supporting six bays of MVM 73 electronics each. Each six-bay module is mounted to a tubular support, as are the solar arrays. This equipment and support structures are, in turn, attached to the primary structure of the SEP module.

To meet the requirements for science-instrument viewing of Encke and to overcome the option-1 viewing problems, the science scan platform was

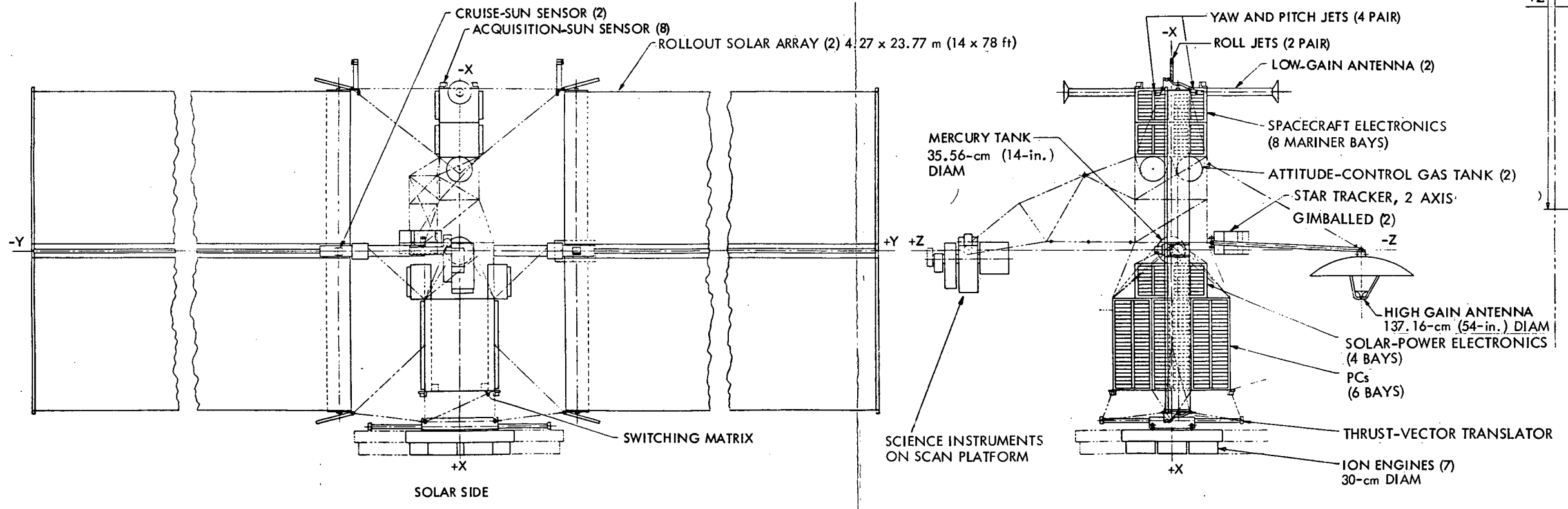

CRUISE FLIGHT MODE

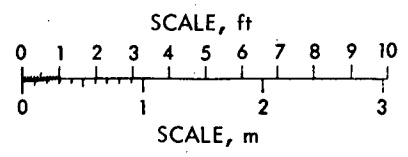

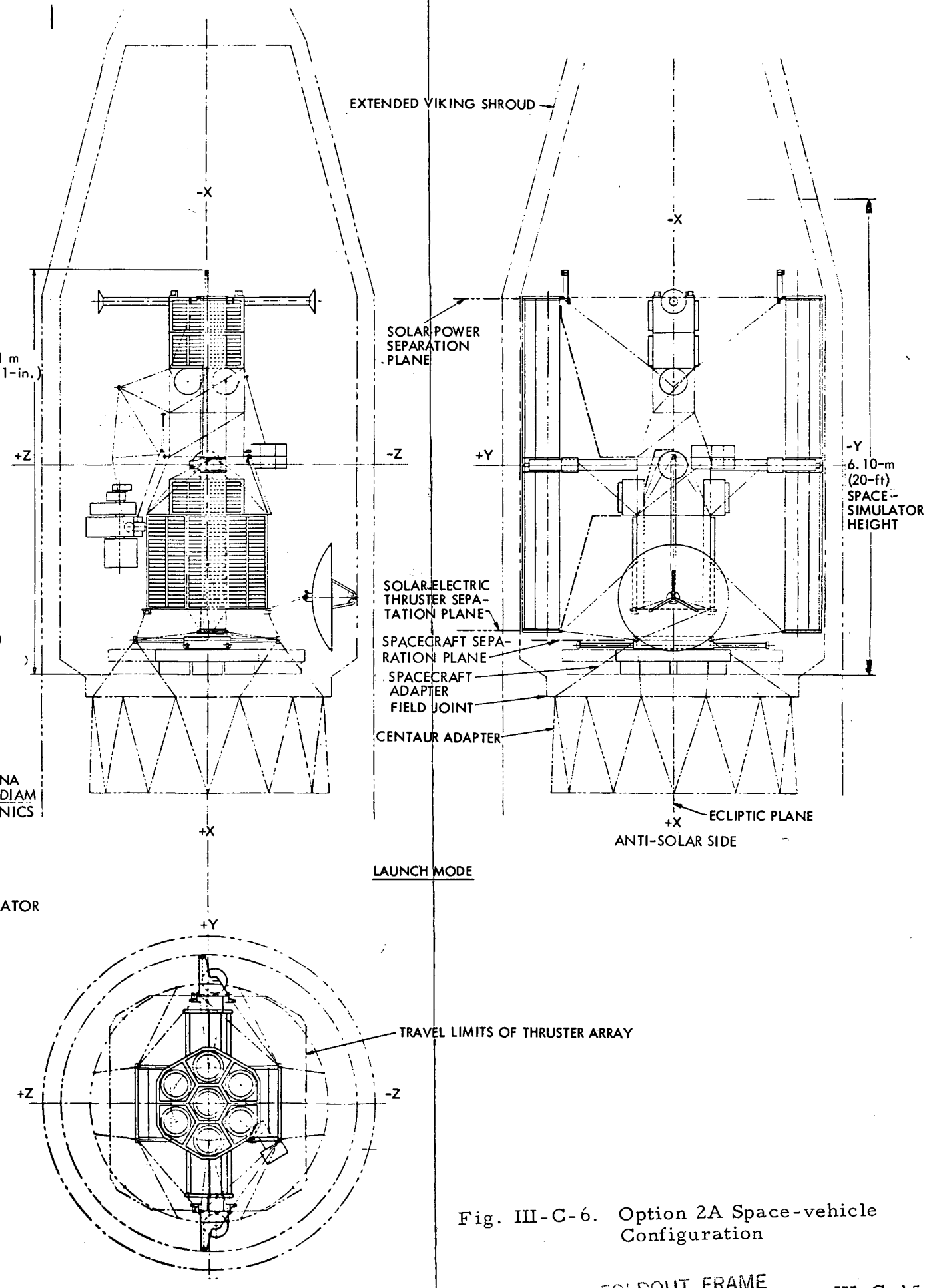

Fig. III-C-6. Option 2A Space-vehicle Configuration

FOLDOUT FRAME 1

FOLDOUT FRAME 2

FOLDOUT FRAME 3

placed on a boom structure, which is deployed in cruise flight. The length of the boom is determined by the need to see past the electric-thruster array at its farthest translated position prior to and during rendezvous. With two axes of rotation and the long boom, the science scan platform has the capability of viewing the comet at pre-determined angles from 60 days prior to and through rendezvous. Thus, this concept appeared to be a satisfactory solution to the option 1 viewing problem.

Study and analysis showed that the option 2 configuration had overcome the disadvantages of configuration 1 except for the high structural weight of equipment added to solve the thermal control problem of the electronic bays. Further analysis of the configuration for temperature control of all electronic equipment led to the conclusion that, if a way could be found to assemble similar equipment, such as PCs and electronic bays, to the primary structure opposite one another, or back-to-back, structural and thermal disadvantages of the option 2 configuration could be minimized or eliminated. Therefore, an intensive study was started on the option 2A configuration emphasizing the new approach of mounting electronics assemblies back-to-back so that, during flight, the louvered surfaces would not be directly illuminated by the sun; i.e., only the edge dimension of the equipment would be perpendicular to the sunline. The option 2A configuration, developed after several iterations of the primary structure and re-location of the electronic equipment, is shown in Fig. III-C-6.

At this time in the study, several other requirements were imposed on the space vehicle. Multimission capability and separation interfaces between the SEP module and spacecraft portions of the vehicle had to be established, at least on a "first iteration" basis. Thus, further electronic packaging studies were necessary to decide whether, functionally, the equipment belonged on the spacecraft side of the separation interface or in the SEP module. Provision for carrying a retropropulsion system for orbiter or flyby missions was developed. The retropropulsion system is attached to the spacecraft as shown in Fig. III-C-4 and III-C-5.

The configuration concept of option 2A proved to be viable, with the problems and disadvantages of the previous options overcome or minimized. Therefore, the option 2 design was selected as a starting point for the option 3 configuration study.

3. Option 3

The objective of the option 3 study was to substitute Viking equipment and electronics in place of Mariner, where feasible. The configuration study was completed under this guideline, and the option 3 space-vehicle design concept was selected as the baseline for FY 1973 studies and is described in detail in the following section.

It was decided to develop the concept in more detail by looking at the spacecraft and SEP-module structure separately.

a. Spacecraft Structure

The spacecraft primary structure consists of a "skin-stringer" box structure, which serves as the spacecraft electronic compartment, and an open truss, which supports the electronic compartment on the SEP module. The electronic compartment is designed with four Viking electronic bays on each of the two sides, parallel to the solar-ray vector.

As shown in Fig. III-C-7, the structure of the electronic compartment consists of six longerons, which connect upper, center, and lower frames to provide support for the electronic chassis. The outer surfaces of the electronic chassis serve as shearplates and also provide meteoroid protection, when used in conjunction with the louver assemblies. The remaining surfaces of the electronic compartment are also stiffened by shear panels and shear-panel intercostals. These surfaces are also required to serve as meteoroid shields.

Besides supporting the spacecraft electronics, the electronic compartment serves as the spacecraft primary structural reference for

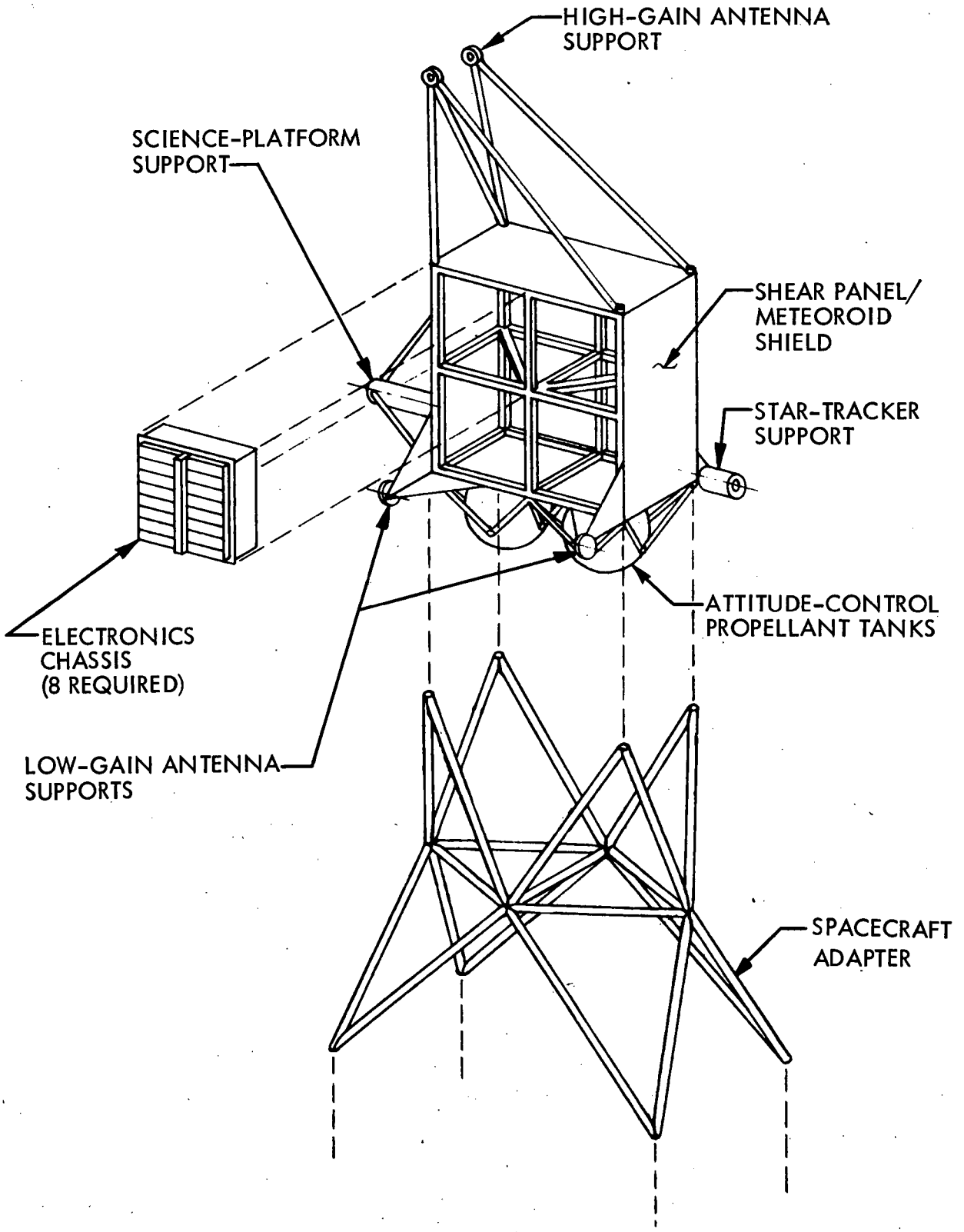

Fig. III-C-7. Option 3 Spacecraft Structure

communication, attitude control, and science-instrument alignment. In this role, it provides structural interfaces for the science platform, the antennas, and the star tracker. Attitude control propellant tanks are also supported from the electronic compartment.

To minimize weight, an open tubular-truss assembly is used to connect the spacecraft electronic compartment to the SEP module. The upper end of the truss is fastened to the electronic compartment during all phases of the mission. The lower end of the truss is attached to the corner longerons of the SEP module with separable fasteners so that it can be separated from the SEP module.

b. SEP Module Structure

The SEP module consists of three primary structural elements; the PC compartment, the SEP electronic compartment, and the solar-array support structure. The main structural members of these elements are shown in Fig. III-C-8. The PC compartment is the largest structural element of the SEP module. It contains the interface with the launch-vehicle adapter and thus supports all other spacecraft structural elements. The structure of the PC compartment consists of eight longerons, which connect upper and lower frames and provide support for the six PC units, which mount on opposite sides of the PC compartment. The outer surfaces of the PC units serve as shear-plates in the structure and also provide meteoroid protection, when used in conjunction with the PC-louver assemblies. The remaining external surfaces of the PC compartment are stiffened by shear panels and shear-panel intercostals. These surfaces are also required to serve as meteoroid shields.

The internal longerons are tied together with intercostals and diagonal bracing to form two deep beams, which run the length of the PC compartment. These beams also support the mercury propellant tank via an eight-member truss.

The bottom frame of the PC compartment provides the interface with the launch-vehicle adapter structure and supports the SEP thruster

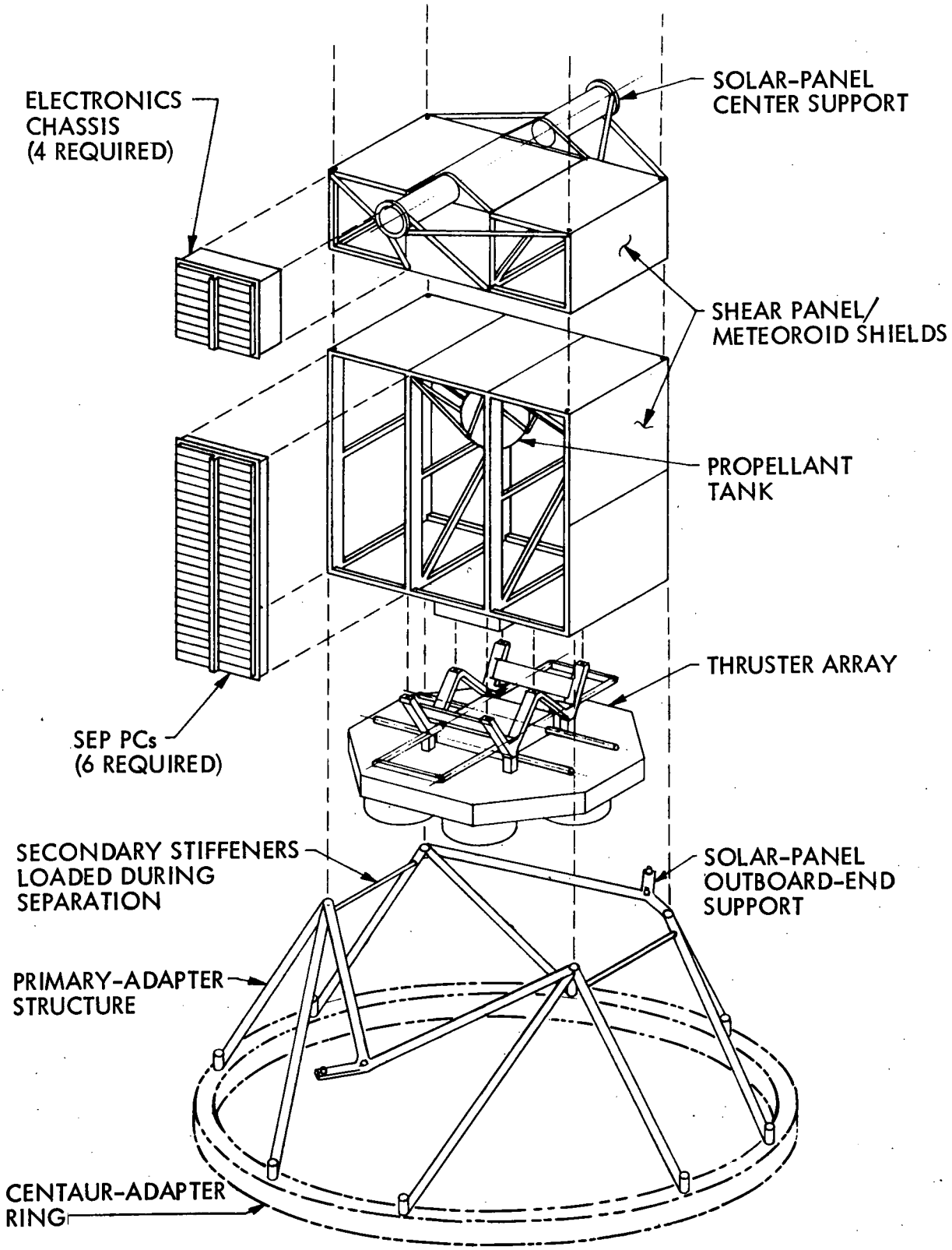

Fig. III-C-8. Option 3 SEP Module Structure

translator assembly and switching matrix. The upper frame provides the separable interface with the SEP electronics compartment.

The construction of the SEP electronics compartment is similar to that of the PC compartment, except that the PC units are replaced with electronic chassis. The bottom frame of the electronic compartment provides the interface with the PC compartment and the top frame provides the separable interface with the spacecraft supporting truss. The electronic compartment also provides the primary structural interface with the solar-array support structure.

c. The Solar-array Support Structure

The solar-array support structure is the third major structural element of the SEP module. As currently configured, the General Electric/JPL rollup solar-array design consists of a primary center support and two secondary outboard-end supports, which are used only during launch. The primary center support is supported on the SEP electronics module by a center support tube and associated braces. To minimize spacecraft weight, the structure required to support the lower ends of the arrays during launch is attached to the launch-vehicle adapter and remains with the launch vehicle following separation.

Although the current solar-array design also requires an upper outboard-end support, an analysis of the solar array interface requirements (Volume III of this report) indicates that the upper supports can be removed in future designs. The upper outboard-end supports have, therefore, not been included on the selected space vehicle design. Their removal simplifies the spacecraft configuration and improves its multimission capability because a solar-array structural interface above the SEP module is not required.

D. BASELINE SPACE-VEHICLE SYSTEM DESCRIPTION

1. Configuration

The space vehicle configuration concept shown in Figs. III-D-1 and 2 evolved after several iterations of a basic modular-assembly approach using open-truss structure Viking technology, and the option 3 configuration.

The space vehicle may be divided into two modules: the spacecraft module and the SEP module. The SEP module is composed of two major assemblies: the SEP module support subsystems and the thrust subsystem, as shown in Fig. III-D-1. All three units are open box-like structures, which serve as the primary structure and provide support for the subsystem equipment mounted thereon.

a. Spacecraft Module

By viewing Fig. III-D-1, it can be seen that the spacecraft module can be separated from the SEP module at the four corners of the connecting truss structure. The spacecraft module carries most of the basic equipment and subsystems found on interplanetary spacecraft. The box structure supports eight bays of electronic assemblies and the required connecting harnesses and cables. Mounted to the forward end of the primary structure is a 1.47-m (58-in.) diameter high-gain antenna with two degrees of freedom to permit earth tracking during various phases of the Encke rendezvous mission. As shown in Fig. III-D-2, the high-gain antenna is stowed and tied to the support structure during launch. After launch, tie-down release devices are actuated to enable the antenna to rotate about its two axes of rotation. Two low-gain antennas are mounted to the spacecraft primary structure on the sides of the box opposite the louvered electronic bays. Using two low-gain antennas on opposite sides of the spacecraft provides 4π steradians of coverage for telecommunications. The star tracker is mounted on the spacecraft anti-sun side (end view of launch configuration) with a two-axis gimbal. The gimballing is necessary to enable the instrument to lock on to several different stars during

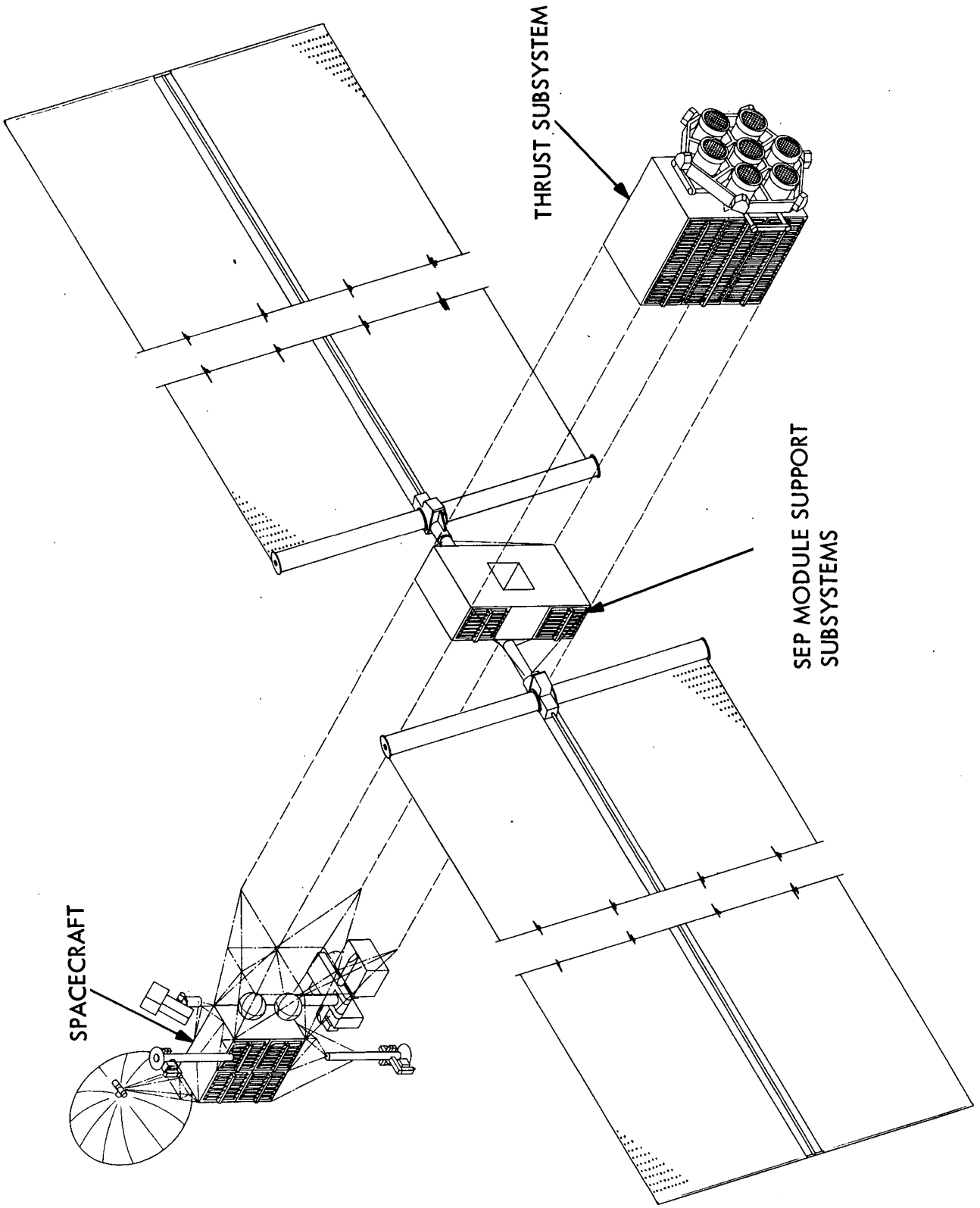

Fig. III-D-1. Option 3 Space Vehicle, Isometric

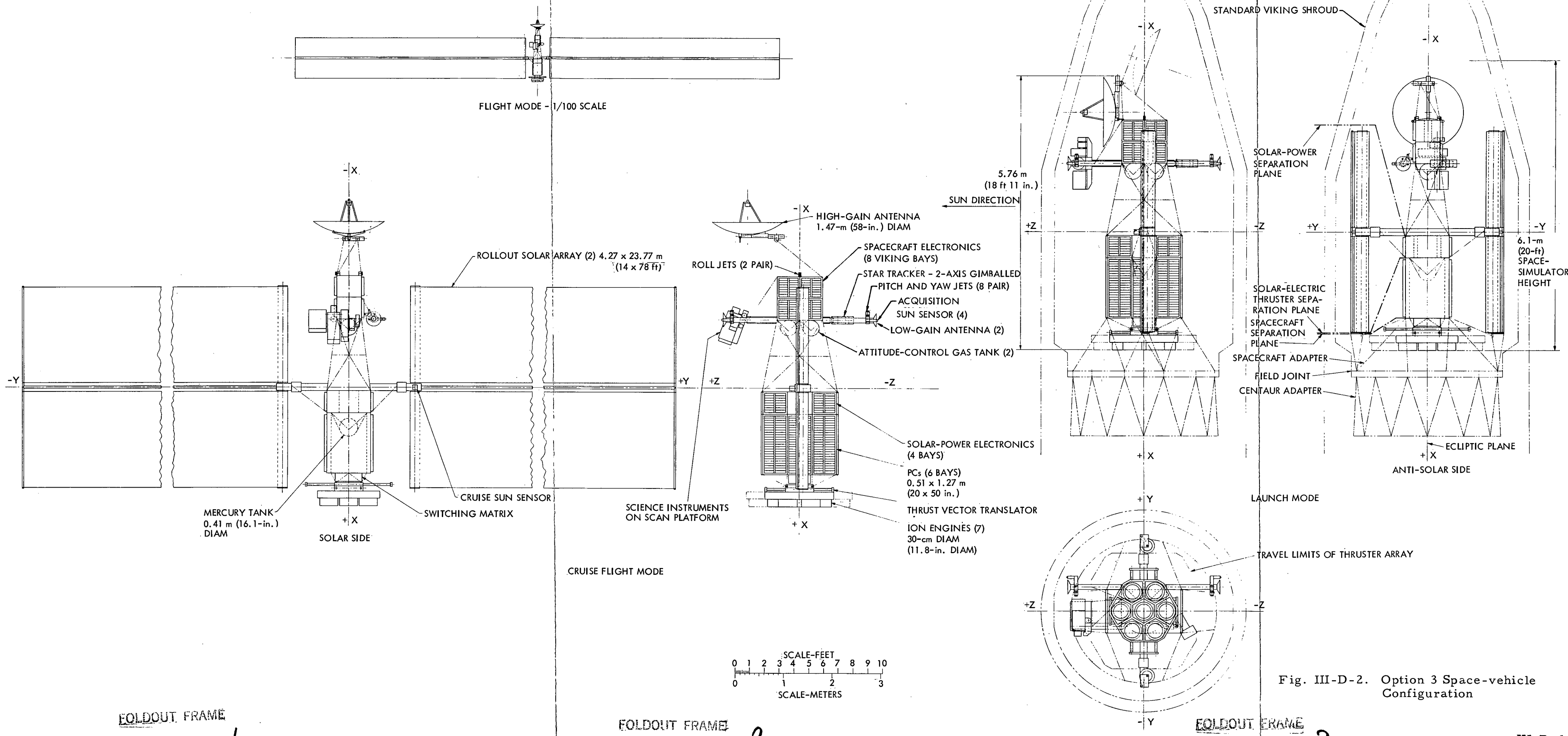

Fig. III-D-2. Option 3 Space-vehicle Configuration

FOLDOUT FRAME 1

FOLDOUT FRAME 2

FOLDOUT FRAME 3

the Encke mission for roll-attitude stabilization without stray light interference from the solar arrays. The science scan platform, depicted on the side opposite the star tracker, has two degrees of freedom. The height of the platform above the structure and the ion-thruster array accommodates viewing the comet from 60 days prior to, and during, rendezvous. Attitude-control gas tanks, nested to the underside of the spacecraft, supply gas to the roll jets mounted on the top side of the box structure near the high-gain antenna and to the pitch and yaw jets mounted on the low-gain antenna masts. Acquisition sun sensors are also mounted on these masts.

b. SEP Module

The center assembly, shown in Fig. III-D-1, is the SEP module support subsystem. The module consists of four electronic bays housing the power subsystem and associated electronics in a box structure. Mounted to the box structure are tubular supports which carry the rollout solar arrays, each of which is 0.27 x 23.77 m (10.6 in. x 78 ft) in size, the deployment actuator, and orientation drive mechanisms. A cruise sun sensor is mounted on the sun side of the deployment actuator (Fig. III-D-2).

The second major assembly in the SEP module is the thrust subsystem. This subsystem comprises six PCs and seven 30-cm thrusters arranged in a hexagonal array. The thrust vector translator, switching matrix, and mercury-propellant tank are shown in Fig. III-D-2 (cruise-flight mode, solar side). All of the equipment mentioned above are mounted to the primary structure. The PCs are mounted to the sides of the structure so that their louvered sides lie in a plane parallel to the plane of the ecliptic during flight. This arrangement meets the temperature control requirement that the PCs should never be subjected to direct solar energy. The thruster array is attached to the box structure of the PCs and is supported by tubular truss members. As shown in the cruise flight mode area of Fig. III-D-2, the switching matrix is nested between the PC structure and the thruster array to maintain minimum cable length. The mercury propellant tank is supported by truss work within the box structure of the PCs.

c. Space Vehicle Adaption to Shuttle

The SEPSIT space vehicle is shown in Fig. III-D-3 in its stowed configuration inside the shuttle bay. Two trusses support the vehicle during launch and flight operations. One truss is an engine mount which adapts the vehicle to the Centaur booster. The second is a "W" truss and supports the space vehicle near the thruster array.

d. Electronic Assembly Packaging

The electronic-equipment packaging arrangement is based on use of standard Viking electronic chassis and subassemblies located in the spacecraft and the SEP modules.

The spacecraft compartment (Fig. III-D-4) contains eight electronic assemblies, five of which consist of identical or slightly modified Viking equipment. The other three assemblies consist primarily of Viking subsystem electronics and include the TV electronics. Approximately 25 percent of the volume of the three assemblies is empty for subsystem change and to comply with science electronic requirements.

The equipment is located to maintain subsystems within an assembly, provide the shortest RF cable to the antenna, distribute the power dissipation within the compartment, minimize power cable losses, and group the signal and logic cables.

The four-bay SEP module compartment contains the electronic assemblies complying with the SEP requirements, including the power distribution module, which is located to minimize system power loss. One bay of the SEP module is available for additional electronics, if required, with 18 percent of the space in the other two electronic bays available. The Viking battery takes a full bay.

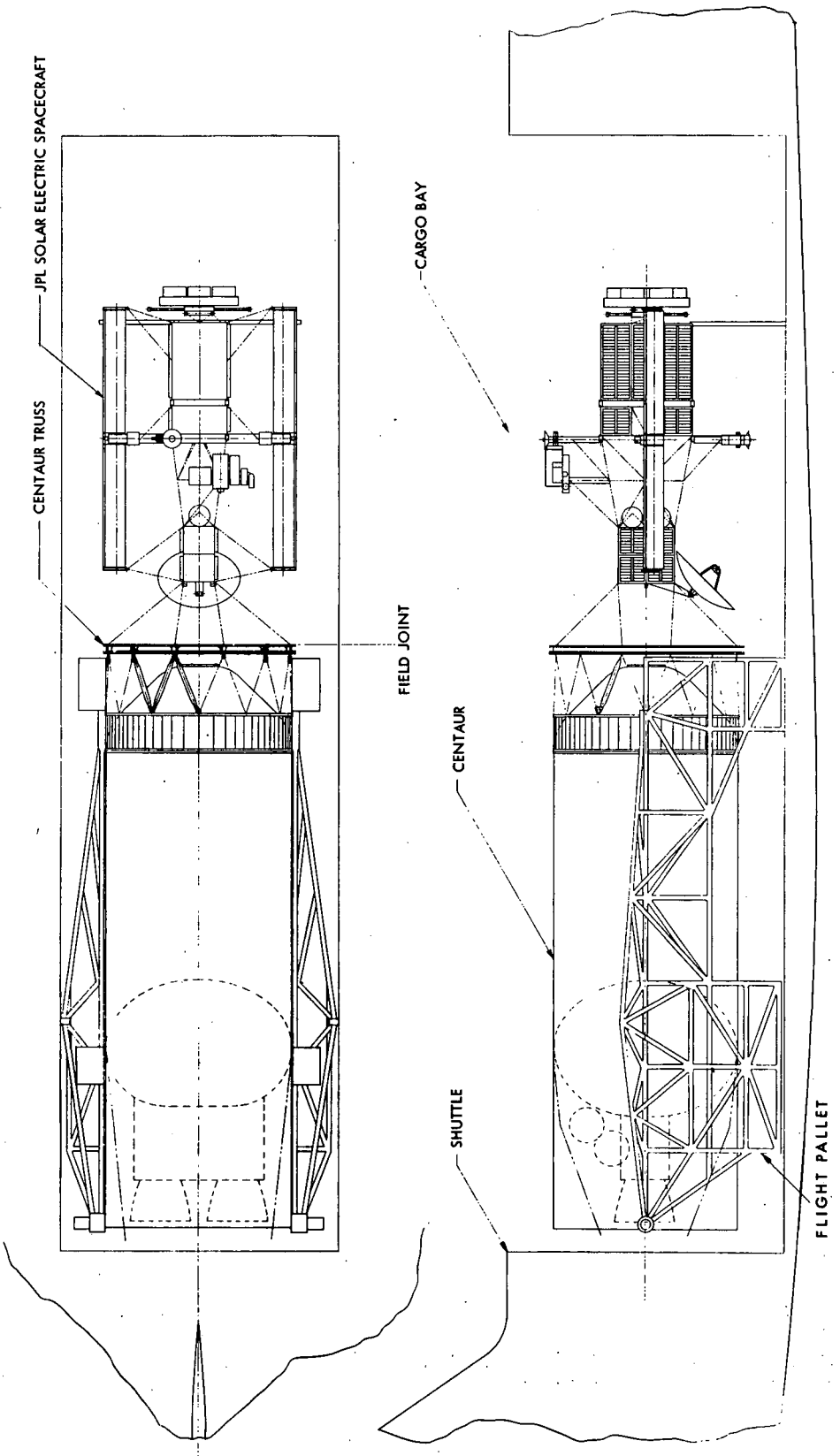

Fig. III-D-3. Space Vehicle Stowed in Shuttle Bay

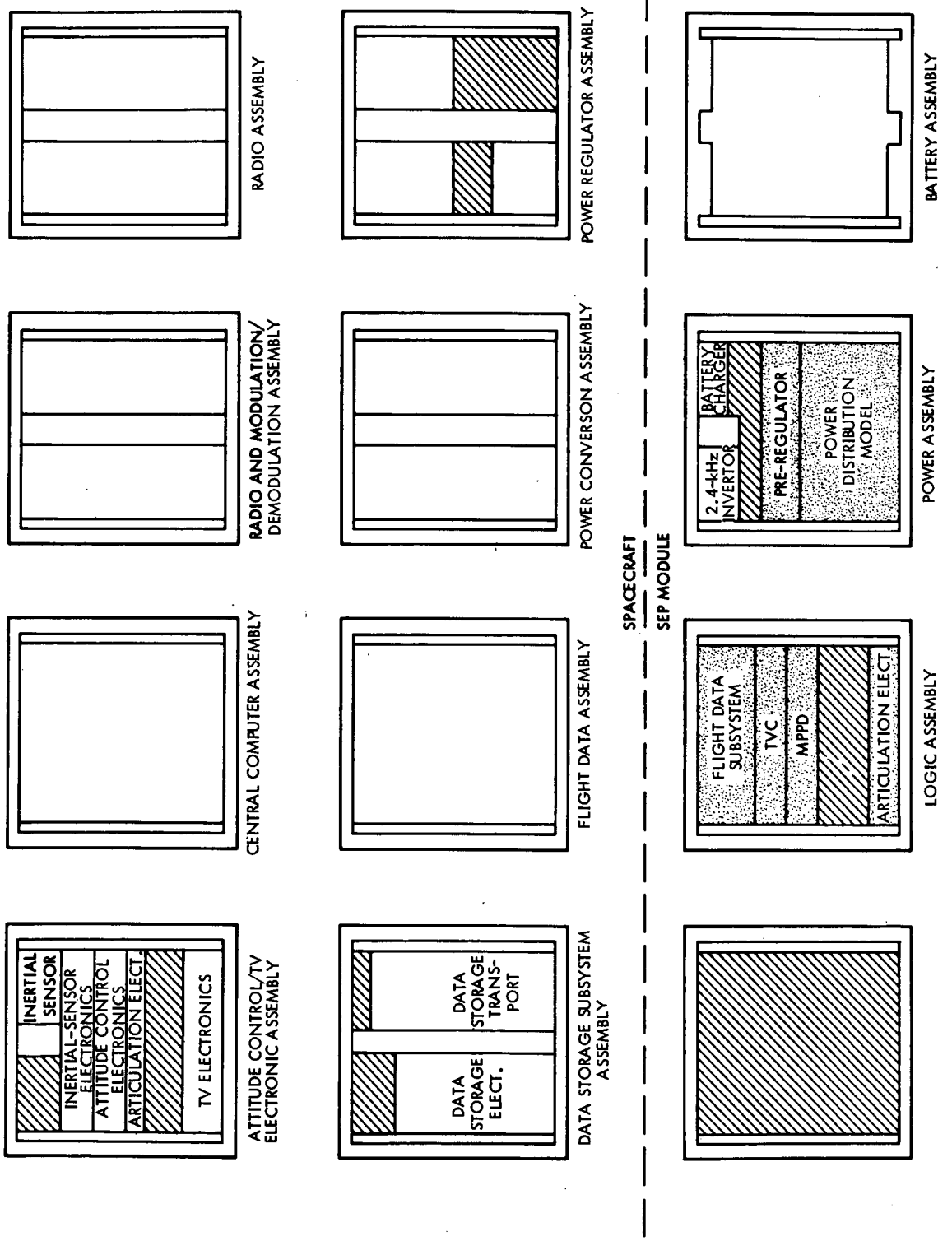

Fig. III-D-4. Option 3 Space-vehicle Compartment Packaging Arrangement

2. Equipment List, Weights, and Space-vehicle Mass Properties

The preliminary gross mass at launch is listed in Table III-D-1. Table III-D-2 gives the weight breakdown for the spacecraft and SEP modules

Table III-D-1. Gross Launch Mass

Elements	Weight	
	kg	lb
Spacecraft	448.1	985.8
SEP module	814.1	1791.0
Launch vehicle adapter	27.2	59.8
Propellant	480.0	1056.0
Total	1769.4	3892.6

and the launch vehicle adapter. Table III-D-3 gives the mass distribution and center of gravity for various flight configurations, as determined by preliminary analyses.

Table III-D-2. Equipment List and Mass Allocations

Item	Mass kg	Mass lb
SPACECRAFT		
Science		
*TV (100 μrad resolution)	17.4	38.3
*Infrared Radiometer	1.9	4.2
*White Light Photometer	2.5	5.5
*Photopolarimeter	4.2	9.2
*Mass Spectrometer	4.5	9.9
*Microwave Altimeter	6.0	2.7
*Radiometer (UV, 1000-4500 A)	2.5	5.5
*Plasma Probe	1.9	4.2
*Mass Spectrometer	4.5	9.9
Optical Particle Detector (Sisyphus)	3.0	6.6
Magnetometer	2.2	4.9
Plasma Wave Detector	4.5	9.9
Langmuir Probe	1.9	4.2
	57.0	125.4
Computer	25.0	55.0
Flight Data	20.0	44.0
Data Storage	28.8	63.3
Telecommunications		
Radio Frequency Subsystem	33.5	73.7
Modulation-Demodulation Subsystem	8.4	18.5
Low-Gain Antenna (2)	3.4	7.5
High-Gain Antenna (1)	5.9	13.0
X-Band Transmitter	1.1	2.4
	52.3	115.1
Mechanical Devices		
High-gain Antenna Articulation	1.0	2.2
High-gain Antenna Latches	3.4	7.5
Scan Platform Latches	6.8	15.0
Star Tracker Articulation	0.5	1.1
Star Tracker Latch	0.9	2.0
Staging Latch	4.5	9.9
Bus Louvers (8)	5.4	11.9
	22.5	49.6
Thermal Control		
Bus Thermal Blankets	1.9	4.2
Scan Platform Thermal Blankets	1.4	3.1
	3.3	7.3
Attitude Control		
Attitude Control Electronics (1)	3.7	8.1
Inertial Electronics (1)	2.7	5.9
Inertial Sensors (1)	2.3	5.1
Sun Gate (1)	0.1	0.2
Acquisition Sun Sensors (4)	0.2	0.4
Star Tracker (1)	4.2	9.2
N_2 Tanks (2)	10.0	22.0
High-Pressure Module (2)	4.7	10.3
Low-Pressure Module (4)	2.6	5.7
Thruster Assemblies	1.2	2.6
N_2	14.1	31.0
Articulation Control Electronics (1)	4.0	8.8
High-Gain Antenna Actuators (2)	2.3	5.1
Scan Control Actuators (2)	4.3	9.5
Star Tracker Actuators (2)	1.0	2.2
	57.4	126.1
Cabling		
Bus Cabling	55.8	122.8
Scan Platform Cabling	4.2	9.2
Power		
Power Sourced Logic	7.1	15.6
Booster Regulator A	3.5	7.7
Booster Regulator B	3.5	7.7
Power Control	2.5	5.5
Power Distribution	4.5	9.9
2.4 kHz Main Inverter	2.1	4.6
2.4 kHz Standby Inverter	2.1	4.6
400 Hz Inverter	1.8	4.0
	27.1	59.6
Structure		
Primary Truss	32.0	70.4
Bus	18.0	39.6
Electronic Chassis (8)	22.0	48.4
Bus Cable Trough	1.2	2.6
Attitude Control Tank Support	1.1	2.4
Scan Platform Frame and Boom	15.9	35.0
Bus Meteoroid Protection	4.5	9.9
	94.7	208.3
Total Spacecraft	448.1	985.8

Item	Mass kg	Mass lb
SEP MODULE		
Thrust		
Thrusters (7)	51.0	112.2
PCs (6)	98.0	215.6
TVC Mechanism	39.7	87.2
Propellant Tankage (1)	15.0	33.0
Switching Matrix (1)	12.3	27.1
Cabling	8.4	18.5
Contingency	10.0	22.0
	234.4	515.6
Power		
Solar Arrays (2)	315.0	693.0
Battery	30.5	67.1
Battery Charger	1.5	3.3
Preregulator	3.5	7.7
Power Distribution	13.6	29.9
2.4 kHz Inverter	1.8	4.0
Maximum Power Point Detector	4.5	9.9
	370.4	814.9
Thrust Vector Control		
TVC Electronics	2.7	5.9
Cruise Sun Sensor	0.2	0.4
Translator Actuators	5.6	12.0
Gimbal Actuators	10.9	24.0
Solar Array Rotators (2)	18.1	39.8
	37.5	82.5
Flight Data		
Master Flight Data Subsystem	9.1	20.0
FDS Slave Allowance	5.0	11.0
	14.1	31.0
Mechanical Devices		
Solar-Array Gimbal Latch (2)	9.1	20.0
Thruster Array Latch (4)	3.6	7.9
Electronic Bay Louvers (4)	2.7	5.9
PC Louvers (6)	16.3	35.9
	31.7	69.7
Cabling		
Power Cabling	11.5	25.3
Signal Cabling	10.0	22.0
	21.5	47.3
Structure		
Primary Truss	24.6	54.1
Solar Array Support	6.4	14.1
PC Frame	31.8	70.0
Propellant Tank Support	11.4	25.1
Switching Matrix Chassis (1)	2.2	4.8
Electronics Chassis (4)	11.0	24.2
Meteoroid Protection	8.2	18.0
Cabling Troughs	2.0	4.4
	97.6	214.7
Thermal Control		
PC Thermal Blankets	3.9	8.6
Bus Thermal Blankets	2.0	4.4
Thruster Array Thermal Blankets	1.0	2.2
	6.9	15.2
Total SEP Module	814.1	1791.0
LAUNCH VEHICLE ADAPTER		
Structure	20.4	44.9
Release Mechanisms	2.5	5.5
Cabling	2.5	5.5
Solar Array End Latches	1.8	4.0
	27.2	59.8
SPACE VEHICLE SUMMARY		
Spacecraft	448.1	985.8
SEP Module	814.1	1791.0
Launch Vehicle Adapter	27.2	59.8
Propellant	480.0	1056.0
Launch Gross	1769.4	3892.7

Table III-D-3. Center of Gravity and Inertial Properties

Mission Mode	Solar-array stowed launch	Solar Array Deployed			
		Launch + 1 hr Drums parallel to X-axis	Launch + 41 days Drums perpendicular to X-axis	Launch + 500 days Drums parallel to X-axis	Launch + 950 days Drums 73 deg from X-axis
Propellant on board, kg	480	480	430	190	10
Center of gravity mm (in.)					
X	221 (8.7)	224 (8.9)	196 (7.7)	97 (3.8)	-3 (-.1)
Y	-8 (-.3)	-13 (-.5)	-13 (-.5)	-15 (-.6)	-15 (-.6)
Z	38 (1.5)	51 (2.0)	53 (2.1)	61 (2.4)	71 (2.8)
Moment of inertia kgm^2 (slug ft^2)					
I_x	908 (670)	48, 356 (35, 666)	48, 769 (35, 971)	48, 348 (35, 660)	48, 722 (35, 936)
I_y	3347 (2469)	3, 250 (2, 397)	3, 235 (2, 386)	3, 200 (2, 360)	3, 070 (2, 264)
I_z	3822 (2819)	51, 180 (37, 749)	50, 750 (37, 432)	51, 133 (37, 714)	50, 622 (37, 337)
Product of inertia kgm^2 (slug ft^2)					
I_{xy}	20 (15)	31 (23)	31 (23)	28 (21)	23 (17)
I_{yz}	-15 (-11)	-26 (-19)	-24 (-18)	-24 (-18)	-28 (-21)
I_{xz}	-150 (-111)	-144 (-106)	-142 (-105)	-138 (-102)	-4, 299 (-3, 171)

E. SEP MODULE ADAPTIONS

Near the end of the FY 1972 study, it was determined that the SEP module, with minor modifications or additions to the electronic equipment, could perform other missions. A study was made of the feasibility of adapting the SEP module to fit various flight configurations, and to determine what changes or additional equipment were required to perform certain inner-and outer-planet missions of high scientific interest.

The first mission studied was an outer-planet orbiter. It was found that, to perform this mission, the space vehicle must include radioisotope thermoelectric generators (RTGs), a high-gain antenna 3.657 m (12 ft) in diameter, and science instruments adapted to the spacecraft part of the space vehicle. Changes to the science instrument payload were also considered, and an allowance made in the vehicle configuration for magnetometers, fields and particles experiments, etc.

Figure III-E-1 is an exploded view of the SEP module configuration for the outer-planet orbiter showing the Mariner Mars 71 retropropulsion system, the RTGs, the high-gain antenna, and the science instruments adapted to the spacecraft. An important feature is that the spacecraft can be separated from the SEP module after the electric thrust subsystem can no longer be powered by the solar array because of the distance from the sun (5 AU or farther). Once separated, the spacecraft receives power from the RTGs to travel on its way to orbit the outer planet.

Figure III-E-2 shows the modification of the space vehicle to perform an inner-planet mission, such as Venus or Mercury orbiter. For this mission, a high-gain antenna 1.219 m (4 ft) in diameter is needed along with a Mariner Mars 71 retropropulsion module. When the spacecraft is separated, the thrust subsystem is left behind, and the solar arrays and power subsystem remain attached to the spacecraft as it continues on its trajectory to orbit the planet. As shown in Fig. III-E-2, the solar arrays have less area exposed to the sun than in the outer-planet mission because of the relatively close distance to the

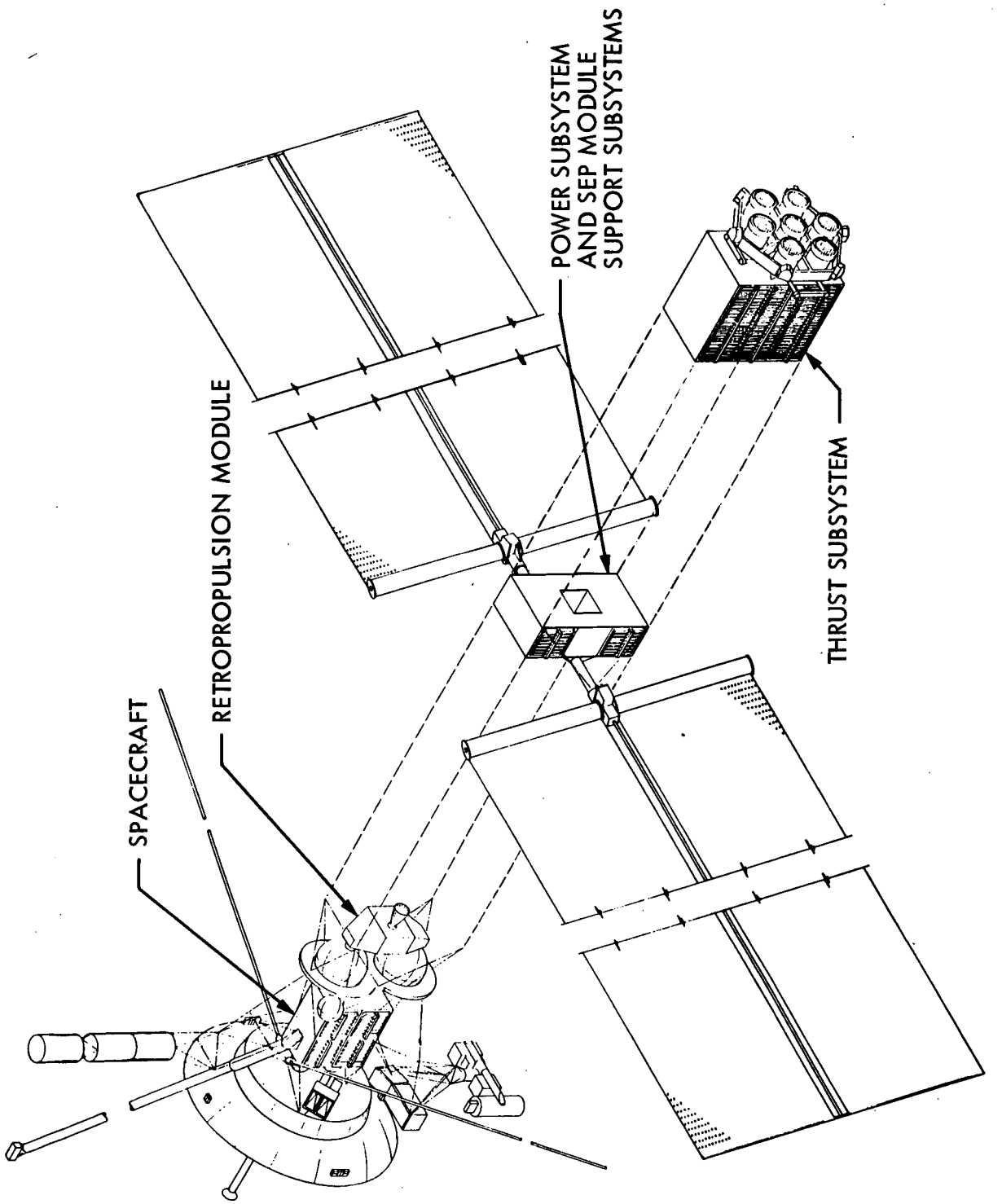

Fig. III-E-1. SEP Module Outer-planet Orbiter

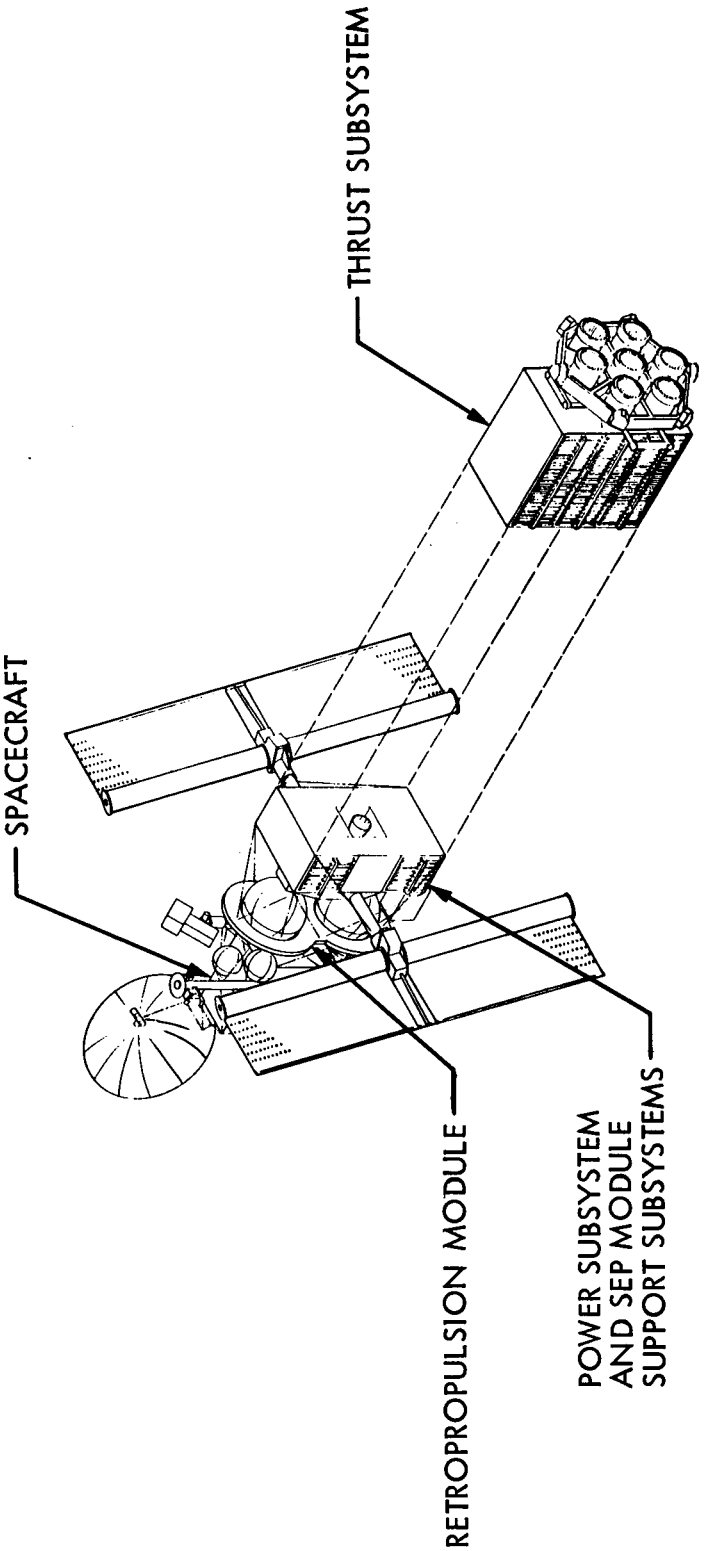

Fig. III-E-2. SEP Module, Inner-planet Orbiter

sun (1 AU or less). At this distance, the array provides enough power to eliminate the need for RTGs to supply auxiliary power. The spacecraft solar-electric power system can provide the needed power during orbital flight.

After the inner-and outer-planet orbiters were studied, the SEP module was examined as a vehicle to transport existing spacecraft on orbiter or flyby trajectories. Figure III-E-3 is an exploded view of the SEP module adapted to a Pioneer spacecraft with an open-truss structure. The Pioneer is separated from the SEP module at a distance from the sun where the solar arrays can no longer power the electric thrust subsystem, and it is then powered by RTGs. A high-gain antenna 1.473 m (4 ft 10 in.) in diameter was added to the SEP module to provide telecommunications during solar-electric cruise flight.

To adapt existing spacecraft, including Pioneer, to the SEP module, it may be necessary to add another electronic subsystem module with a capacity for four electronic subsystems.

The adaptation of the Helios spacecraft to the SEP module concluded the study. Fig. III-E-4 shows this configuration, which is identical to that of the Pioneer with the exception of the type of truss used to adapt the spacecraft to the SEP module. A different truss adapter is required for each of the spacecraft studied.

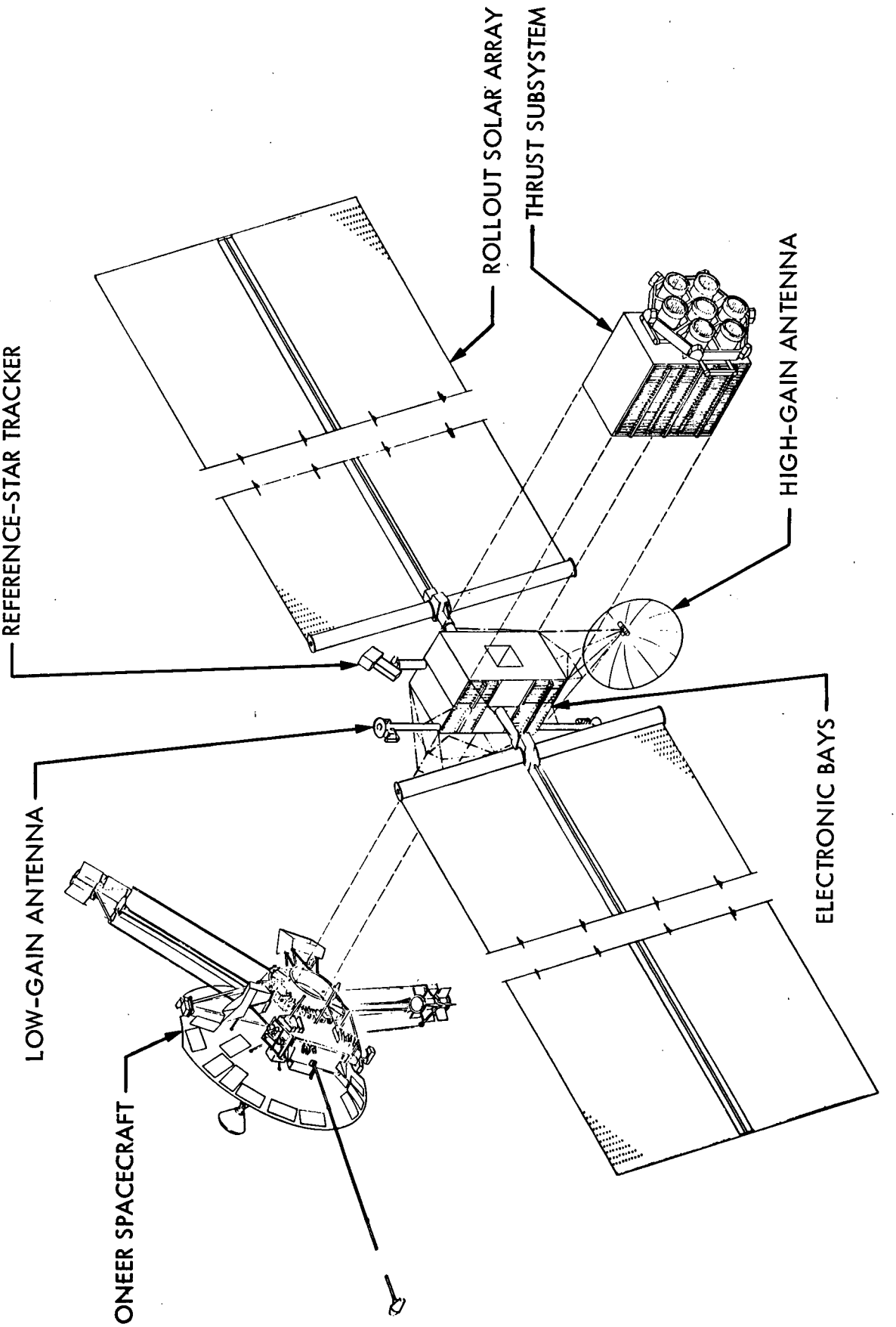

Fig. III-E-3. SEP Module, Pioneer Spacecraft Configuration

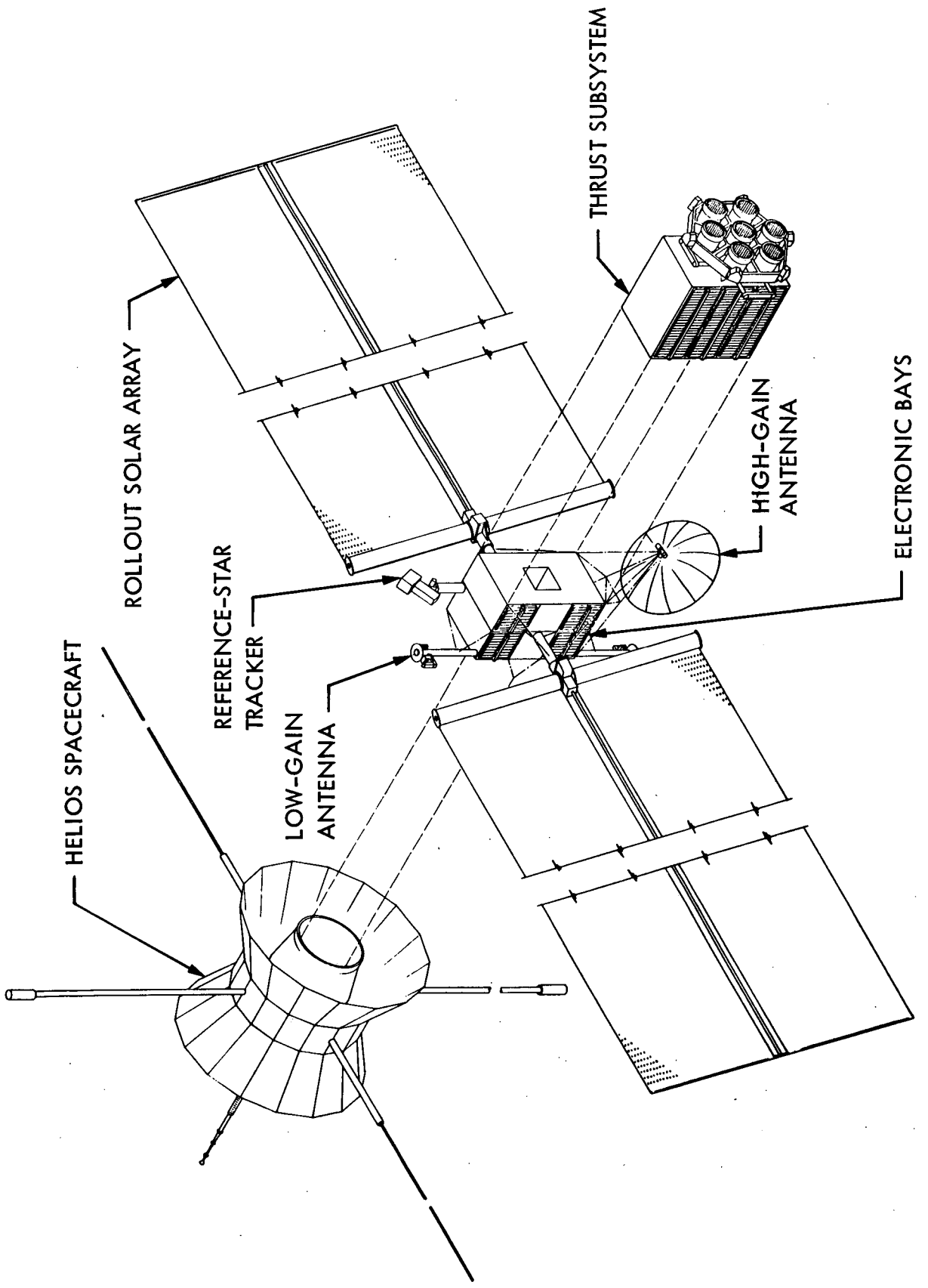

Fig. III-E-4. SEP Module, Helios Spacecraft Configuration

SECTION IV

SUPPORTING ANALYSES

A. INTRODUCTION

The analyses summarized in this section were performed in support of the design-point selection for the SEP module thrust-subsystem, as embodied in the thrust-subsystem functional description document, Appendix A, Volume II of this report. The analyses in detail appear in Volume III. Each of these analyses had at least one of the following objectives:

(1) To aid in the specification of parameters which affect the performance of elements within the thrust subsystem.
(2) To improve understanding of thrust subsystem interface requirements with the goal of optimizing interfaces wherever possible.
(3) To assure feasibility of some of the more critical technological aspects of SEP application.

Table IV-A-1 summarizes the relationship of each of the analyses to the above objectives. The table, as well as this section, is subdivided into studies which are related directly to the Encke rendezvous mission application, thrust-subsystem studies, power-subsystem studies, and other supporting subsystem studies. Specific output goals of each analyses are contained within the body of Table IV-A-1.

All studies which required a mission and/or space vehicle design were based, for the most part, on the SEP module/Viking-based spacecraft applied to the 1980 Encke rendezvous mission, as described in Volume II of this report. Deviations from this rule are caused by the initiation of some studies before the baseline design was made final. In all cases, however, these deviations are minor in nature and do not affect the conclusions of the studies.

Table IV-A-1. Relationship of Supporting Analyses to SEPSIT Study Goals

SEPSIT STUDY SUPPORTING ANALYSES		SEPSIT STUDY GOALS		
		Specify Thrust-subsystem Element Characteristics	Identify and Define Thrust-subsystem Interface Requirements	Establish Feasibility of Key SEP Technology Requirements
Mission Studies	SEP Thrust-subsystem performance sensitivity analysis	Examine the sensitivity of trajectory performance to variations in power level, specific impulse, thrust-subsystem efficiency, thruster-beam divergence, thrust-beam double ion content, and establish tolerance limits for these parameters.		
	Navigation studies	Develop a time-dependent model of thrust-subsystem performance dispersions, as determined by variations in thruster-beam voltage, current, divergence angle, single and double ion content, thruster grid alignment and erosion, celestial-sensor performance and thrust-vector control actuator performance, and establish tolerance limits for these parameters consistent with acceptable navigation accuracies.		Evaluate the feasibility of advanced orbit-determination methods which would permit successful navigation in spite of the unusually large random accelerations attendant to low-thrust systems. Develop a feasible terminal navigation scheme and investigate the requirements imposed on spacecraft imaging instruments.
	SEP mission risk-factor analysis	Evaluate the impact of thrust-subsystem size, reliability and operational strategy on the probability of mission success, thereby providing a data base to aid in the allocation of thrust-subsystem reliability.		
Thrust-Subsystem Studies	Power-conditioner selection and SEP-module integration study	Define size, electrical, thermal, and structural characteristics of thrust-subsystem power conditioners.	Determine optimum thermal and structural interfaces of multiple power-conditioner assembly with SEP module configuration.	
	Switching-matrix tradeoff study	Select best power-conditioner-to-thruster-connection method based on weight and probability of mission success tradeoffs, and supply data which would aid in allocating power conditioner, connecting switch, and thruster reliability.		
	Switching matrix development analyses	Provide a preliminary design of selected power-conditioner-to-thruster switch as determined by the switching matrix tradeoff study.		
	Thruster-array thermal analysis	Determine impact of thruster thermal control methods such as thermal coatings, shields, and heat pipes on maintaining thruster components within acceptable temperature limits, and specify a preferred thermal control approach.	Evaluate the thermal interface requirements imposed on thrusters by surrounding SEP module elements such as thrust vector control actuators, propellant lines, and power conditioner assemblies.	
	Thrust-vector-control tradeoff study	Compare the merits of the JPL gimbal-translator with the TRW collar-gimbal thrust-vector control approaches; and select tentative best method for future thrust-subsystem applications.		
Power-Subsystem Studies	Power-subsystem operating-voltage selection	Specify thrust-subsystem input voltage range.	Select power-subsystem operating-voltage range based on consideration of solar array, power conditioning, and distribution benefits.	
	Solar Array Analyses: Dynamic interactions with attitude control			Develop a linear dynamic attitude-control simulation of a space vehicle with large, flexible solar arrays. Evaluate the feasibility of using a SEP thrust-vector control system as an attitude-control device for various solar-array sizes and dynamic characteristics.
	Solar Array Analyses: Structural Interface with SEP module			Identify the feasibility and specify means of structurally integrating large flexible solar arrays into a SEP module. Special attention is given to the interaction of the arrays with the SEP module during large displacement, low frequency, launch vibration modes.
	Solar Array Analyses: Thermal Analyses			Evaluate the combined effects of solar-array edge-curl and high solar intensity environment (.34 AU) on the feasibility of maintaining solar arrays within acceptable temperature limits.
	Maximum power-point detector concept survey			Examine closed and open loop methods of operating solar arrays at or near their maximum power output; list advantages of each method.
Support-Subsystem Studies	Data handling		Determine the command, control, and sequencing requirements of a SEP thrust subsystem, including the response times required, parameters to be measured, failures to be handled (both transient and permanent), parameters to be controlled, data storage, and data transmission. Evaluate the various hardware implementations in relation to: complexity, cost effectiveness in satisfying the requirements, reliability, noise tolerance [electromagnetic interference (EMI) and radio frequency interference (RFI)], and weight; and, from the evaluation, to arrive at a preferred data system configuration.	
	Telecommunications - SEP interaction studies		Provide data whereby thruster ion-beam effects on telecommunications performance might be understood and possibly minimized.	Evaluate the effects of "Bremsstrahlung radiation" generated by the ion-thruster exhaust beam on telecommunications uplink performance; and develop a model to evaluate the effect of a general dispersive media, e.g., solar corona or ion beam, on telecommunications performance.

B. MISSION STUDIES

1. SEP Thrust-subsystem Performance Sensitivity

The objective of the performance sensitivity study was to examine the sensitivity of mission performance to the combined SEP thrust subsystem parameters η_{TSS} (overall efficiency) and I_{sp} (specific impulse) and thereby to derive the constraints which should be imposed on the thrust subsystem hardware. The approach taken was to sequentially examine the available contingencies and their effect on necessary thrust-subsystem performance, starting from an assumed selected mission and spacecraft preliminary design. The effect of variations of η_{TSS} and I_{sp} on these contingencies was next examined, and constraint boundaries for subsystem performance were determined. Finally, the effect of changes in the design on these constraint boundaries were determined.

As a fundamental guideline for the sensitivity study, mission success was defined as: (a) reaching the desired position and velocity, (b) with the required amount of hardware, (c) in a specified amount of time. The controls available to achieve this success include the combined subsystem parameters under investigation, I_{sp} and η_{TSS}, the amount of time the system is operated, the initial mass which must be accelerated, and the time history of the thrust-pointing vector. Ideally, each control should be optimized in the sense that histories (e.g., thrust coast-times and pointing vector) would be selected which ensured mission success, but which place minimum restrictions on the thrust-subsystem operating specifications. The goal should be to determine the set of paths over a desired launch opportunity which exhibit these features:

(a) A relatively low amount of thrust time, thereby increasing reliability through a reduction of hardware operation time.

(b) Regularly spaced coasts, which could be used as thrust periods to increase mission tolerance to substandard hardware performance.

(c) A thrust-pointing history minimizing the number of vehicle inertial-attitude changes.

(d) Mission success over a wide range of I_{sp} and η_{TSS}.

The study guideline selected was the determination of the set of paths exhibiting feature (d) under the constraint of feature (a). Thus, trajectories were required to have coast phases, but accurate quantitative thrust times were not determined, nor were the effects of thrust-period placement or constrained thrust angles on the tolerances for the collective parameters, I_{sp} and η_{TSS}, examined. The omission of features (b) and (c) leaves the probability of significant future changes in the acceptable hardware-performance limits. The importance of early specifications for hardware development raises the priority for securing fast, accurate, flexible, and inexpensive hardware simulation programs to alleviate the guideline restrictions of this study.

To provide a basis for tolerance studies, boundaries were required for measuring mission success. The logic detailed in Volume III, Section II A, led to the summary of mission boundaries used to set hardware tolerances based on performance (Table IV-B-1).

Table IV-B-1. Summary of Mission Boundaries

Parameter	Boundary
Arrival	50 days prior to comet perihelion
Velocity	Matching at the comet (VHP = 0)
Launch Operations	Any time during a 30-day opportunity
Coast Periods	A reasonable amount of coast time
Thrust-Vector Pointing	No limitations placed on thrust pointing history for this study

The parameter selected as most important in relating thrust-subsystem hardware technology development to performance is the final mass, m_f. The force which delivers the final mass is embodied in the kinetic energy contained in the thrust exhaust beam. Mass and beam power occur as a ratio in the equation for instantaneous acceleration, and this ratio provides a convenient parameter for use as an objective function in setting hardware boundaries for individual trajectories. A similar parameter combination was used to account for propellant requirements.

Setting limits or specifications for thrust-subsystem design and operations requires understanding available mission contingencies or controls, such as arrival date, launch period, and coasts. For arrival time and launch period, contingency is added to a system meeting the success boundaries, if the mission boundary definition can be altered to allow later arrivals and/or shorter launch periods. Because coast periods were not adequately investigated in this study, final decisions about this contingency effect are dependent upon further study.

Other contingencies, not considered explicitly as mission success criteria, are important as controls indirectly affecting mission success. In general, the ability to change the controls, which define the low-thrust mission mode, is available during the three pre-target phases: (a) the initial design, (b) post-hardware delivery, and (c) post-launch. The number of controls available for re-specification diminishes with each phase. Table IV-B-2 summarizes

Table IV-B-2. Available Contingencies and Controls

Controls	Initial Design Phase	Post Hardware Delivery	Post Launch
Launch Excess Capability	X	X	
Launch Period	X	X	
Arrival Date	X	X	X
Coast Periods	X	X	X
Vehicle Design Mass (de-fueled)	X		
Solar Power Reserve	X	X	X
Propellant Mass (reserve)	X	X	
Thrust Pointing Capability	X	X	X

the controls available during each phase. The table shows that, during the initial design and construction phase, limits can be set and tradeoffs can be made among mission and hardware parameters to define mission success and set hardware specifications. Adjustments can still be made should late considerations demand redefinition of mission goals. After launch, however, thrust subsystem anomalies can only be handled by adjusting the planned coasting periods, accepting later arrival at the target, using the planned solar-power reserve, and altering the path with a new thrust-pointing profile. For clarification of the relationship of these control alternatives to the objective of setting hardware specifications, see Vol. III, Section II-A. A typical example of the basic mission data used in determining mission tolerance to hardware anomalies is given in Fig. IV-B-1. The data are based upon the 50-day pre-perihelion arrival selected as a mission success boundary and illustrate a delivered thrust-subsystem with an I_{sp} of 3000 sec. The auxiliary power allowance is given as a ratio, which includes the thrust-subsystem efficiency, η_{TSS}. The solid lines represent various values of the objective function, m_f/P_j. Each point is a possible trajectory for the vehicle with that m_f/P_j. The path flown depends on the launch date. All the displayed trajectories include some amount of coast, except those connected by the dotted line, which denotes the continuous thrust boundary. The paths farthest to the left of this boundary have the largest amount of coast. Allowance for use of planned coasts as contingency was accomplished by constraining the allowed launch dates with the second dotted line denoted "launch period closed". This line is arbitrarily placed to provide a "reasonable" allowance of coast time and to reserve available paths for in-flight contingency use (post-launch phase). The propellant load ratio must be based on using the contingency.

The system considered is a 1261-kg spacecraft, with 20 kW installed power at 1 AU, and with 16 kW delivered to the thrust subsystem. The thrust subsystem specific impulse is 3000 sec with an efficiency of 0.65. For this system to be within the selected mission-success boundaries, the hardware constraints are that there be a minimum allowable delivered I_{sp} of 2910 sec and a minimum efficiency of 0.615. To provide these tolerances, it is necessary to design for a propellant reserve of 56 kg.

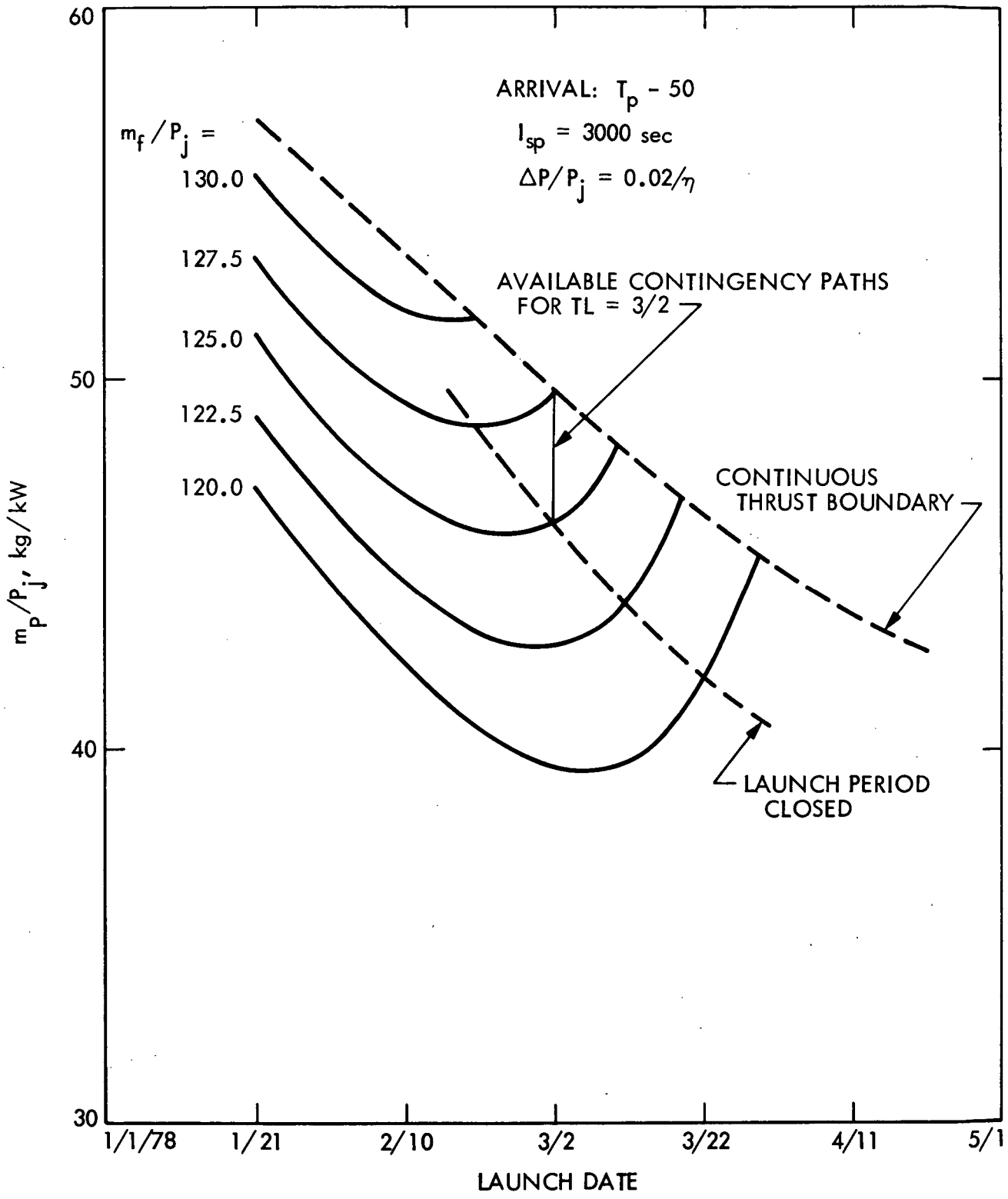

Fig. IV-B-1. Mission Contingencies Available in Launch Period

The subsystem efficiency was based on the assumption that the fraction of single ions in the beam, η_1, was 0.9; the double ion content, η_2, was zero; and beam divergence, gimbal misalignment, and thrust-vector misalignment angles were all zero. The thrust recovery factor, ζ, was 1.0.

As these parameters are varied, both I_{sp} and efficiency vary. Variation of beam divergence, $\bar{\theta}$, and η_2 were specifically examined, and limits found for the nominal mission. The results indicated that only small variations in these parameters can be tolerated. For example, for $\bar{\theta}$ = 5 deg, the maximum allowable value of η_2 is about .035.

The study also showed that the constraints on the hardware performance can be relaxed by the addition of more power, as illustrated in Fig. IV-B-2, wherein constraint boundaries on η_{TSS} at several values of I_{sp} have been plotted for various power levels. These curves are based on assumed vehicle dry masses of 1261, 1281, and 1301 kg for 16, 17, and 18 kW, respectively, of initial power to the thrust subsystem. The curves inherently include a given I_{sp} versus η_{TSS} relationship, and they must be updated to include variable I_{sp} systems. The figure also shows a band, which covers the "nominal" subsystem performance over its entire operating range. This band accounts for efficiency variations with power level. It can be deduced from this figure that, as long as the path of the thrust-subsystem operation from the "nominal" point, A, to some other point, B, does not cross the appropriate mission success boundary, then success, as measured by the delivered final mass for the selected power level, will be achieved. Such a path could result from throttling, etc. If, however, the path crosses the boundary, as typically shown at C, then mission failure occurs.

The figure shows that the operational range and, consequently, the interaction with mission success boundaries is strongly influenced by $\bar{\theta}$ and η_2. For example, suppose point C is reached by some throttling function which maintains $\bar{\theta}$ and η_2 at zero. Several possibilities are then added which can translate C as shown. If constant I_{sp} is maintained, the dotted path results. This path reduces the effects of $\bar{\theta}$ and η_2, showing that a system of 17 kW and

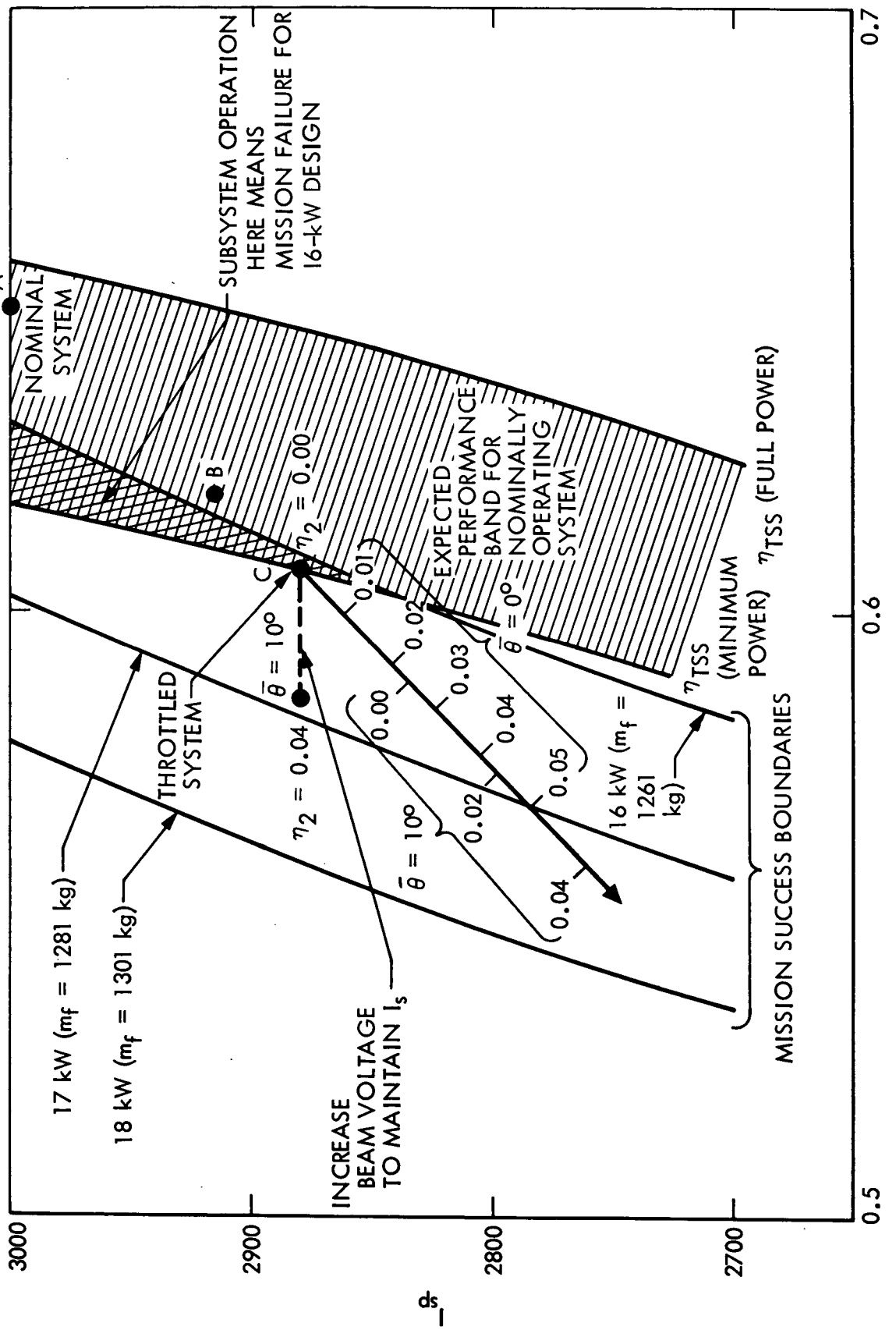

Fig. IV-B-2. Constraint Boundaries and Nominal Expected Performance for Thrust-subsystem Efficiency, η_{TSS}

m_f = 1281 kg is still successful at full throttling with $\overline{\theta}$ = 10 deg and η_2 = .04. Without constant I_{sp} being maintained, the same values of $\overline{\theta}$ and η_2 result in mission failure for the 17 kW system. However, by initially designing for 18 kW, substantial variations in the various parameters can be tolerated within the corresponding mission success boundary. Further, if the true values of $\overline{\theta}$ and η_2 are known, a basis is provided for selection of the design power level. For instance, given a $\overline{\theta}$ = 10 deg and η_2 = .04, a boundary of 17 kW can be chosen for a strategy which increases the beam voltage to maintain constant I_{sp}.

The conclusion to be drawn from this is that it is important to know, at the time of preliminary design, the exact values of such parameters as $\overline{\theta}$ and η_2. Unplanned values for these parameters can be accommodated by increasing the design-power level; but, because this directly affects cost, the cost of minimizing allowable variances in subsystem parameters must be traded off against the cost of the additional power required to accommodate them.

Increasing the power level to the thrust subsystem by 1 kW, for example, drops the minimum acceptable efficiency at 3000 sec to 0.602, and at 2900 sec to 0.586. Thus, the power level selected influences the hardware constraints. Because power, however, is a major cost item, there is strong motivation to hold power level to a practical minimum. To do this requires good knowledge of the true performance of the thrust subsystem at the time of power-level selection and tight constraints, thereafter, on meeting the performance used to select the power.

The major conclusions reached in this study are:

(a) Uncertainties in achievable performance in the elemental parameters of the thrust subsystem have significant effects and must be considered in selecting both the power level of the spacecraft and the ion-beam voltage.

(b) Any reasonable variance in the thrust-subsystem performance can be accommodated by increasing the power level.

(c) Once the power level and beam voltage have been selected, hard limits are set on thrust-subsystem performance. Violation of these limits will make the mission unattainable.

(d) On the basis of the above, an accurate knowledge of true subsystem performance is essential prior to the final selection of a design power level and beam voltage.

2. Navigation Studies

A navigation development team (NDT) was formed to investigate in depth the requirements and feasibility of a SEP Encke rendezvous mission. This section includes the general background of low-thrust navigation and the results of the specific studies undertaken by the NDT. Summary results of the thrust-subsystem error modeling study and the orbit determination studies are presented. Also, the new error modeling developments are described because they are fundamental to the orbit determination and guidance studies. These studies lead to the definition of a feasible navigation scheme for a low-thrust rendezvous mission to Encke.

In addition, the terminal-maneuver strategy also has an important impact on thrust-subsystem tolerance specifications. This viewpoint was investigated by the NDT, and it was proven that it is feasible to accomplish terminal guidance using a practical optical imaging design in the presence of random acceleration errors as large as five percent.

a. The Low-thrust Navigation Problem

Navigation, in the broader sense, describes a multifunctional system comprised of three integrated areas: orbit determination, maneuver strategies, and guidance. The interfaces binding these operations are even stronger for low-thrust missions than for ballistic missions, so that a low-thrust navigation system must be designed as an entity.

Current navigation methods rely totally on an earth-based command and control system. Feedback control of the spacecraft depends

entirely on an earth-based tracking system, known as Mark I (Mk I), which employs conventional doppler and range data. Mk I navigation has been improved by reducing the data-error sources to a point where planetary excursions to the terrestrial planets are well within the capability of the system.

Although earth-based navigation will continue to improve, most missions over the next two decades will require some additional navigational support from the spacecraft itself. Figure IV-B-3 illustrates the evolution of navigation against a "timeline" of mission options. The navigation technology represented by the systems in Fig. IV-B-3 applies equally well to ballistic and low-thrust missions except that the low-thrust system requires Mk II for the planetary missions. However, it is worthy to note the general commonality, a duality that is most beneficial to the low-thrust technology development program.

Current studies have shown that low thrust is very attractive for small-body and comet missions. Consequently, a low-thrust rendezvous mission to Encke in 1980 was selected as a definitive means of focusing low-thrust technology development. The low-thrust navigation system to be developed for this mission clearly falls within a Mk II class of system. The ephemerides for small-body and comets are the major source of error or uncertainty. Physical properties of these targets limit the capability to improve their ephemerides by earth-based tracking; but earth-based data, supplemented with spacecraft-based data, dramatically reduces ephemeral errors from a dominant source to a level commensurate with platform-error sources, such as DSN station-location errors.

Figure IV-B-4 conceptualizes a Mk II navigation system (Ref. IV-B-1). Development of a particular navigation system begins with these basic ideas and then transforms each of the block concepts into a working process with compatible interfaces. This transformation is not routine, even for a mission needing only well developed existing technology, for there are many design options to be considered in each area. For example, for orbit

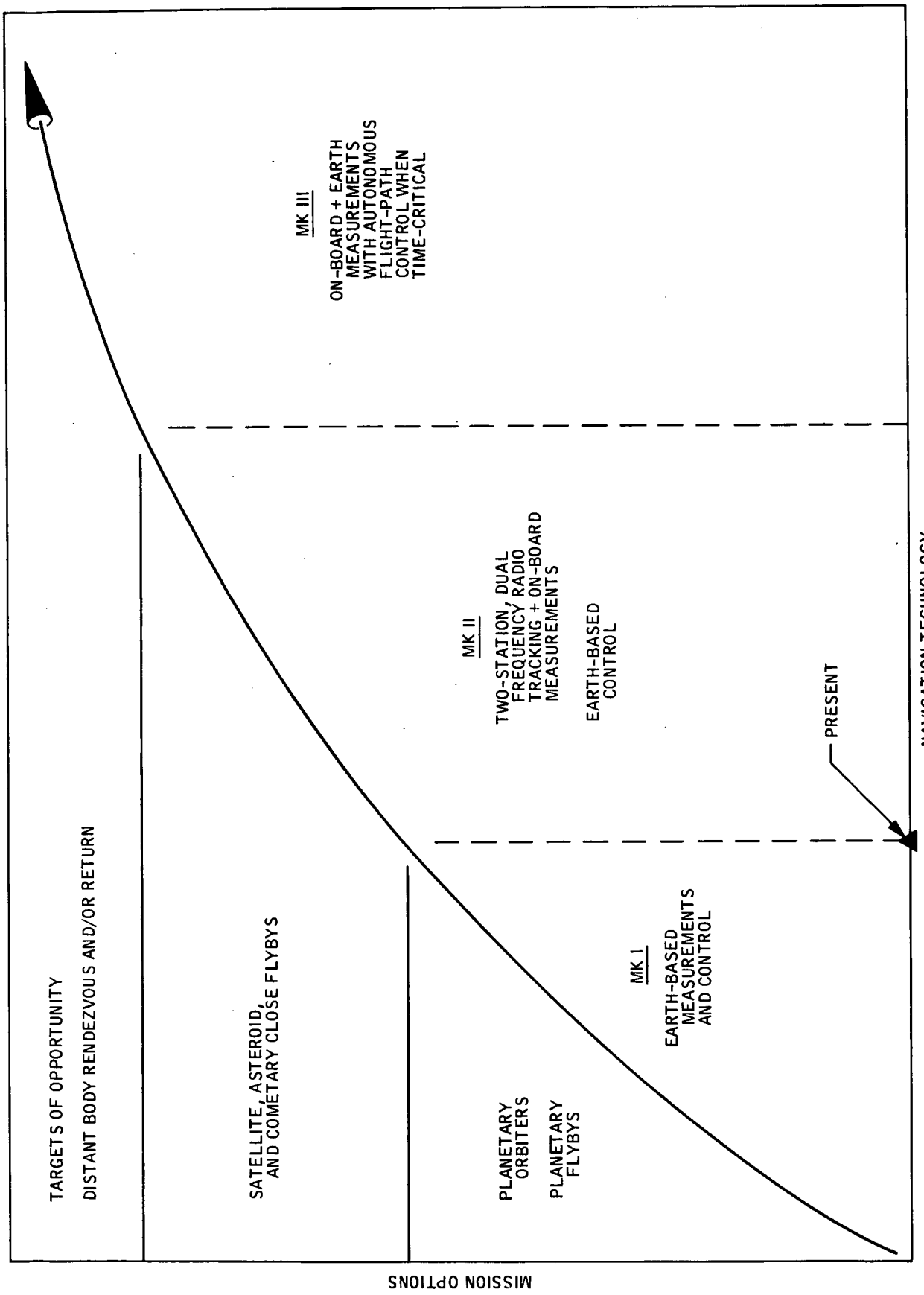

Fig. IV-B-3. Mission Options versus Navigation Technology

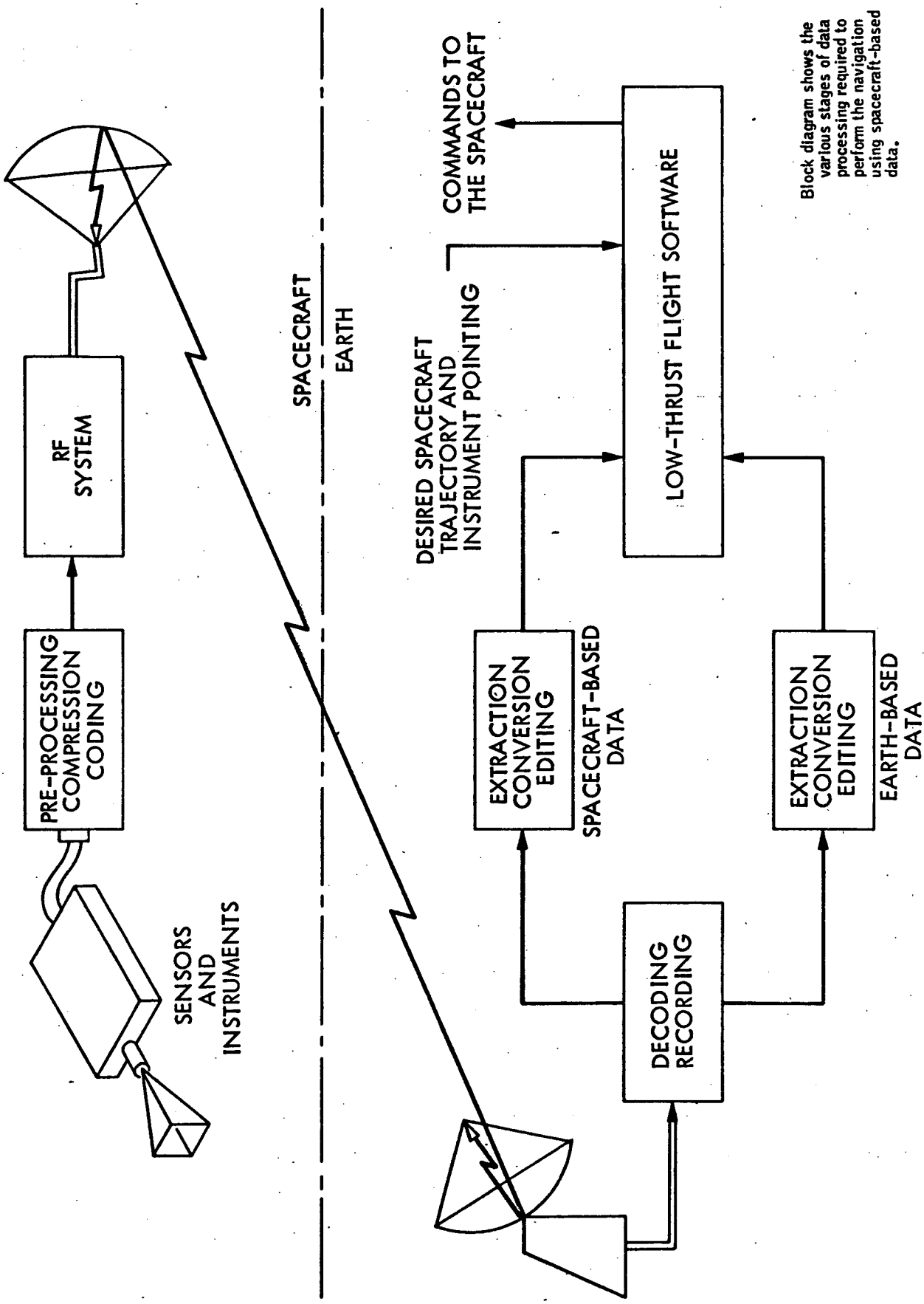

Fig. IV-B-4. Mark II Navigation System

estimation, the best combination of available types of data must be selected according to a set of overall system requirements, of which accuracy would certainly be a prime factor.

Not all technology for navigating a low-thrust spacecraft is fully developed. A SEP thrust system has unpredictable variations in accelerations, which dominate the navigational problem. These continual random acceleration dispersions (process noise) are typically three orders of magnitude larger than the nongravitational acceleration dispersions encountered on ballistic missions.

The comparison shown in Fig. IV-B-5 illustrates the effect of process noise on conventional doppler data. The degrading effect in estimating position accuracy as acceleration noise is increased can be seen. Two popular orbit estimation techniques are illustrated. Because the current system is expected to produce acceleration errors up to 10^{-8} km/sec^2 in magnitude, innovations are necessary to reduce the impact of noise on accuracy, with an ultimate goal of approaching the accuracies of ballistic missions.

Batch processing of low thrust data is not appropriate. Sequential estimation is more promising, but current filters may not be adequate. Better filters can be devised, but this may require better models of the random noise process; this is difficult. The best filter would possibly be an adaptive type, second-order filter which can approach "ideal" performance even in a changing environment, although even this may not be good enough.

Another approach would be an attempt to directly measure the acceleration disturbance, instead of trying to model its behavior. Still another approach would be to find some unique type of data (other than conventional doppler), which would be insensitive to this kind of disturbance. Because all of these possibilities, and others, may have some merit, technology studies are necessary for the design of a low-thrust navigation system.

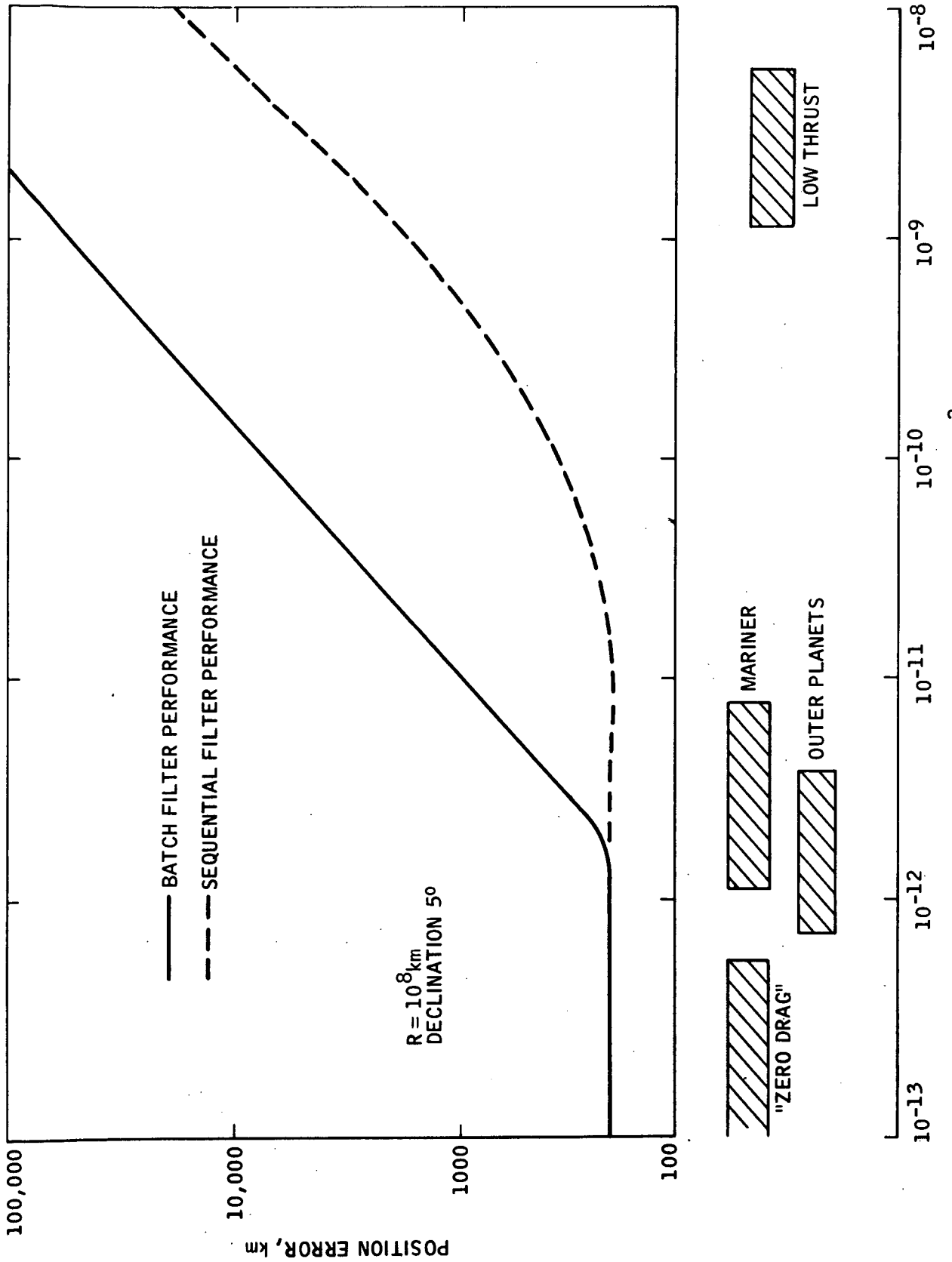

Fig. IV-B-5. Comparison of Batch and Sequential Filter Performance

In addition to the acceleration noise problem, there are other problems caused by the level of available propulsive acceleration: (1) control with a low continuous acceleration precludes conventional ballistic maneuver strategies and (2) large corrections are often required near comet rendezvous because of dramatic improvements in ephemeris information; thus, controllability problems may be encountered.

After a feasible low-thrust navigation system is defined and developed, sensitivity studies can be performed to investigate the parameter effects on navigation performance. The most significant parameters are those used to model the random acceleration dispersions of the thrust subsystem. Studies of this kind not only solidify the navigation system design, but the results can also be used in a reverse role by thrust designers, who, on the basis of navigation performance, can determine the best set of thrust subsystem tolerances for design criteria.

b. Summary of Navigation Development Team Study Results

Four main task areas need to be studied for Mk II navigation: (1) error modeling, (2) orbit estimation, (3) maneuver strategies, and (4) optical guidance. These tasks are related in pairs, respectively. An initial task for study of (1) and (2) is to model the unpredictable random accelerations dispersion of the thrust subsystem.

The other pair of tasks, (3) and (4), is related in that adequate maneuver strategies and feasible guidance schemes to implement them must be determined. Because of Encke's dominant ephemeris uncertainty, navigation is separated into a cruise phase and a terminal phase. Cruise navigation of the spacecraft to within the ephemeris uncertainty of the comet is

routine. However, once the spacecraft is in the vicinity of the comet, terminal navigation becomes critical in that rendezvous accuracies of ≤ 1000 km must be achieved within a very short period, typically, less than 20% of the cruise time. Therefore, controllability may be a serious navigational problem, depending largely on how soon spacecraft optics can acquire the comet.

1) Thrust Subsystem Error Model. Previous low-thrust studies have modeled the low-thrust subsystem acceleration errors as purely random stationary processes, with equal components in all three body axes (spherically distributed). No biases were assumed to exist in acceleration errors. There are arguments that this approach is conservative; however, it does not lend itself readily to relating accuracy sensitivities to specific hardware parameter sensitivities. As mentioned earlier, a more complete model is needed to provide data for specifications of acceptable tolerances, useful for both operational design and manufacturing.

The basic approach is to first obtain parametric models of the thrust subsystem. Analytical parameter models are then converted to statistical models, with only those parameters which contribute significantly to eventual acceleration errors retained. Next, time-varying statistics are mapped into tractable random processes along both a principal thrust direction and perpendicular cross-axis components. These random processes are assumed to be stationary, unbiased, and time correlated (exponential, auto-correlated processes). Biases in these components are treated by superposition of a time-varying, first-order random process onto a similar process, whose time correlation value is infinite.

Unlike previous models, the major error sources were found to be basically dual in nature: those which are statistically independent (do not share a common error source), and those which are dependent, (common errors).

Thrust subsystem parameters such as beam current, beam voltage, mass utilization efficiencies, and beam-angle divergence can be treated as independent error sources. These error sources are rss proportional to the square root of the number of engines on the basis of total thrust. Dependent error sources occur because of errors introduced through a common source such as the celestial sensor-attitude reference system, or the thrust-vector control system. In contrast to statistically independent errors, common errors increase in proportion to the number of engines. Consequently, the current model yields acceleration errors which are not symmetrical about the thrust axis.

The independent error sources and their standard deviations are given in Table IV-B-3. The rss value of these errors (except the angle, β) represents the total time-varying standard deviation in acceleration error along the principal thrust axis caused by one engine. This value is calculated as 3.5% (6.35% is the maximum value, i.e., when the errors are summed). Correspondingly, the rss of the biases is 2.2%.

Cross-axis acceleration errors result from both independent and dependent error sources. The independent errors, such as plate warpage, $\overline{\beta}$, do not actually vary with time, since plate warpage attains a permanent set. The long correlation time reflects the bias nature of this quantity. A 1-σ value of this component was estimated at 1.2%.

The dependent error contribution, caused by pointing errors, is much less significant. A time-varying drift in the celestial reference system produced acceleration errors less than 1%, with a bias contribution less than 0.1%. Also, a candidate thrust-vector control system was examined as a dependent contributor to the cross-axis acceleration errors. It is shown that, if a closed-loop control system, such as the translating system proposed at JPL, is used, maximum acceleration errors are produced on the order of only 0.5%; these errors are quite negligible. However, there are other systems currently being proposed, which produce significantly larger errors, on the order of one radian. Consequently, to cover all possibilities, conservative estimates of this component, which amount to 1%, are used in the orbit determination analysis.

Table IV-B-3. Thruster Performance Summary Data

Parameter	Nominal Value	Calibration Accuracy (% Nominal)	A Priori Process Standard Deviation	Correlation Time	Contribution to $\Delta T/T$		
					Bias	Time Varying Component	
I_B	Programmed	±0.5	±1.5%	weeks	0.5%	1.5%	6.35% maximum
V_B	1 - 2 kV	±0.5	±1.0%	weeks	0.25%	0.5%	
cos θ	0.96	±2.0	±3.0%	weeks	2.0%	3.0%	
η_1	0.8 - 0.85	±1.0	±5.0%	days-weeks	0.02 - 0.05%	0.1 - 0.2%	
η_2	0.04 - 0.07	±20.0	±25.0%	days-weeks	0.5 - 1.25%	0.5 - 1.0%	
ϵ	0.005	±30.0	±30.0%	days-weeks	0.15%	0.15%	
					rss 2.2%	rss 3.5%	
$\bar{\beta}$	0.0	--	±2°/3	months	1.2% cross axis		
Pointing Errors	0.0	--	.01 rad	hours	0.1%	1.0% cross axis	

Lastly, statistical independence of the parameter vectors was assumed. This assumption is justified under normal operations; however, operation in certain failure modes could invalidate this model. Notwithstanding the degree of sophistication, the error model still serves adequately as a basis for a much needed sensitivity analysis, which relates hardware parameter errors to orbit estimation performances.

2) Orbit Determination. An integrated program was undertaken whereby a software development program and a mission navigation study were merged. From the outset, design of orbit estimation processes to resolve the ambiguities caused by the presence of unpredictable acceleration dispersions dominated the early activities of the NDT.

As discussed previously, the spacecraft can remain in cruise configuration, navigating within the earth-based ephemeris uncertainty of the comet up to the terminal phase, when a Mk II navigation system is required. This fact establishes the framework for the design of the orbit determination software, consisting of filter models and tracking strategies. Proper filter design and tracking strategies can be adequately designed through accuracy comparisons of steady-state orbit parameter estimates (position and velocity at some epoch), and by the rate at which the estimation filter attains steady-state values. Steady-state values can be obtained from a single data arc, strategically located, so that the results are representative of all such data arcs. A typical 30-day arc, which can be used for both the cruise and terminal phases, was selected to be located near the end of the mission.

The following possible solutions to the "process noise" problem (unpredictable random acceleration errors) were considered:

(a) Precise error modeling (second order models).
(b) Adaptive filtering (real time identification of process noise statistics).
(c) Inertial (accelerometer) data.
(d) Types of data insensitive to process noise (optical and radio).

It would be logical to analyze types of data first, although the reasons for this choice are not obvious. For example, consider approach (c). Concurrent studies by the University of Texas have shown that the use of inertial accelerometer data is not feasible unless "precise gyro platform alignment (within 0.01 deg) and very low noise-to-signal ratios (0.07) in the accelerometers are maintained." However, this type of data could still be effective in combination with one or more of the alternative schemes. Furthermore, first-order error models may be sufficient for the first two solutions, and the improvements of various types of data should be studied before more complex software with second-order error models, and adaptive filtering are investigated. Consequently, the fourth proposition was initially selected for further detailed orbit determination studies.

Orbit estimation processes are often characterized by the filter model and the baseline standard deviations assumed. A batch-sequential (discrete sequential filter), square-root filter design was developed to effectively utilize as much of the ballistic batch software as possible. Companion orbit estimation algorithms were constructed with filter models compatible with the error modeling discussed in Volume III, Section II-B-3. Baseline standard deviations for thrust-axis errors were used. These deviations correspond to a configuration for four thrusters assumed operating over the entire 30-day data arc. Assumptions for the baseline values in the cross-axis directions were conservative compared to the model estimates indicated in Section II-B-3 of Volume III. The estimates were representative of worst-case spacecraft designs and amount to nearly 2.0 percent. Assessments of the cross-axis standard deviations of future designs appear to be approximately equal to one half of the baseline values used. However, since one of the primary study-objectives involves a sensitivity analysis, baseline selections can be somewhat arbitrary.

Several tracking strategies, representative of the cruise portion of the mission, were compared. Tracking strategies for the cruise phase consist of using various configurations and operations of earth-based tracking stations, from single-station tracking to multiple-station configurations.

2

However, the actual measurements to be taken by each station still consist of standard doppler and range data. Projected 1980 data-measurement accuracies were taken to be 3 m and 1 mm/sec for two-way range and doppler data, respectively.

Figure IV-B-6 represents a rather complete picture of the final results which are discussed in the following pages. The orbit determination results were not totally unexpected. An 'optimal' filter model (theoretically, the best that can be done) with a multistation configuration, representing a type of combined data consisting of two-way and three-way data processed simultaneously, virtually eliminates the process noise problem. Steady state rms position accuracies are on the order of 35 km. QVLBI is a similar type of data, except that the two-way and three-way data are explicitly differenced. This type of data yields even better values of position accuracy (24 km). On the other hand, if only single-station conventional doppler is used, there is a severe order of magnitude degradation in accuracy. The precise accuracies obtainable from the multistation types of data are not required for cruise in the Encke mission because the ephemeris uncertainty is on the order of 30,000 km before recovery. According to the optimal filter results, single station doppler with range yields accuracies well within Encke's ephemeris uncertainty. A preliminary conclusion would indicate the use of single-station tracking during cruise, and multiple stations during the terminal phase.

However, the optimal filter approach assumed the modeling to be perfect, and this will certainly not be the case. Some indication of the impact of less perfect knowledge on the accuracy can be observed from the batch filter results, which indicate the accuracies when almost the worst model is used instead of the best. The batch filter models only the bias effects. The multistation type of data, QVLBI, degrades 2680 km, while the other data types are orders of magnitude larger. It is through these magnification effects produced by modeling errors that the real advantages of the QVLBI data are realized.

However, in reality, our knowledge of modeling errors is expected to be considerably better, although some uncertainty is expected.

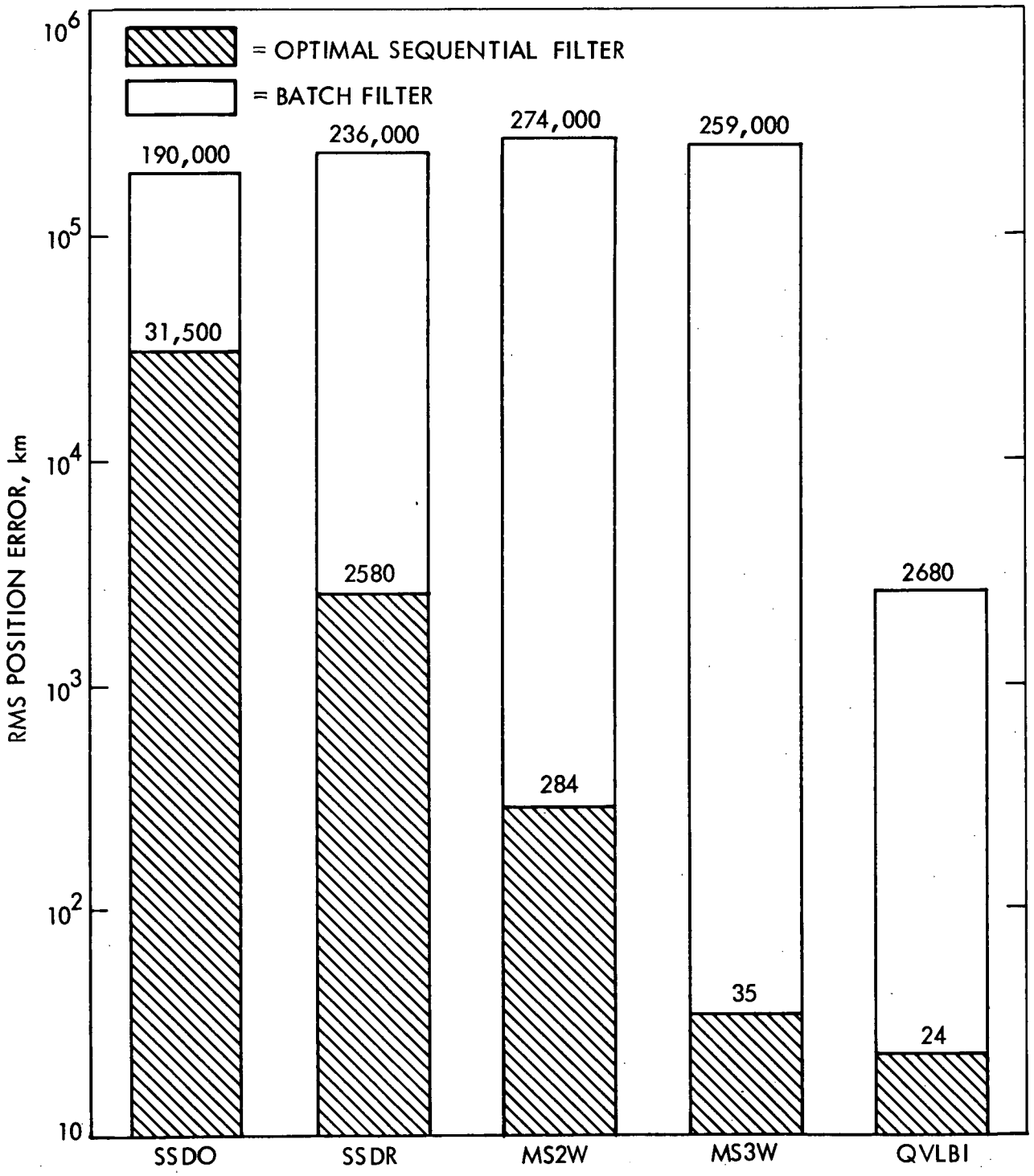

Fig. IV-B-6. Baseline Navigation Performance for Various Tracking Strategies

For example, if needed, second-order models (or other conventional filter techniques) can always be used to reduce model error effects to some degree. Since the worst-case results can be tempered, preliminary conclusions can still be valid, even if model errors degrade optimal accuracies by one order of magnitude.

Realistic answers to these modeling error effects are important to the practical operation of the DSN tracking facilities. Daily tracking with multiple stations for 900 days is unrealistic, but it is feasible over short periods, such as the 60-day terminal phase, when it is really needed. Even this may be an inordinate requirement. However, during the terminal phase, additional optical data, which is also insensitive to process noise, will be available to compensate for the effects of tracking less frequently with the DSN.

However, the more important question to assess is the cruise-tracking DSN duty requirements over approximately 80% of mission time. As mentioned earlier, even with a one order of magnitude degradation in accuracy, cruise tracking can still be accomplished by conventional, single-station techniques. Tracking frequency analysis indicates that a tracking data pass taken only once per week is a reasonable DSN duty cycle to provide the needed cruise-accuracy requirements.

Orbit determination analysis provided several other results, such as the effect of station location errors, SEP thrust-subsystem parameter sensitivity analysis, and rudimentary simulation results to enhance existing knowledge of the realistic impact of imperfect modeling. Sensitivity studies were made to investigate the impact of the optimal filter performance caused by fluctuations in the baseline standard error deviations of the thrust-subsystem parameter error model. The sensitivity studies show that the multistation data, MS3W and QVLBI, are generally less sensitive to baseline changes of the thrust-subsystem error model than other tracking strategies. Of the other strategies, single-station accuracy sensitivities indicate that these types of data are more sensitive to changes in the model error assumptions

related to orientation angles than to changes in the expected errors of the thrust magnitude parameters.

3) Maneuver Strategies. Orbit determination provides the current-state estimate required as input to any control guidance scheme employing any one of a variety of possible maneuver strategies. The control policy will usually depend on the current estimate of the vehicular state and the definition of the performance criteria. Admissible control corrections will in all probability be subject to one or more control constraints. Maneuver strategies employing a feedback control system can either be linear or nonlinear, depending upon the model assumed for the transfer function. A linear system was selected as the initial basis upon which a more general software design can be adapted, if needed.

It is well documented that the low-thrust spacecraft can be navigated, during the cruise portion of the mission, to within Encke's large ephemeris uncertainties. Typically, only a single continuous correction less than 100 m/sec near the midpoint of the cruise phase is sufficient to maintain accuracies well within these ephemeris uncertainties, requiring almost a negligible amount of fuel. However, as the spacecraft nears encounter, the ephemeris uncertainty can suddenly improve after acquisition by the onboard optical sensors; however, the spacecraft may not have enough time to obtain the required orbit correction using only the low-thrust system, and the question of controllability could become critical. In any case, the terminal guidance problem has significantly more impact on the low-thrust navigation design, especially since final rendezvous accuracy will be uniquely determined by the performance of the terminal guidance system.

A linear terminal maneuvering strategy was constructed to study the accuracy limitations associated with terminal guidance. In particular, guidance accuracy sensitivities to the level of the process noise (acceleration errors) can be used as a means of determining thrust-subsystem tolerance limitations on various model parameters. By using both the QVLBI and optical data as the means of performing the orbit estimation, some limiting

steady-state accuracy can be achieved, virtually independent of the level of process noise present. However, the spacecraft can never achieve this accuracy because random acceleration errors continually inhibit its ability to completely make the necessary orbit corrections. Unlike the orbit estimation problem, an increase in the process noise can degrade the terminal accuracies achievable because of an increased guidance inefficiency. As a supplement to this important study, the effectiveness of onboard ranging, as an additional device to improve accuracy, can be evaluated in conjunction with the effects of various approach geometries.

The guidance scheme simulated attempts to control state deviations from a reference path, using at most only three control parameters. The scheme is general enough to consider hardware bounds on the control parameters and weight certain state deviations over others. A control policy is devised to avoid the possibility of controllability problems which characterize many conventional terminal controllers. This new policy requires that the current control effort must minimize the projected terminal errors without regard to future control opportunities, so that every effort is put forth in reducing terminal errors as soon as possible.

For purposes of numerical studies, in particular, the thrust-subsystem sensitivity study, conservative estimates were assumed wherever numerical values were needed. The initial ephemeris uncertainty in the position of Encke was assumed to 30,000 km, a value representative of Encke's ephemeris uncertainty before earth recovery. The velocity uncertainty was on the order of tens of meters per second. In the various studies discussed, the standard deviations of the angle measurement error were taken to be 100 arc sec, 10 and 1 km, respectively. Control bounds of $u_{max} \approx 5^\circ$ (1σ) were imposed to limit the possible thrust vector angle deviations. An acceleration percentage of $\sim$1.8% (four thrusters), spherically distributed, was assumed for a process noise baseline value.

The guidance scheme itself possesses several unique and desirable features which avoid the controllability problems associated with

conventional terminal regulators. As such, a scheme based on these principles is a feasible candidate for a low-thrust guidance breadboard program.

Numerical results presented in Fig. IV-B-7 contain a complete set of parametric data, relating all possible terminal velocity accuracies obtainable to all possible terminal position accuracies obtainable, given a terminal guidance time to rendezvous for several possible choices of weighting factors. Regions of feasible rendezvous and flyby possibilities are superimposed to indicate areas of probable interest. Also superimposed on this data is a locus of points to indicate the relative guidance performance caused by the presence of a certain amount of process noise.

The strategy discussed is the more demanding maneuver of reaching rendezvous accuracies without delay. There are other, less stringent strategies proposed which employ a series of delayed maneuvers, permitting ample time for corrections to be made.

The following preliminary conclusions were reached:

(a) In spite of the large ephemeris uncertainties of Encke, rendezvous is possible if onboard navigation is initiated no later than 40 days prior to nominal encounter.

(b) The reduction of terminal state errors becomes more difficult as the process noise levels are increased (Fig. IV-B-5). At levels above 5% of the nominal thrust acceleration, rendezvous cannot be achieved if terminal navigation begins later than 50 days prior to encounter.

The last important result of this study concerns the design of a feasible navigation system. Optical data contain no range information, so that, in lieu of an onboard ranging device, many previous studies have included an offset bias during the final approach so that range information

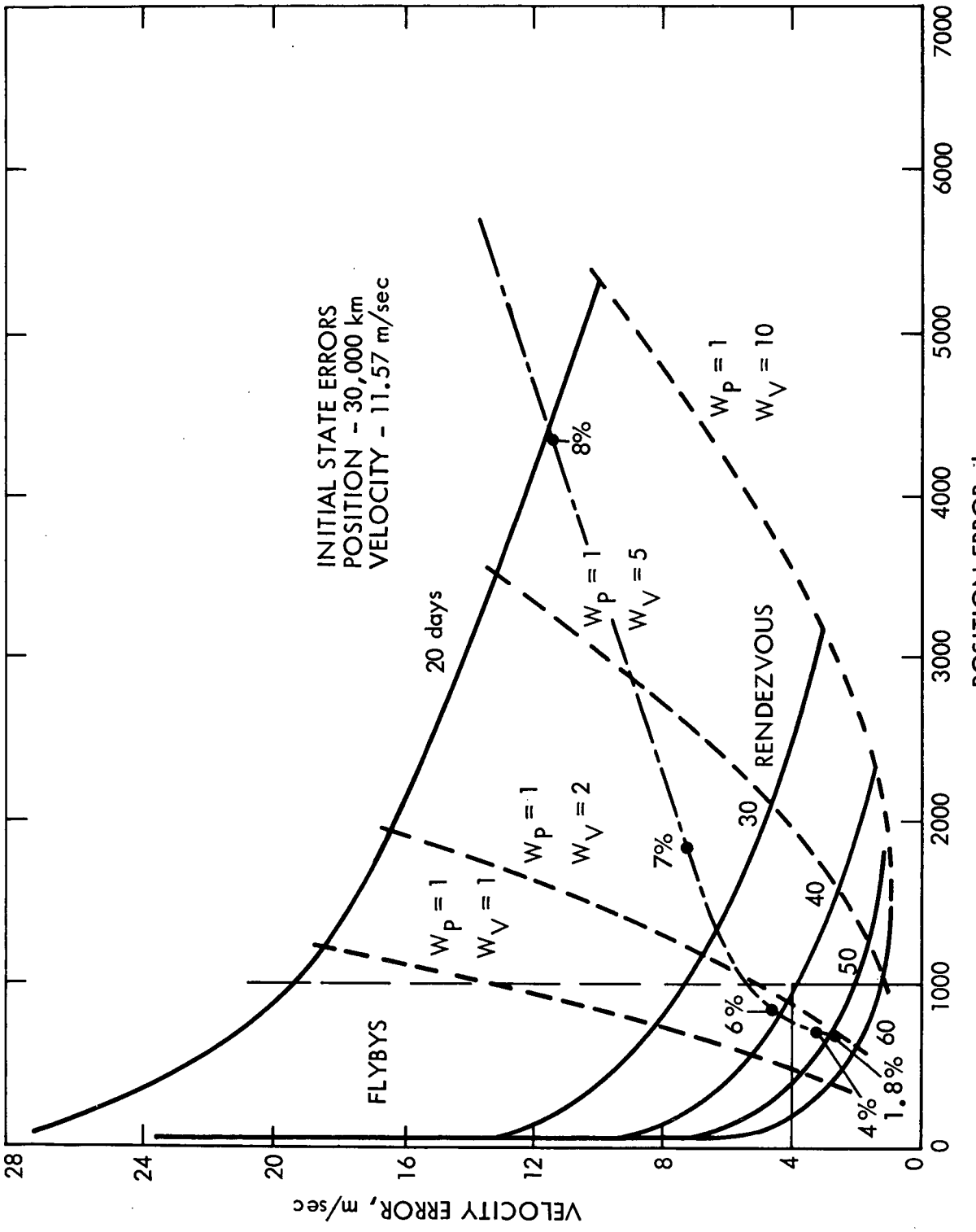

Fig. IV-B-7. The rms Final State Errors versus Flight Time and Weighting Parameters

can be inferred from the optical data. However, this analysis shows that the use of a curved nominal approach trajectory permits orbit determination without relative range measurements and without the use of an artificially imposed bias.

4) Optical Guidance Analysis. The previous analysis was done to develop the necessary maneuver strategies applicable to the terminal rendezvous phase. However, maneuver strategies are only part of an overall guidance system which must execute the maneuvers. For this low-thrust mission, the chief design problem critical to successful execution of the corrective maneuvers is the onboard optical system. Therefore, a guidance study was performed to investigate potential problem areas.

To begin with, a candidate optical system must be able to see the comet before executing any terminal maneuvers. In addition, guidance considerations fix a lower bound on the time to execute the maneuvers, given a certain level of process noise. On the other hand, the earlier the comet can be detected, the less stringent the requirements on thruster-subsystem tolerances and guidance effort. For example, the terminal maneuver analysis indicates that, if the comet can be detected before encounter time minus fifty days (E-50 days), a 5% level of process noise is still acceptable for a successful mission. With these design tradeoffs in mind, it is easy to see the importance of an optical sensor analysis.

The only real data available on the performance of an imaging system are the experimentally derived detectability data for the Mariner B (telephoto) camera. The source of the data was the Mariner Mars 71 optical navigation demonstration (OND). Everything else is pure hypothesis. However, the impact of various hypotheses can be assessed by synthesizing the postulated photometric characteristics of the comet in terms of Mariner camera nominal parameters.

More specifically, the fundamental approach used in the optics analysis for guidance was to combine the suggested comet brightness models and integrated photometric data with the experimentally derived detectability data.

For a 100% confidence level, a star detectivity threshold of 7.5^{m} was used as the reference for visual magnitude comparisons, with integrated surface brightness assumed to be imaged over a single picture element. In this manner, different surface brightness models can be compared to assess the impact of imprecise comet photometric knowledge on the design of a practical optics system.

Basically, magnitude curves for the brightness of the pertinent components of the comet model are generated as a function of comet geocentric distance with time to encounter. Given a set of optical parameters, nominal integration times can be determined for both point source and central halo radii of 100 km to 2500 km, respectively. Nominal recovery is assumed to occur at E-60 days to account for uncertainties in the photometric model.

The results are most significant. If an ample margin of integration time is designed into the optics system to allow for brightness variations (exposure time or shutter speed), optical recovery can be made as early as E-60 days regardless of whether the comet appears as a point source or an extended source. When factors are weighted toward the extended source models, then the design margin on the integration time amounts to about 11 sec on the average. The extra integration time amounts to an additional 20%, but it provides for a detectability range in terms of visual magnitude of 2 about a reference of 7.5^{m}. If the probable uncertainty in visual magnitude is assumed to be larger, longer integration times should be designed into the system.

In addition, these results were found to hold true for a range of Mariner camera designs, from a maximum sensitivity design, having a focal length of 150 mm (aperture diameter was assumed to be 20 cm), to a much less sensitive design having a focal length of 400 mm.

3. SEP Mission Risk-factor Analysis

A quantitative analysis of risk assessment for a SEP mission was made. The main area of concern is the uncertainties associated with thruster

performance, such as a limited thruster life and the frequency of thrust-subsystem component failures. In a power-varying, continuous-thrust mode, the characteristics of the failure modes and their impact on the mission goal are considerably different from those of a ballistic mission. These characteristics present a new, complex problem unique to low-thrust missions.

In this study, development of a method to predict the probability of success of a given mission was emphasized. The method devised and the results derived from it can serve as a tool to identify key risk factors in a mission, both in hardware and trajectory design, thus contributing to the design of an optimal, low-risk, SEP mission. In this analysis, the method was applied to a 1980 Encke rendezvous mission.

To assess mission risk, the profile of the operational sequence of the proposed mission must be understood. To execute a thrust program using a given thrust subsystem, an operational policy is applied to decide which thrusters will be used at each phase of the mission. Once this operational profile is determined, probable thruster failure events may be simulated, their probabilities of occurrence predicted, and their impact on the mission goal evaluated. The probabilities of thruster failure are computed using a thruster-reliability model. As a result of thruster failure, one of the following three operations may occur: (a) abort the mission, (b) continue on the nominal trajectory with a revised operational profile, or (c) change the path (i.e., the thrust program) and the operational profile. Because of difficulty in generating low-thrust trajectories, the usual Monte Carlo (failure + retarget) procedure was avoided. Instead, a "tree" of failure effects was constructed by investigating the effects of various failures at chronologically ordered, finite failure-points, which can be used to represent approximately any failure occurring between the investigated points.

Fig. IV-B-8 shows the pertinent risk factors and their relationship to the assessed risk.

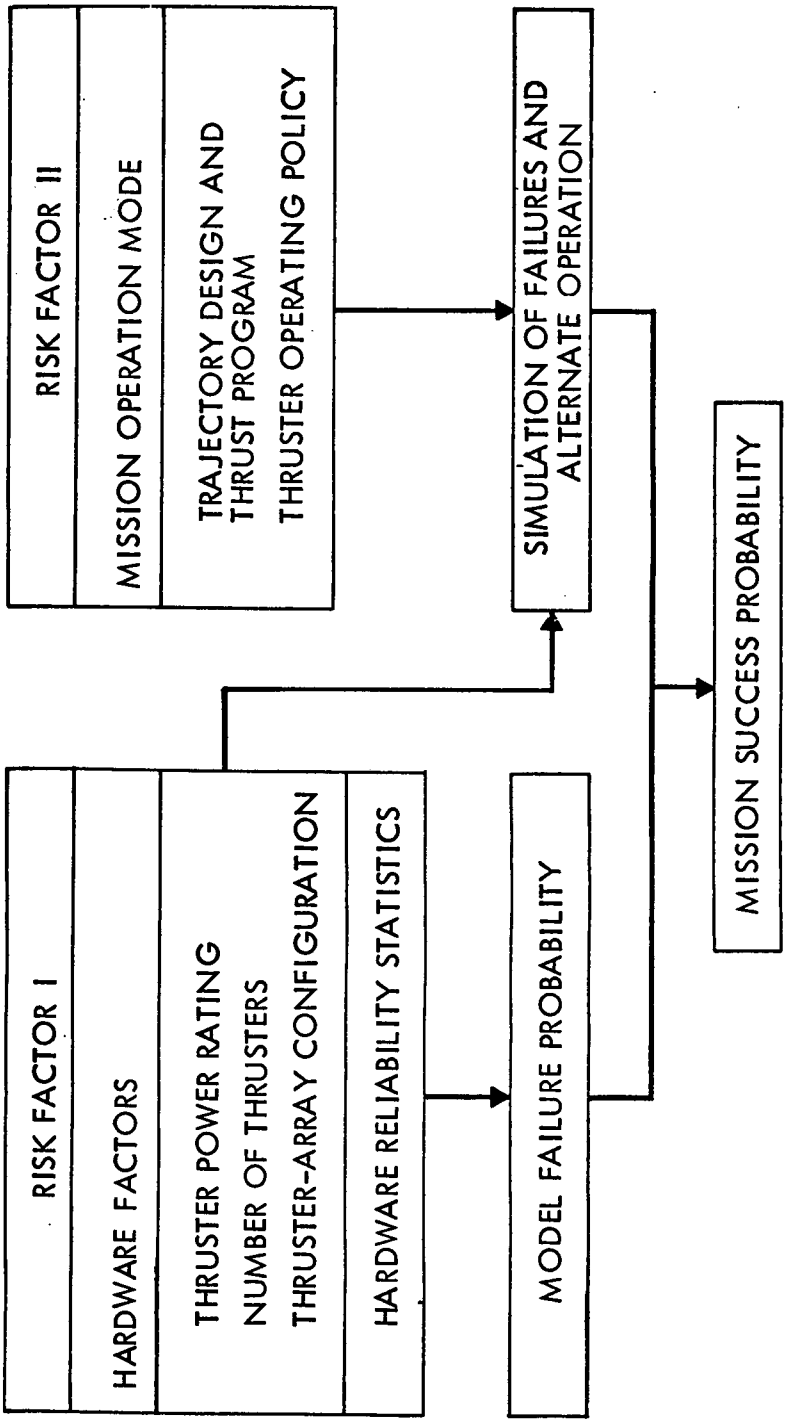

Fig. IV-B-8. Risk Factors

A range of thruster failure data was assumed and the risks for a 16.6-kW 1980 Encke rendezvous mission were estimated. The results were then analyzed in terms of the different risk factors considered.

Two classes of mission objectives were defined.

(a) Class I, the selected mission mode. In this mode, rendezvous with Encke occurs at the desired rendezvous time of -47 days to time of perihelion (T_P).

(b) Class II, a degraded but acceptable rendezvous mode. Herein, the mission goals are considered attained, if the spacecraft can achieve rendezvous with Encke any time before -27 days to T_P.

a. Hardware Factors and Risk

(1) If 2.8-kW (30-cm) thrusters are used, if thruster life is 400 days or longer, and if failure rate for the thrust-subsystem components is $20/(10^6$ hr) or less, then a seven-thruster system assures a 95 percent or better chance of mission success.

(2) The limiting factor in attaining a higher reliability, as well as the need for a seventh thruster in this mission, is due to the quoted high, steady, component-failure rate.

b. Trajectory Design Factor

(1) A significant difference in predicted risk was noted between the two classes of mission objectives as defined above. A mission design allowing a 20-day encounter margin, as in a class II mission, appears to compensate effectively the risks caused by the failures of the components. This fact indicates that a careful

trajectory design with risk consideration (such as designed coast phase, earlier encounter time, etc.) may prove to be more effective than additional redundant hardware in compensating for uncertain hardware performance.

c. Effects of Thruster Operating Policy

The main characteristics of the power profile in the Encke mission are its long duration (~1000 days) and wide variation of power levels (higher at the beginning and during the terminal phase of the mission). To match such a power profile using thrusters with finite lifetime, a policy whereby the load of burn on each thruster is equally distributed assures a better chance of mission success because it mathematically simulates maximum reliability. However, when as many as seven thrusters are recommended (because of the higher failure rates), a policy whereby thrusters are replaced only when the failures occur does not seem to affect the success probability significantly.

REFERENCES

IV-B-1. William G. Breckenridge and Thomas C. Duxbury, "Defining a Spacecraft-Based Navigation System", Astronautics and Aeronautics, pp. 44 to 49, May 1970.

C. SEP MODULE THRUST SUBSYSTEM STUDIES

1. Power Conditioner Study

This study was conducted to assess the applicability of SEPST III type of PC (Ref. IV-C-1) to a 1980 Encke rendezvous mission using the JPL proposed SEP module attached to a Viking based spacecraft, and, if necessary, to recommend modifications for that mission application. Because the Encke rendezvous mission provides the most severe environmental and performance requirements of all proposed SEP missions, the PC design recommendations which emerge should be an appropriate basis for PC design for any foreseeable SEP mission.

A functional block diagram of the selected electrical design (shown in Fig. IV-C-1) closely follows the SEPST III design concept. The major deviations proposed for the SEPSIT design are (a) to raise the input voltage from a range of 53 to 80 V to a range of 200 to 400 V, (Section IV-D-1), (b) to modify the output characteristics to accommodate the LeRC 30-cm thruster design, (c) to raise the power-transistor junction temperature from 55 to 110°C, and (d) to modify circuit designs, cabling, and circuit locations to minimize electromagnetic interference (EMI) effects. The packaging design departs from the SEPST III design because: (a) the preferred electrical design differs from that of the SEPST III units in both total power output (and resulting dissipated power) and maximum allowable power-transistor junction temperatures; (b) recent dynamic tests of the SEPST III units (Ref. IV-C-2) indicate that the design was inadequate to survive expected launch loads; and (c) heater power required to maintain dormant PCs at minimum design temperatures was deemed excessive for past SEP module/PC integration schemes.

Figure IV-C-2 illustrates the proposed SEP module/PC integration scheme. The six PCs required for the Encke rendezvous mission are shown with variable-emittance louver assemblies attached, mounted back-to-back with their shearplates perpendicular to the solar-array axis of rotation. By maintaining an angle of 90 deg between this axis and the sun-space vehicle line, direct solar illumination of the louvered PC surfaces is avoided.

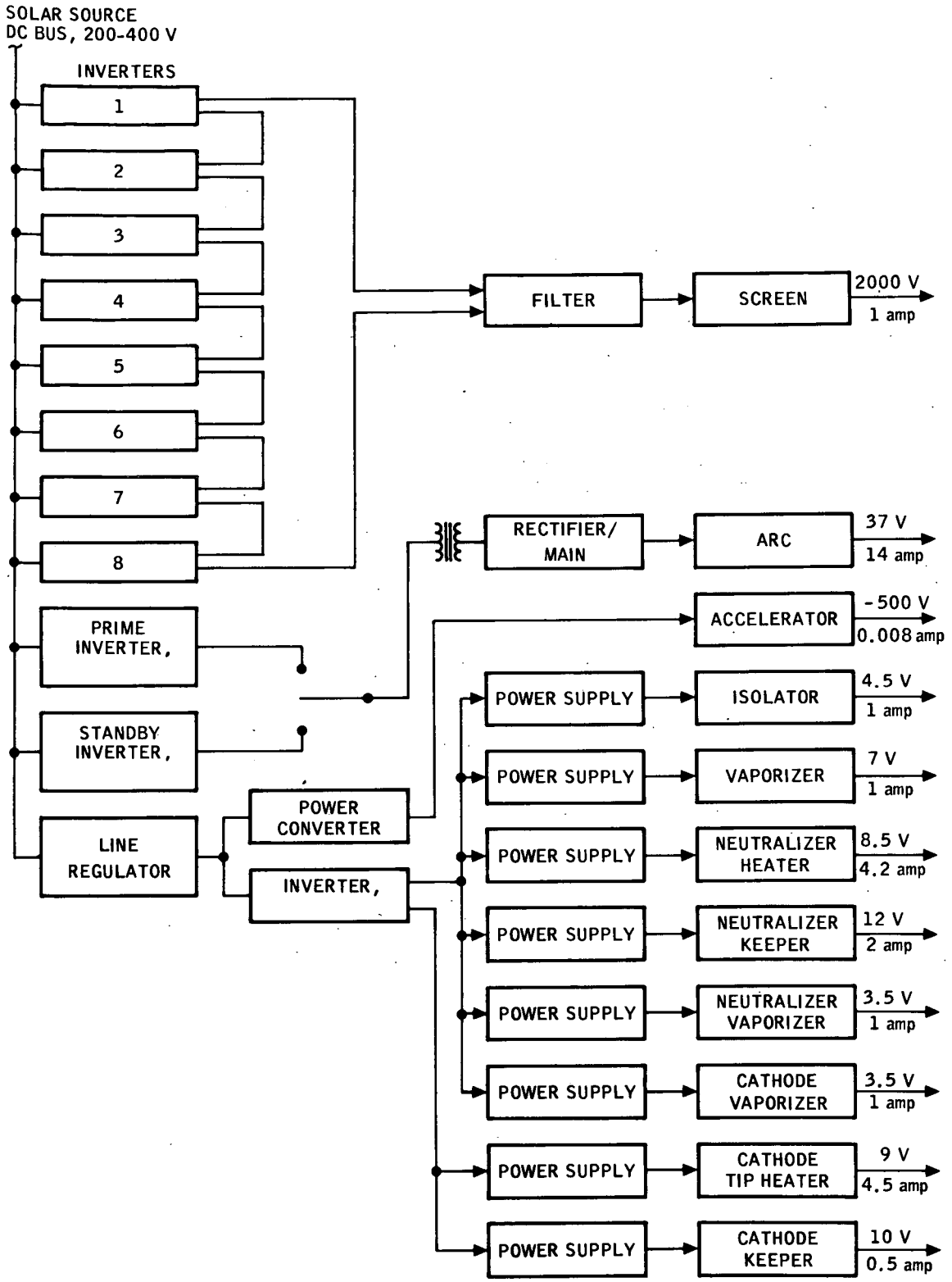

Fig. IV-C-1. Selected PC Functional Block Diagram

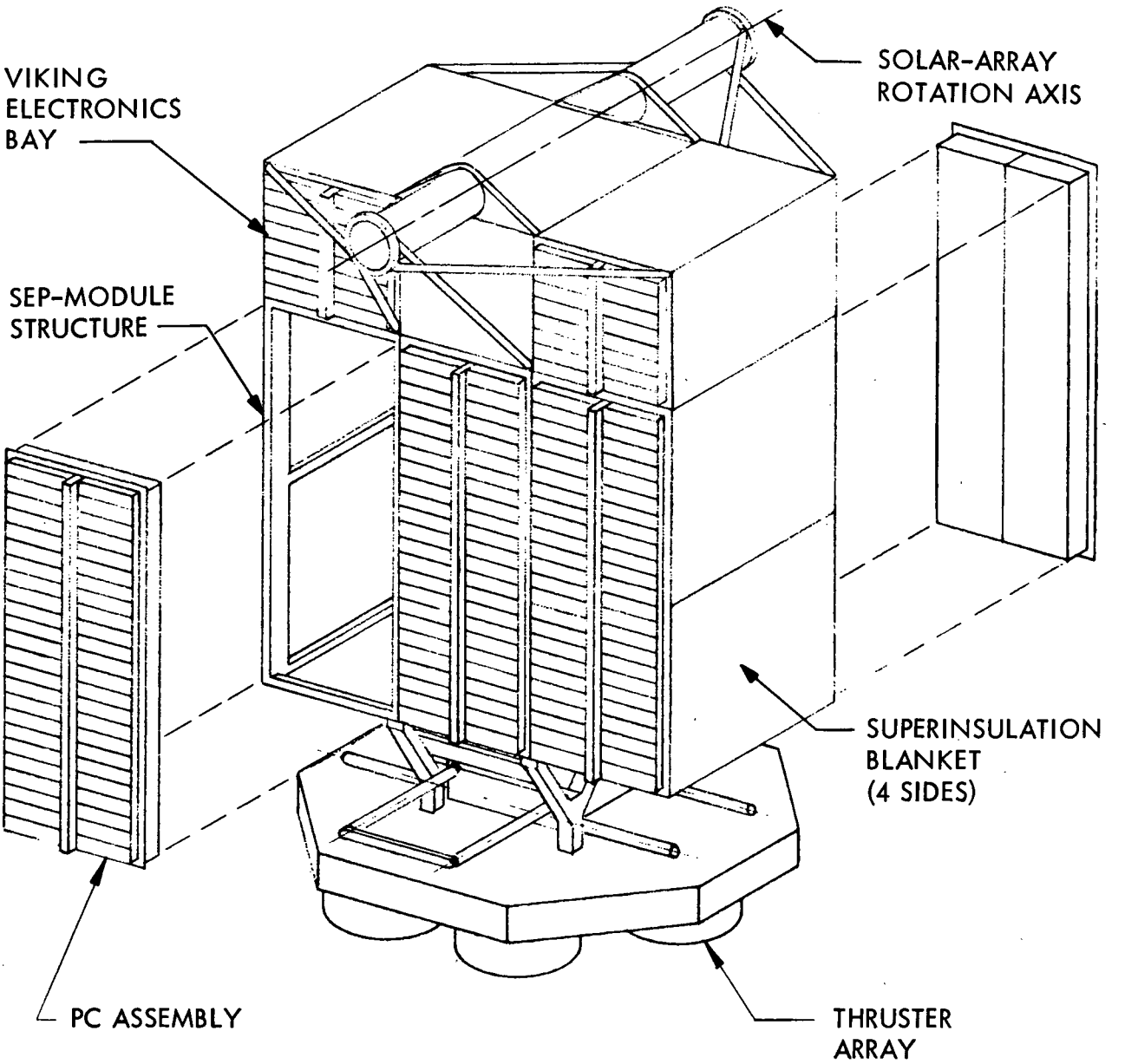

Fig. IV-C-2. PC Assembly within the SEP Module

The proposed PC configuration utilizes the SEPST III flat-pack design concept for high-power dissipation modules, in which components are mounted directly to radiator/shearplate modules mounted, in turn, to the PC chassis. Individual modules are mounted from the rear of the PC chassis to allow module removal for post-assembly repairs without requiring removal of the delicate louver assembly. The two-module width provides compatibility with SEPST III module component layouts. Module rows are separated by a cabling support on which are mounted individual module plug-in connectors and the primary PC input and output connectors. Figure IV-C-3 shows some of the details of two opposing PCs.

As a result of this study, it became apparent that a PC concept which employs a modular integrated-electronic-packaging/structure approach is not only feasible but provides significant weight and operational improvements over the SEPST III design. In addition to being influenced by the electrical requirements of providing voltages, currents, and closed-loop control of a thruster, the PC design is strongly influenced by thermal and structural interfaces with the remainder of the space vehicle. Although the preferred design size, which has emerged, is specifically suited to a JPL SEP module for Encke rendezvous application, the design concept and criteria, which it reflects, are considered appropriate for all foreseen applications. With this in mind, the following preliminary design requirements for a thruster PC are offered:

(a) The PC should operate over an input voltage range of 200 to 400 V using high-voltage transistors* in the screen power supplies.

(b) Output characteristics should be compatible with the LeRC 30-cm thruster.

(c) Reverse currents should not be imposed on the solar-array bus.

(d) To allow for maximum solar-array power utilization, the input current ripple should be limited to 1% of peak-to-peak

*The merits of silicon-controlled-rectifier (SCR) power circuitry should be investigated as more data becomes available.

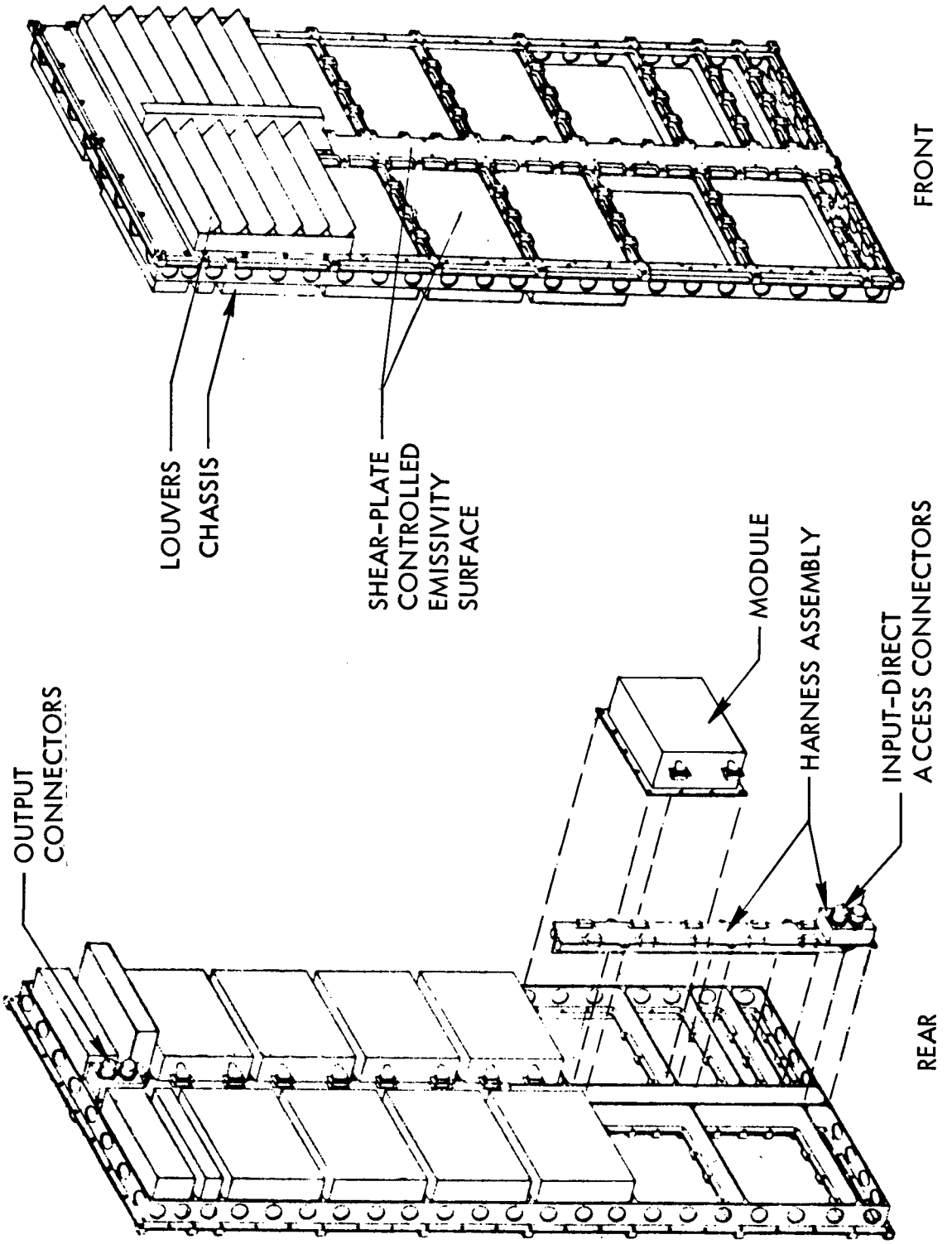

Fig. IV-C-3. Detailed View of Two Opposing PCs within the SEP Module

value of the operating current under all conditions including transients.

(e) The circuit design will provide required voltages and currents within specification for operation at shearplate/radiator temperatures between +75°C and 0°C and will be capable of startup at -20°C and of surviving in a dormant state at -40°C.

(f) The power transistor junction temperature will not exceed 110°C operating at maximum power with a 75°C shearplate/radiator temperature.

(g) All electrical parts, packaging parts, and materials used in the PC will be properly derated to meet reliability requirements while operating within the specified temperature range.

(h) Effective EMI protection and suppression techniques should be considered and included in the design.

(i) Cable routing lengths should be minimized by proper connector placement, application of power-flow concept to module placement, and connector assignments.

(j) Provisions for cable routing and support will be included in the structure design.

(k) Input and output connectors should be located to minimize cable lengths within the SEP module.

(l) The PC structure will be designed for a minimum resonant frequency of 200 Hz.

(m) The module shearplate/radiator surface shall carry in-plane shearloads and provide meteorite protection.

(n) The PC structure will provide a mounting surface and interface attachment for a specified louver assembly to cover at least 80% of the surface area.

(o) The minimum area for the PC shearplate/radiator surface will be 6451.60 cm^2 (1000 $in.^2$) and have an integrated surface emittance greater than .85.

(p) The assembly will be packaged with electronic functional, removable, and replaceable modules. The flatpack planar approach is recommended for high power dissipators, and

approved efficient techniques must be used to minimize shearplate/radiator area for low dissipation modules.

(q) High-voltage cabling design shall meet requirements of JPL specifications*.

(r) The PC will be installed as a complete assembly with only mechanical fasteners and connector mating required.

(s) Preliminary analyses indicates that the selected PC should be packaged within a 50.80 x 139.7-cm (20 x 55-in.) rectangular frame.

2. Switching Matrix Tradeoff Study

This study examines alternate methods of connecting PCs to thrusters in the context of a 1980 Encke rendezvous mission. The objective of the study is to select the preferred connection method. Probability of mission success and SEP thrust subsystem mass are key factors in the selection process.

Three methods of connecting PCs to thrusters were investigated; hard wiring, complete switching, and partial switching. The complete switching approach permits the connecting of any PC to any thruster and is accomplished with a rotary multiposition switch for each PC. In the partial switching approach, only designated spare thrusters are connected to any PC. A switch, in this case, will have one position more than the number of spare thrusters, i.e., one position will connect a PC to its normally assigned thruster, the second position will connect a PC to the spare thruster.

In the study, partial and complete switching between PCs and thrusters was investigated for the following combinations: five PCs/six thrusters (one spare thruster), five PCs/seven thrusters (two spare thrusters), six PCs/seven thrusters (two spare thrusters and one spare PC). Hard-wired systems involving five, six and seven PCs and thrusters were also studied.

*JPL Specification DM505139 (a JPL internal document).

The Encke mission requires that the thrust subsystem provide thrust during the entire mission for a trajectory which extends from earth to 3.3 AU and which returns to 1.0 AU for rendezvous with the comet. At the beginning of the mission, the solar-array power available is sufficient to operate five 3.1-kW, 30-cm thrusters. As the solar-array power output decays, throttling of the thrusters is required, and thrusters are shut down as necessary. The reverse process is employed during the inbound portion of the mission.

The tradeoffs were performed by examining the mission reliability for each of the thrust-subsystem designs with different switching. A Monte Carlo analysis with 5000 simulations per data point was used as the basis for this reliability analysis.

The failure rates of the components considered in the study have been derived from data and information available from manufacturers, experts in the field, and from JPL component-part failure rates based on previous spacecraft experience. Because the data obtained are only best estimates, all the important failure-rate parameters were varied to some extent to determine their effect on the mission reliability.

Both random failure and wear-out failure modes were considered for the thrusters. At present, there is insufficient test data to obtain good estimates for either. Estimates of wear-out life by experts in the field indicate that, by proper grid and cathode design, a 30-cm thruster can be fabricated with a mean wear-out life of at least 14,000 hr and possibly up to 20,000 hr. In this study, two thruster-wear-out curves were used to temper these estimates with currently planned thruster lifetime goals. One curve shows wear-out starting after 6000 hr with a mean wear-out life of about 10,000 hr (early wear-out); the other wear-out model has wear-out starting after 8000 hr with a mean life of about 12,000 hr (late wear-out). The random failure rate was varied between $1/10^6$ hr to $50/10^6$ hr. It was assumed that the PCs have random failure modes only. A failure rate of $5/10^6$ hr were also examined to determine the effect of this parameter on mission reliability. An 0.1-dormancy factor was used for the PCs.

The rotary-switch failure rate was estimated at $20/10^6$ hr for the complete switch with seven thruster-contact positions per switch. For the switch with three positions capable of connecting two spare thrusters to any PC, an estimate for the failure rate was $11/10^6$ hr. For the switch with two positions capable of connecting one spare thruster to any PC, a failure rate of $3/10^6$ hr was computed.

Three switch failure modes were considered:

(a) A "stuck-at" failure, when a PC remains connected to a particular thruster and can not be switched to any other thruster. This could occur, for example, if the switch motor failed.

(b) An "open" failure, when a contact to one of the thrusters has opened, thus preventing the PC from operating that particular thruster. This could occur because a wire or contact is broken or because a switch terminal is contaminated.

(c) A "complete" failure, when the PC assigned to the switch can not be switched to any thruster; it is totally disabled. This failure mode is equivalent to a PC-failure, and it could occur, for example, if one of the switch wafers should crack.

The probability that any of the above failures can occur is based on test data and previous experience with rotary switches. From the information available, the following conditional probabilities apply:

(a) "Stuck at" failure, 0.35.

(b) "Open" failure, 0.5.

(c) "Complete" failure, 0.15.

Two definitions of mission success were considered. A class I success is obtained when the spacecraft follows a trajectory which rendezvous with the comet at least 40 days before Encke perihelion. A class II success is a slightly degraded success in which rendezvous occurs at least 27 days before

Encke perihelion. The latter was used as the basis for most of this study. Thus, the reliability analysis gives a probability of obtaining at least a class II success.

Mission reliability was computed for all the configurations under study, and the results were plotted. A typical example is shown in Fig. IV-C-4. The results show that:

(a) The combination of six PCs connected to seven thrusters by the complete switching method is the most reliable of the combinations studied, regardless of the wear-out and random failures of the thrusters.

(b) Of all cases considered, the system with the minimum mission reliability is that of four PCs hard-wired to four thrusters. This was true for all failure rates examined.

(c) The reliability of thruster-failure rates greater than $20/10^6$ hr is unacceptable, especially if the thruster mean-lifetime is not greater than 10,000 hr.

(d) Increasing the random failure rate of the PCs from $5/10^6$ hr to $10/10^6$ hr has no effect on the selection of the switching approach.

(e) The complete switching cases were superior to hard-wired cases and to equivalent limited switching cases (same number of thrusters), except as noted in (f) below.

(f) For the five-PC, seven-thruster system, the complete switching method becomes more reliable than the limited switching method as the thruster failure rate increases. At very low thruster failure rates, the limited switching is the more reliable. The crossover point depends on the thruster wear-out parameter, but it usually occurs when the thruster failure rate is between $1/10^6$ hr and $6/10^6$ hr.

When thrusters are more reliable, with a random failure rate of $6/10^6$ hr with late wear-out and a mean life at 12,000 hr, then the five PCs connected to seven thrusters via the limited

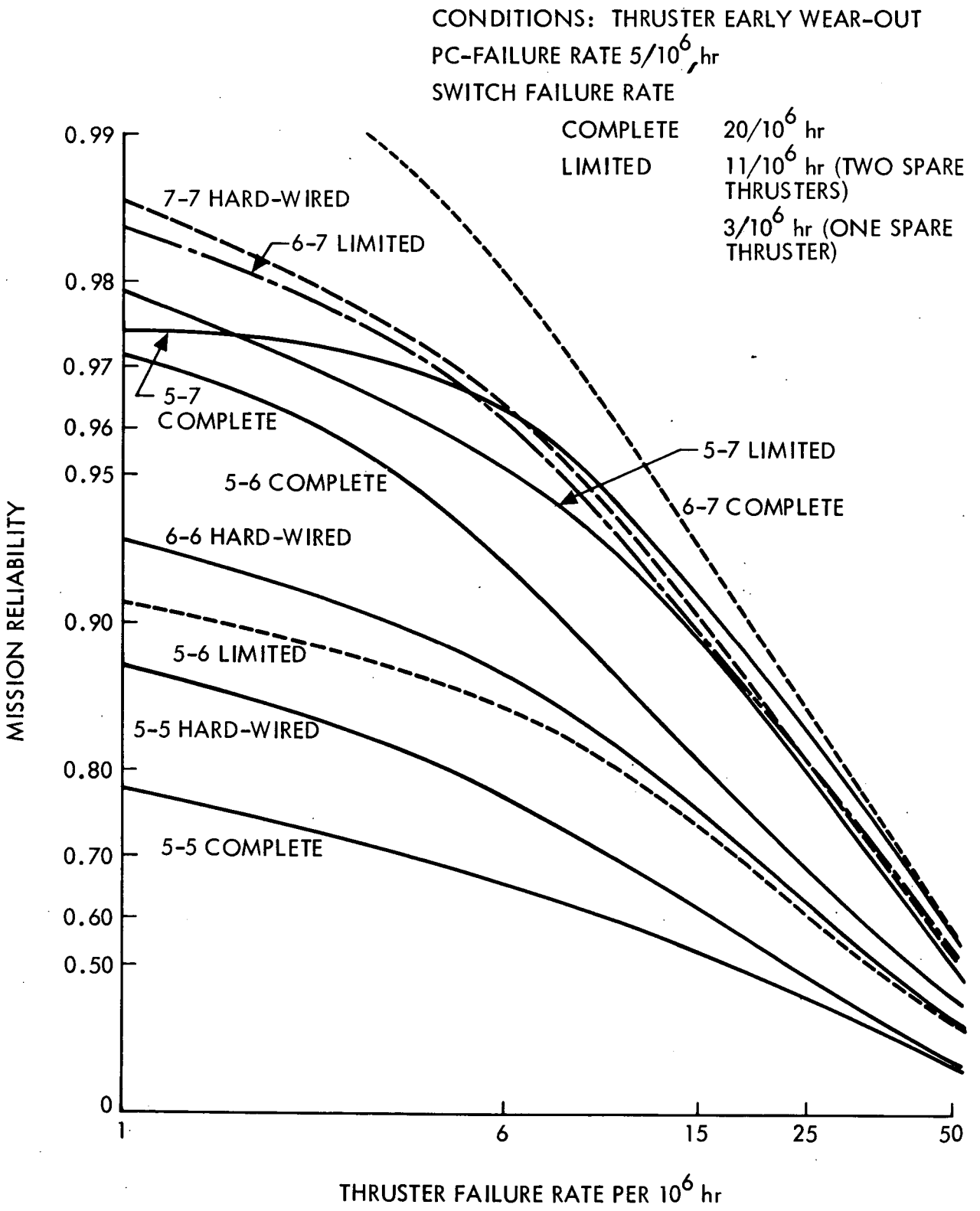

Fig. IV-C-4. Encke Comet Mission Reliability versus Thruster Failure Rate, Monte Carlo Simulation, Case 1

switching method is more reliable than the complete switching connection method; this is because the higher switch failure rate for the complete switch connection begins to influence the reliability. On the other hand, with a thruster random failure rate higher than $1.5/10^6$ hr and early wear-out, or with a thruster random failure rate higher than $6/10^6$ hr and late wear-out, complete switching connection of the five PCs to the seven thrusters is more reliable than limited switching. Complete switching is also more reliable under these circumstances than seven PCs hard-wired to seven thrusters. These results are not surprising because the connection flexibility offered by complete switching becomes more advantageous as thrusters fail more frequently.

(g) Variations in the switch failure rate do not have a significant effect on the selection of the best switching approach, as long as the same ratio between the failure rates for the complete and for the limited switching is maintained. The plots move up or down as the ratio of the failure rate decreases or increases about the estimated value. There is no major change on the crossover points, particularly those of the five-PC/seven-thruster complete switching connections and the five-PC/seven-thruster limited switching connections.

(h) In addition to the switch tradeoff, the results also show the effect of various thrust subsystems on mission reliability, and from this, an acceptable thruster-failure rate can be allocated.

(i) In limited switching systems, the choice of which thruster(s) should be the spare(s) is an important, but not always obvious, decision. As a typical example, the 6 to 7 case was computed using two different choices for the spare thruster. Differences in reliability which appeared were caused by symmetry requirements necessary for attitude control.

Individual component weights were calculated for each element of the system. Using these weights and the computed mission reliability data, mission reliability versus subsystem weight was plotted. Figure IV-C-5 shows the results when a thruster random-failure rate of $6/10^6$ and a mean life of 10,000 hr was assumed. The following comments can be made about this data:

(a) Mission reliability increases with weight (additional spare units). However, those cases which are not on the increasing reliability line do not follow this rule and are not recommended for the thrust subsystem.

(b) In most cases, the complete connection method improved the mission reliability.

(c) These weight curves will be used mainly as a tool for the spacecraft designer in deciding the thrust-subsystem configuration for the mission, and in weight tradeoffs for increased reliability. The weight difference between the lightest and heaviest configuration studied is approximately more than 45 kg (100 lb).

From the results of computed mission simulations and the results of the weight tradeoff, it is apparent that some kind of switching adds to the mission reliability.

For the Encke rendezvous mission, the complete switching connection method has advantages over the limited switching connection, as is evident in the mission reliability data for the following cases:

(a) Six PC to seven thrusters for all thruster failure conditions.

(b) Five PCs to seven thrusters for all thruster failure conditions except when they are very good; i.e., they have very late wear-out and low random-failure rate.

Based on this data, it is recommended that complete switching connections be used for the Encke mission. Higher reliability was obtained

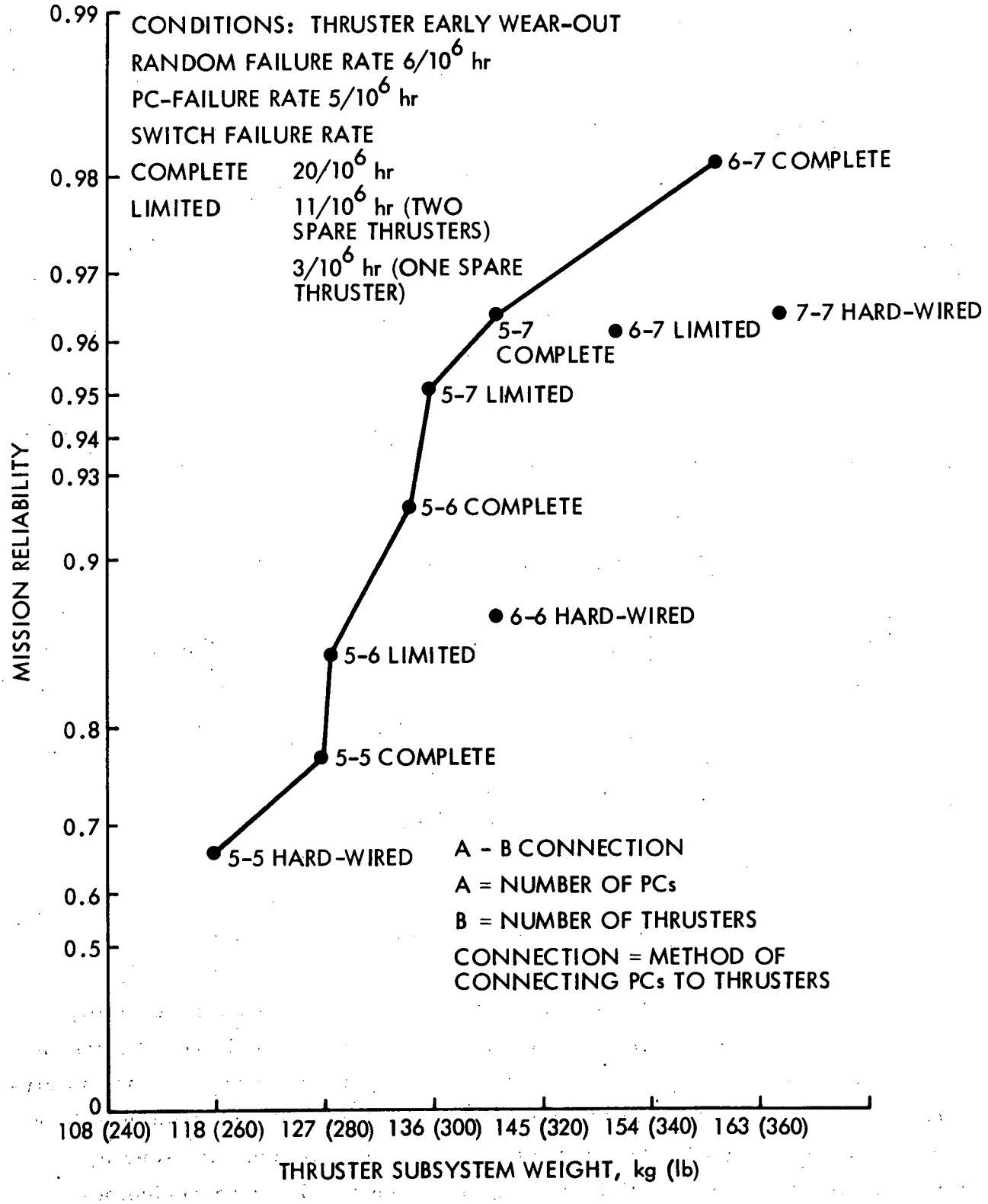

Fig. IV-C-5. Encke Comet Mission Reliability versus Thrust-subsystem Weight

with a relatively low weight penalty. The flexibility of operating any PC with any thruster, provided by complete switching connections, can also conveniently be used to locate trouble in the thrust subsystem during ground operations and even in flight.

3. Switching Matrix Development Analysis

A design review of the SEPST III switch indicated that an improved design, incorporating two features, was needed to meet thrust subsystem requirements. First, a new switch design, providing improved high voltage/high current capability at reduced weight and volume, was proposed. Secondly, the integration of the proposed switch into a matrix assembly, providing switch mounting, common output connection, and clean structural and mechanical interfaces, was proposed. This section describes the development of these designs.

The SEPST III switch is a hermetically sealed, conventional two-circuit per deck, wafer switch. This unit has a variety of mechanical alignment, electrical, size, and weight problems. The new design overcomes these problems and takes advantages of some rather unusual constraints, as follows:

(a) The required voltages can be conveniently arranged into four high and low voltage groups.
(b) Switching is done with no load applied.
(c) A low number of cycles are required.
(d) Reduction in weight is second only to reliability in importance.
(e) Repair or replacement capability is desired.

Figure IV-C-6 shows details of the proposed switch assembly. High-voltage circuits are grouped on one wafer pair, low-voltage circuits on another wafer pair, and the -1000 V accelerator and position information circuits on a "half" wafer. Encapsulation of the wafers and insulation barriers provide improved high-voltage capability. Switching is accomplished by stepping the rotor through eight 45-deg increments. Short rotor-jumper

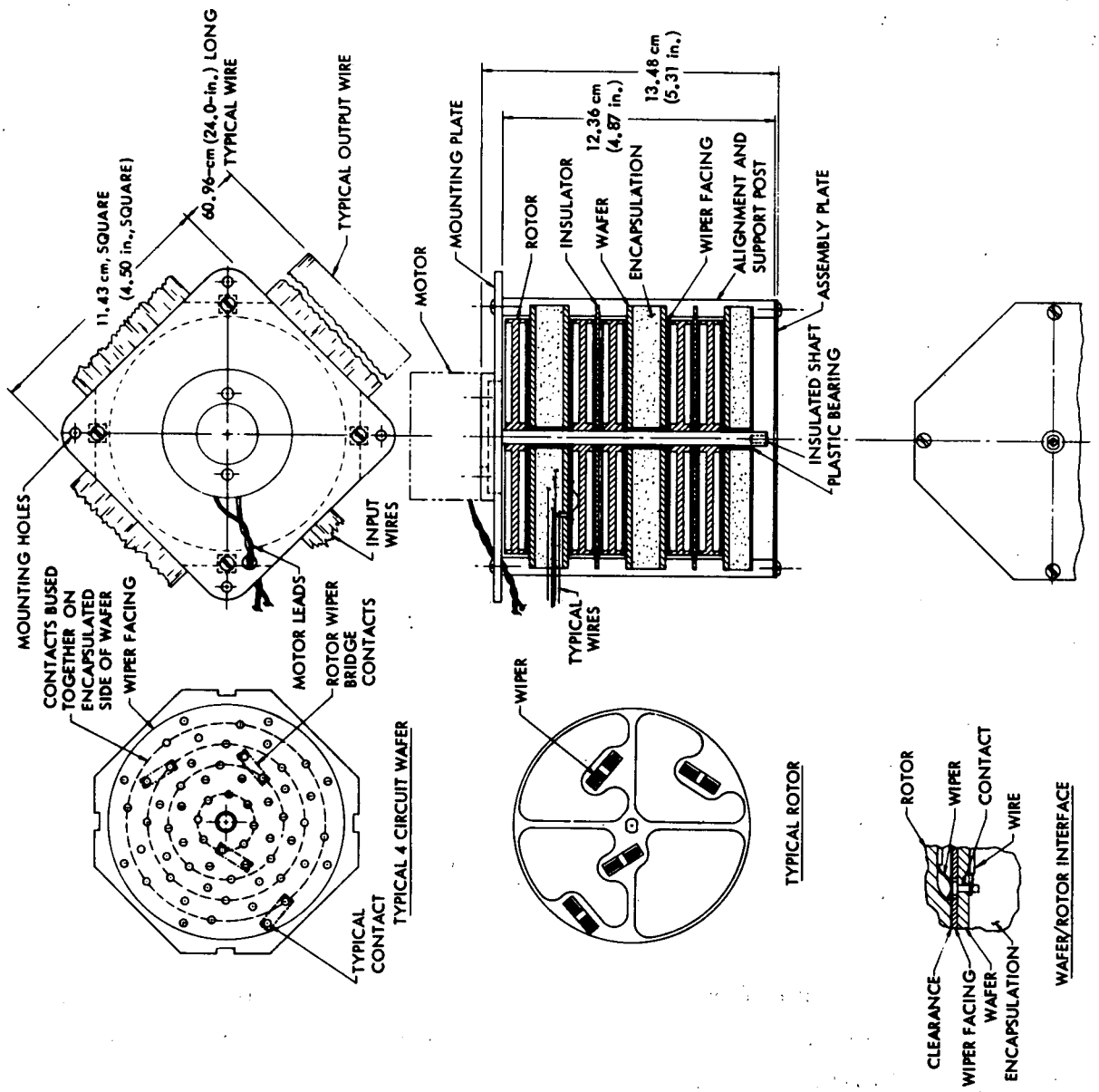

Fig. IV-C-6. Rotary Stepping Switch

contacts bridge between bused input contacts and the output contacts. Design of the wafer/rotor interface and design of the high voltage/high current contact are important technological items in the development of this switch.

To demonstrate this design, it was proposed that the mounting plate for alignments of support posts and at least one wafer pair with its associated contacts and wipers be fabricated as an engineering model. The contact resistances, especially under high-current conditions, the torque required to rotate the switch, high-voltage-withstanding capability, and the estimated life can be obtained from tests of this model. Based on the torque requirement, the appropriate motor can then be sized and obtained for the switch. With this configuration, the weight can be estimated, and the packaging techniques evaluated for assembling and connecting six of the required switches. Tests would be made at sea-level pressures and at high-vacuum conditions to assure that effective leakdown of trapped air would occur to prevent operation of the switch in the critical pressure region.

The SEPST III switch gear was connected to terminal boards near system interfaces, which resulted in long wire runs, "daisy-chain" jumpers, potential high-voltage breakdown, and minimal EMI protection. The incorporation of the proposed switches into a switching matrix assembly would offer substantially improved capabilities, as follows:

(a) A standard switch-mounting interface.
(b) Support for input/output wiring.
(c) Clean electrical and mechanical interfaces.
(d) Dust and contamination protection.
(e) An effective EMI enclosure.
(f) A method for connecting the various switch outputs to the identical output of the other switches and to the thruster inputs.
(g) Ease of access for installation, maintenance, repair and/or replacement.

(h) Suitable high-voltage protection in accordance with specifications*.

(i) Minimal weight and volume.

The switching of six PCs to any of seven thrusters requires connecting 672 switch outputs to 112 thruster inputs, for a total of 784 wires to be spliced. These circuits need to be grouped and routed by voltage and thruster assignment and should be designed to facilitate assembly, installation, repair, and replacement.

A conceptual sketch of the proposed assembly is shown in Fig. IV-C-7. Six switches are mounted in a chassis approximately 18 x 45 x 55 cm. The assembly is not hermetically sealed. Suitable RF gaskets for penetrations and special finishes on mounting surfaces are provided for EMI protection. Three switches are mounted at each end close to the associated PC-input connectors. The in-line arrangement permits the assembly width to increase, if additional switches are to be incorporated. Switch outputs are cabled and routed to the connection matrix located in the center. Outputs from the matrix go to high and low voltage connectors mounted on opposite side walls.

Three design approaches were considered for the connection matrix. The first uses a stack of laminated bus boards with special high-voltage/high-current contacts along the edges. The second approach uses a commercially available crimp contact plugged into individually insulated bus-blocks. The third approach uses a new design for a crimp-splice retention device which has the potential for substantial weight savings. Engineering models of these three approaches would be tested in conjunction with the rotary-switch model to evaluate circuit resistance, high-voltage capability, matrix weight, and to make assembly design tradeoffs.

The following conclusion can be drawn from the design analysis described above:

*JPL Design Specification DM505139 (a JPL internal document).

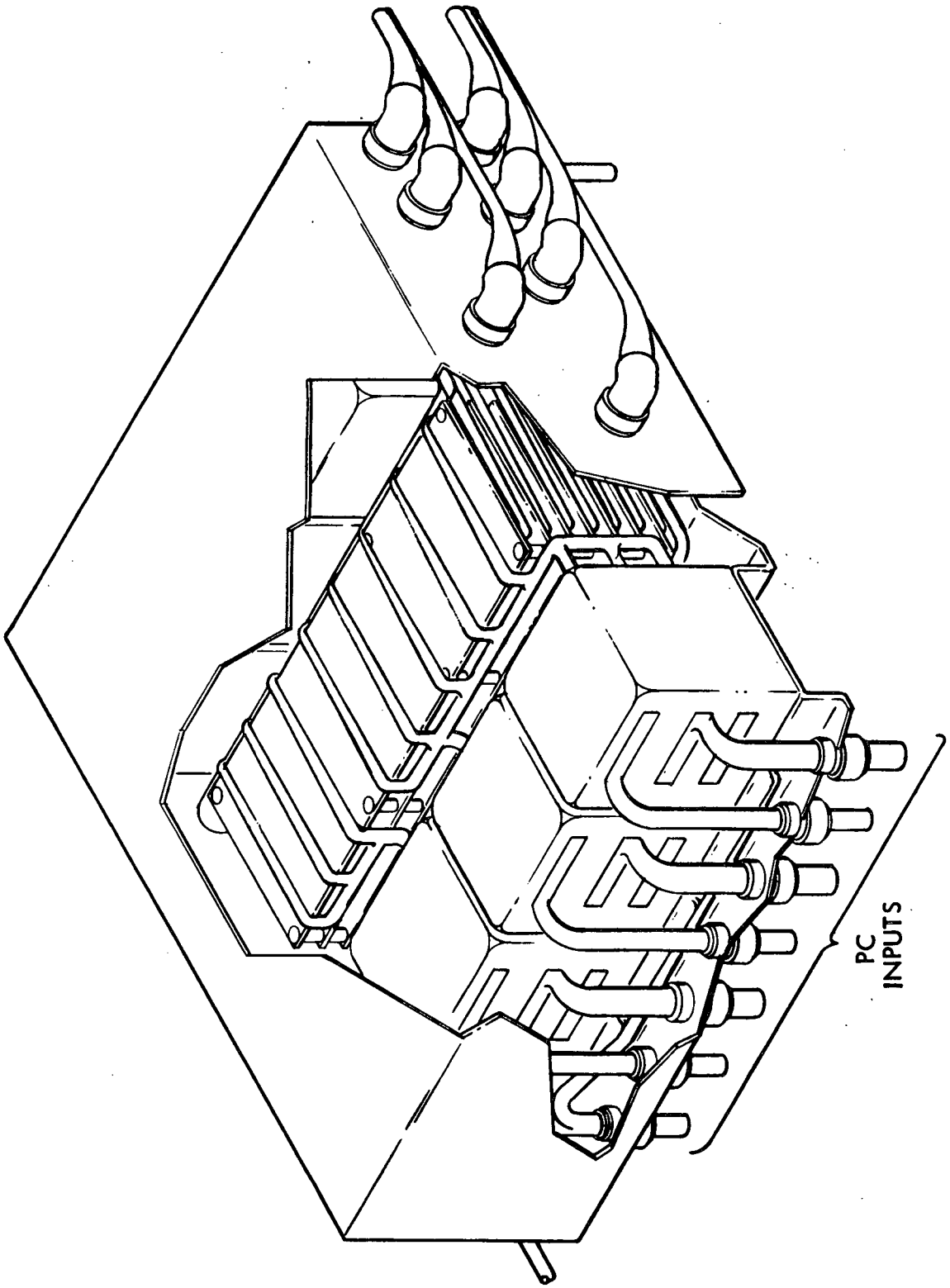

Fig. IV-C-7. Cutaway View of Switching Matrix

(a) Based on this study, the original design of the hermetically sealed SEPST III swtich does not satisfy the optimum design constraints for this application.

(b) A special design, as described, should be capable of meeting the requirements for smaller size, reduced weight, repairability, and reliability.

(c) An engineering model of a switch wafer pair to demonstrate the design feasibility should be fabricated.

(d) The described preliminary design for a switching-matrix assembly can incorporate the rotary-switch design and the required circuit connections.

(e) Three design approaches to the connection matrix appear feasible.

(f) Engineering models of the three matrix concepts should be fabricated.

4. Thruster-array Thermal Analysis

A seven-thruster clustered array, consisting of thrusters 30 cm in diameter and of related gimbal devices is the baseline array configuration. Thruster operating-temperature levels under various possible solar-heating modes and thruster operating-conditions were investigated for several thermal arrangement schemes. Because of the lack of definitive design criteria and detailed thruster thermal characteristics, the present study offers only a qualitative discussion of several design alternatives. One of the major objectives is to identify potential thermal problems for further detailed investigations.

The analysis considered five thrusters operated at full power over a variable solar environment. The peak thermal loading occurs at spacecraft perihelion (.34 AU) where solar irradiance up to a 10-sun level may come in at any angle with respect to the thrust axis in a plane parallel to the PC shear-plates. The high-irradiance solar heating, in addition to the thruster power dissipation, estimated at 500 W per thruster, would cause the thruster to operate at excessively high temperatures. To ensure proper thruster operation,

the maximum temperature levels of all thrust-subsystem components have to be kept within the upper temperature limits through proper configuration and application of thermal-control devices.

On the other hand, at spacecraft aphelion (3.5 AU), only one thruster is operated at one-half power level, and the solar irradiance becomes less than one percent of the level at spacecraft perihelion. Thermal control measures are required to keep all components above their lower temperature limits. Most component temperature limits and thermal constraints are not yet identified. Therefore, results of thermal analyses can be used only as a qualitative guide for design concepts until further detailed investigations are made. In the present study, a 250°C maximum temperature for the cathode vaporizer and a lower limit of -39°C for the mercury feedline are used as the basic constraints in evaluating the various thermal arrangements of the clustered array.

It was concluded from a previous study (Ref. IV-C-3) that, for a clustered array, the most efficient way of rejecting thruster internal-heat dissipation is radiation through the back surfaces. However, it is also desirable to minimize the thermal interaction between the thrusters and the remaining parts of the SEP module to protect the PCs and control mechanisms from overheating because of thruster heat dissipation. Before designing an improved integration scheme between the thruster array and the rest of the SEP module, it is essential to investigate a limiting worst-case situation. For the preliminary investigation, it was assumed that the back surface of the thruster array is insulated with a super-insulation blanket. Such an arrangement definitely increases the thruster operating-temperature and is one of the major sources of overheating problems in inbound missions. However, an insulated mounting plate helps to keep all standby thrusters warmer at the spacecraft aphelion, when only one thruster is operating at half-power level.

The following conclusions have been drawn from the study results:

(a) When the mounting plate is insulated and there are no additional thermal control devices, the thruster will overheat during full power operation even without solar heating.

(b) A radiator surface combined with a heat pipe/fluid loop is required to maintain thruster controllability in inbound missions, when the mounting plate is insulated. A louver arrangement or louver system that can be jettisoned in an environment of high solar irradiance should be considered to accommodate the need for variable surface emittance for the extreme heat-load variation imposed by the SEPSIT-Encke mission. The thermal response of the thruster array with the heat pipe/louver application is shown in Fig. IV-C-8 for two limiting operating conditions.

(c) The constraints with an insulated mounting plate appear to be undesirable because the application of heat pipe/fluid loop devices would increase the weight, as well as the uncertainties of performance reliability.

(d) The following areas are crucial to the temperature control of the thruster-array assembly and require further detailed investigation:

(1) Detailed experimental and analytical study of the thermal characteristics and performance of the specified 30-cm thruster.

(2) Establishment of definitive thermal constraints on all thrust-subsystem components.

(3) Experimental investigation of thruster-array assembly under a realistic environmental simulation, in particular, the effects of the solar irradiance level and angle of incidence.

(4) Detailed investigation of thermal interactions between the thruster array and related subsystem elements, such as the PCs and the control mechanisms. The investigation should aim at a feasible integration scheme, which would accommodate all the component thermal constraints without insulating the mounting plate.

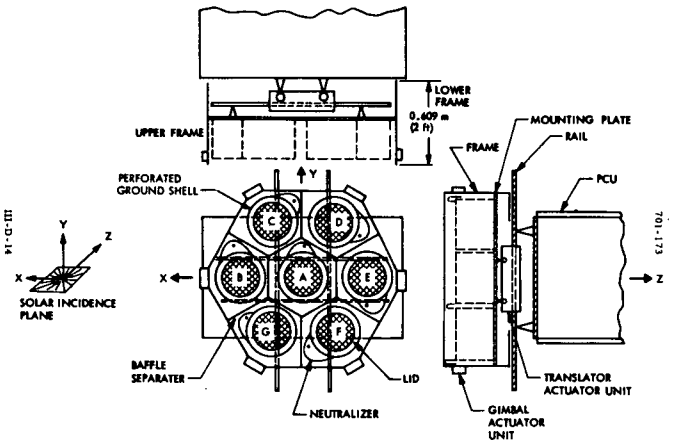

(a) Basic Thruster-array Configuration

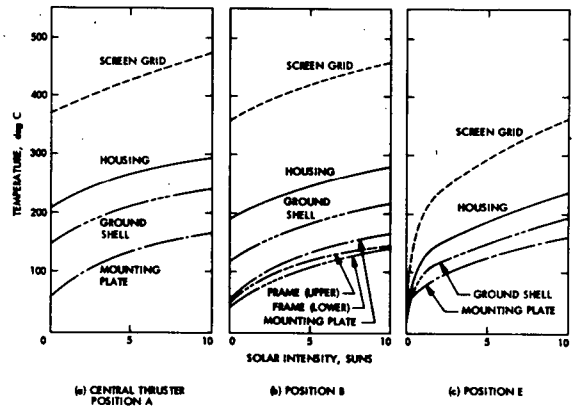

(b) Thrusters A, B, C, D, and G Operating at Full Power, Solar Incidence Parallel to Thruster Axis

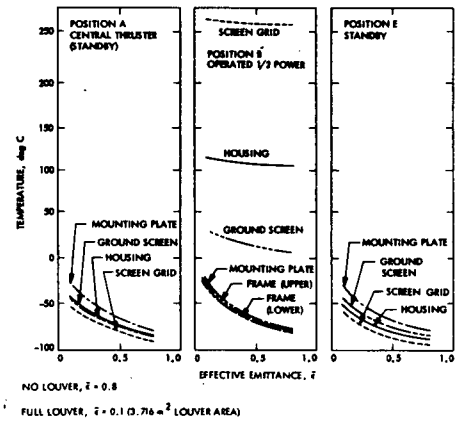

(c) Thruster B Operated at One-half Power, No Solar Heating

Fig. IV-C-8. Thermal Response of Thruster Array with Heat Pipe/Louver Application

5. Thrust Vector Control Tradeoff Study

In keeping with the major 1972 study objective of establishing the functional specifications for the electric propulsion subsystem, a tradeoff study of the various thrust vector control (TVC) concepts was undertaken. The following four areas were selected for investigation:

(a) JPL translator-gimballing concept.
(b) TRW gimballing-twisting concept.
(c) NASA-LeRC electrostatic gimballing concept.
(d) NASA-LeRC electrostatic-mechanical gimballing concept.

The study was concentrated on the JPL and TRW designs because the NASA/LeRC designs are in the experimental stage and will require new technology for implementation, whereas the JPL and TRW concepts can be implemented by existing technology. Furthermore, the JPL design exists in actual hardware form and is currently being used in the SEPST program. No engineering model of the TRW design has yet been built.

It may be argued that comparison between an actual piece of hardware and a mere concept is impossible and that such comparison invites inevitable bias. An attempt has been made to circumvent this problem by hypothesizing certain characteristics for the TRW idea, thus providing a firmer basis for comparison. As an example, although no electronic circuitry for the TRW scheme is available, an attempt has been made to approximate its complexity and general nature. On comparison with the existing JPL circuitry, the conclusion favors TRW on the basis of simplicity of design. However, modifications of the JPL design could reduce its electronics to a level compatible with that hypothesized for the TRW model.

Despite the attempt to establish a firm basis for comparison, one conclusion in favor of the translator-gimballing concept is inescapable, i.e., that building an engineering model of the gimballing-twisting concept and bringing it up to the level of testing reached for the translator-gimballing concept will be expensive and time-consuming.

Figure IV-C-9 shows the TRW thruster array of six thrusters arranged in a circular pattern. All six thrusters are mounted to a gimbal ring

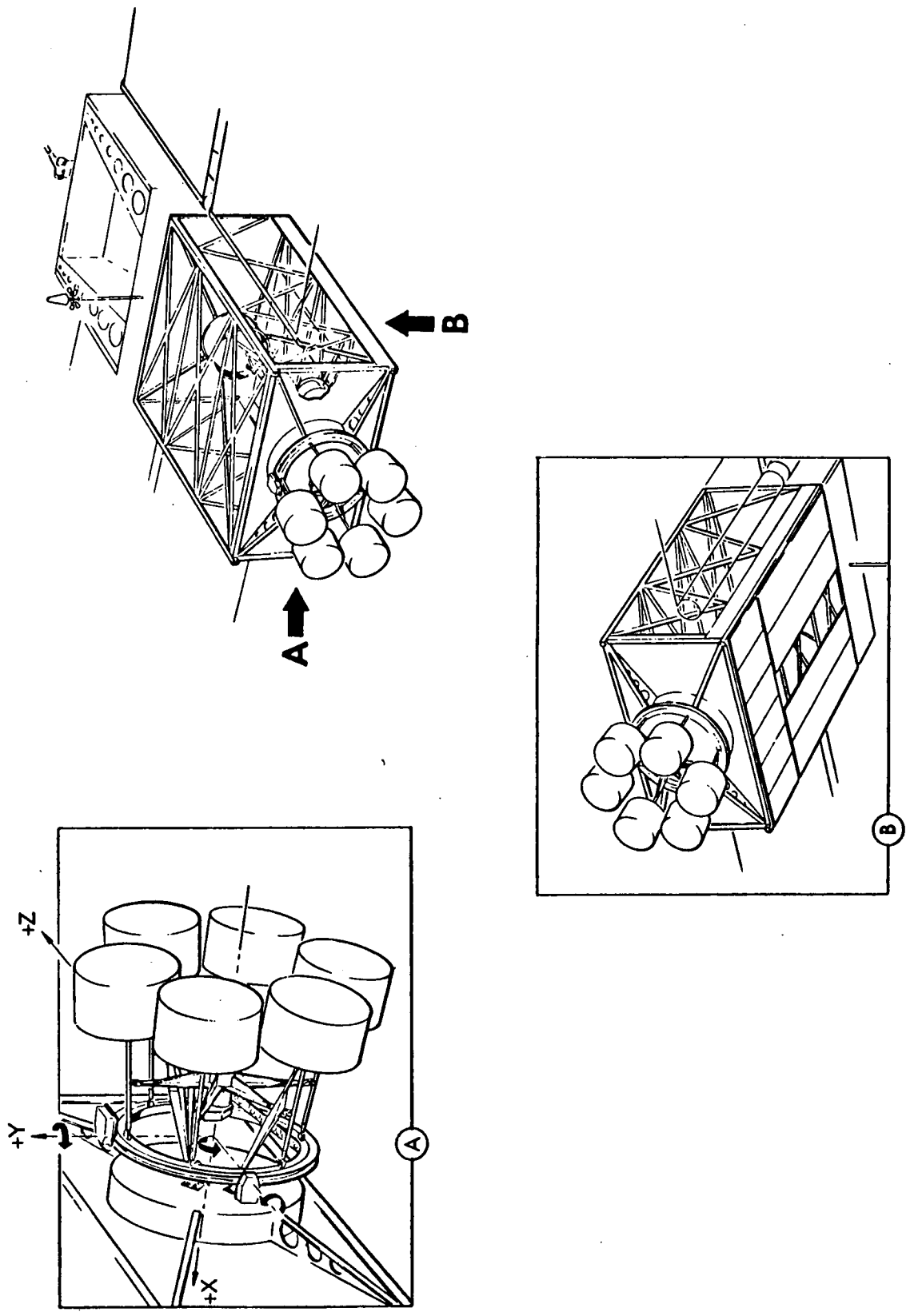

Fig. IV-C-9. TRW Electric Propulsion Module

in such a way that the thrust axis of each is canted to the pitch axis by an angle of 9 deg. The intent is to orient each thruster so that its thrust vector nominally points through the vehicle mass center. Hence, for unsymmetrical thrusting situations, no unbalance moment is exerted.

The gimbal referred to is mounted to an outer gimbal ring. Rotation of these gimbal rings about axes parallel to roll and yaw diverts the thrust vector from the mass center and produces control torques about the roll and yaw axes. Pitch control is provided by rotation of the star-shaped structure (Fig. IV-C-9) attached to the struts supporting the thrusters. The resultant twisting motion of the thrusters produces the pitch control torque.

Figure IV-C-10 shows the JPL thruster-array configuration. Six

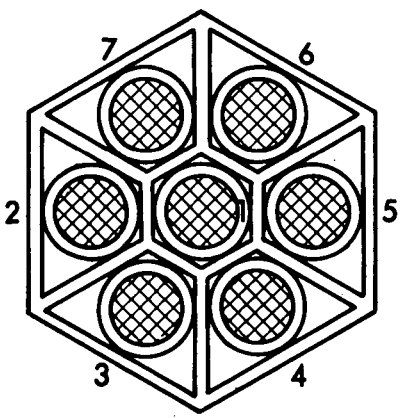

Fig. IV-C-10. JPL Thruster Configuration

outer thrusters are arranged symmetrically in a hexagonal frame about a center thruster. The plane of the frame is parallel to the roll-yaw plane. For the situation where no attitude control moments are required, the thrust direction for each thruster is parallel to the pitch axis.

Roll and yaw control are obtained by translating the entire thruster array parallel to the yaw and roll axes, respectively. In translating parallel to the yaw axis, the resultant thrust vector remains parallel to the pitch axis

and no longer passes through the roll axis. Consequently, a torque about the roll axis is generated. On the other hand, translation parallel to the roll axis dictates that the thrust vector no longer passes through the yaw axis and, hence, a torque about this axis is generated.

For pitch-axis control, outside thrusters are gimballed about axes passing through the array center. For example, gimballing thrusters 2 and 5 by equal and opposite amounts produces a couple on the vehicle about the pitch axis. This couple is used for control purposes.

After detailed examination of the two concepts, a conclusion favoring the JPL design was reached. Tables IV-C-1 through 3 lists some of the pros and cons of the two designs. Substantial detail verifying these comments appears in Volume III. It should be remembered, however, that additional work needs to be done to flight-qualify either design.

Table IV-C-1. Comparisons Based on the Basic Attitude Control Function

	Translator-gimballing TVC Concept	Gimballing-twisting TVC Concept
Canting	No canting No thrust loss No higher thrust level No additional power Initial unbalance torque for unsymmetric thrust configuration compensated for by translation No thrust vector reorientation for unsymmetric thrust configuration No need to reorient thrust vector or solar arrays No celestial sensor bias No need to know mass center location exactly No gimballing required for mass center shifts Distance between mass center and thruster array not important Large roll or yaw torque requires large translation	Approximately 9° through mass center Approximate 1.2° thrust loss Higher thrust level required Higher power to provide higher thrust No unbalance torque for unsymmetric thrust configuration Thrust vector reorientation required for unsymmetric thrust configuration Possible lower solar power level due to reorienting thrust vector Celestial sensor bias required to establish new null position Mass center location needs to be known Gimballing required to compensate for mass center shifts Long separation between mass center and thruster array Large roll or yaw torque obtained with small gimbal angle
Lateral Thrust	No lateral thrust in roll or yaw control No need to compensate for lateral thrust	Lateral thrust in roll or yaw control Increased electronics complexity to compensate for lateral thrust
Cross Coupling	Third order coupling No pitch axis coupling	Second order coupling Coupling in all three axes
Failure Modes	Failure of a gimbal actuator not catastrophic No current redundancy for translator actuators. Possible redundancy using gimbal actuators	Failure of twist actuator is catastrophic. No redundancy provided No current redundancy for gimbal actuators
Other	Tail-wags-dog effect not a problem Heavier mechanism. However, has redundancy Feed-line and power-cable-line problems equivalent	Tail-wags-dog effect not a problem Lighter mechanism. Has no redundancy Feed-line and power-cable-line problems equivalent

Table IV-C-2. Comparisons Based on the Actuator Designs

Current Translator-gimballing Baseline Design	Gimballing-twisting Design
Requires 2 different designs, 6 gimbal actuators, 2 translator actuators	Requires single actuator design. Requires 3 JPL design gimbal actuators. No translator actuator designs
All concepts of the configuration built and life tested (proven design)	Design complete only, no hardware
Uses ball bushings and rails (conventional	Uses multiple flexible pivots (conventional)
May require bellows covers on rails for space environment	Flexure pivots can withstand space environment
Tortuous path feedline and power cable design - Larger motions (qualified design)	Tortuous path feedline and power cable design. Small motions involved
Simpler launch environment design. Stiffer system Single simple caging, low height	Complicated launch environment design inherently less stiff. Multiple caging, more height
Resultant motion straightforward	Uncertainty in resultant motion (cross-coupling)
Maximum redundancy a) Each engine gimbals independently b) Gimbal motion could provide backup for translational motion	No redundancy - motion for all engines fail/axis
More easily adaptable to changes in configuration (i.e., number of engines required)	Less adaptability
Few moving parts (fewer moving parts when caging is accounted for)	Few moving parts
Weight somewhat known based on hardware (somewhat dependent on launch environment design)	Weight unknown - could be greater when caging (launch environment) accounted for

Table IV-C-3. Comparisons Based on the TVC Electronic Design

Parameter	Translator-gimballing	Gimballing-twisting
Basic control problem	Same for both systems	Same for both systems
Gain change in pitch axis	Not required because only two motors gimballed at a time	May be required because all 6 motors on the perimeter are gimballed
Electronic control of cross axis coupling	Can probably be ignored in both systems (i.e., small translations or gimballing)	Can probably be ignored in both systems (i.e., small twist or gimballing)
Mode switching for pitch axis control	Sophisticated electronics required to choose which of 3 couples to use for control	No switching required because all engines gimballed by one actuator
Pitch axis gimbal skewing	Requires special circuitry to realign gimbal couple	No skewing inherent in this design - gimbals mechanically linked
Reliability	The increased parts count and electronic sophistication of the JPL design invites reliability problems. However, approximately one half of the electronics is unique to gimbal couples, therefore offering redundancy in case of a failure	Reliable because there is no more switching. However, there is no redundancy in case of an electronic or mechanical failure

REFERENCES

IV-C-1. T. M. Masek, Integration of a Flight Prototype Power Conditioner with a 20-cm Ion Thruster. AIAA Paper No. 71-159, presented in the 9th Aerospace Sciences Meeting, January 25-27, 1971.

IV-C-2. D. C. Hamilton and W. R. Morgan, Radiant-Interchange Configuration Factors, Purdue University, December 1952.

IV-C-3. L. Wen, D. Crotty and E. V. Pawlik, Ion Thruster Thermal Characteristics and Performance, AIAA Paper No. 72-476, presented at the 9th Electric Propulsion Conference, Bethesda, Md., April 17-19, 1972.

D. SEP MODULE POWER SUBSYSTEM STUDIES

1. Power Subsystem Operating Voltage Selection

The power subsystem of a SEP spacecraft generates, processes, and distributes many kilowatts of electrical power, which results in extremely high current and heat dissipation losses.

The potential advantages of operating at higher voltages, which result in reduced currents, higher efficiency, and lower weight, were investigated. However, the advantages may be offset by technical problems in design, fabrication-qualification testing, safety and component limitations.

A tradeoff study, based upon this analysis of the power-subsystem designs, was initiated to determine an optimum operating voltage range between 50 to 400 V. An upper limit of 400 V was established for the subsystem operating voltage because of the unavailability of JPL-approved components at higher power levels. The voltage ranges, based upon propulsion PC designs in development, are: (a) 50 to 100 V, (b) 100 to 200 V, and (c) 200 to 400 V, respectively. The effect of the operating voltage on the following parameters was considered during the selection process:

(a) Subsystem specific mass.
(b) Subsystem efficiency.
(c) Subsystem reliability.
(d) Device limitations.
(e) Maximum utilization of existing designs.

The above considerations were used in the analyses of the power-subsystem major elements (solar array; power conditioning, excluding the thruster-subsystem PC; and distribution).

a. Power-subsystem Description

The block diagram of the SEP spacecraft power subsystem is shown in Fig. IV-D-1. Power is generated by the rollout solar arrays, which deploy outward from the spacecraft in a plane normal to the sun. Power from the solar array is delivered via the power-distribution module to the thrust-subsystem PCs and to the pre-regulator. The pre-regulator provides regulated power to the SEP module housekeeping PCs and to the payload-module power subsystem. The output voltage of the pre-regulator will be from 40 to 50 V for compatibility with the existing Mariner or Viking power subsystem designs. The SEP module housekeeping-power inverter provides regulated alternating current to the engineering subsystems necessary for the operation of the thrusters. Spacecraft battery power will be delivered to the power distribution module for use by the pyrotechnic subsystem of the SEP module during sun occultation periods.

The maximum power point detector (MPPD) is used to determine the maximum solar-array power available at any time throughout the mission. This permits the use of maximum power for spacecraft thrust.

b. Solar-array Design Study

Two rollout solar arrays are required to provide the power of an electrically propelled spacecraft. Each solar array is made up of two flexible substrates composed of sectors individually fabricated and tested. The conceptual designs for a 2.5-, 5-and 10-kW rollout solar array of 50, 100 and 200 V (near earth) at operating voltage of 60°C were examined. The various element weights and sizes with their resultant power-to-weight ratio, determined for this study, are shown in Table IV-D-1. This analysis was performed using the PSRUSA computer program developed during the 66-W/kg (30-W/lb) program and a 9-g launch acceleration. Results obtained with a launch acceleration of 4.5 g are shown to indicate the potential increase in the power-to-weight ratio, which may be possible.

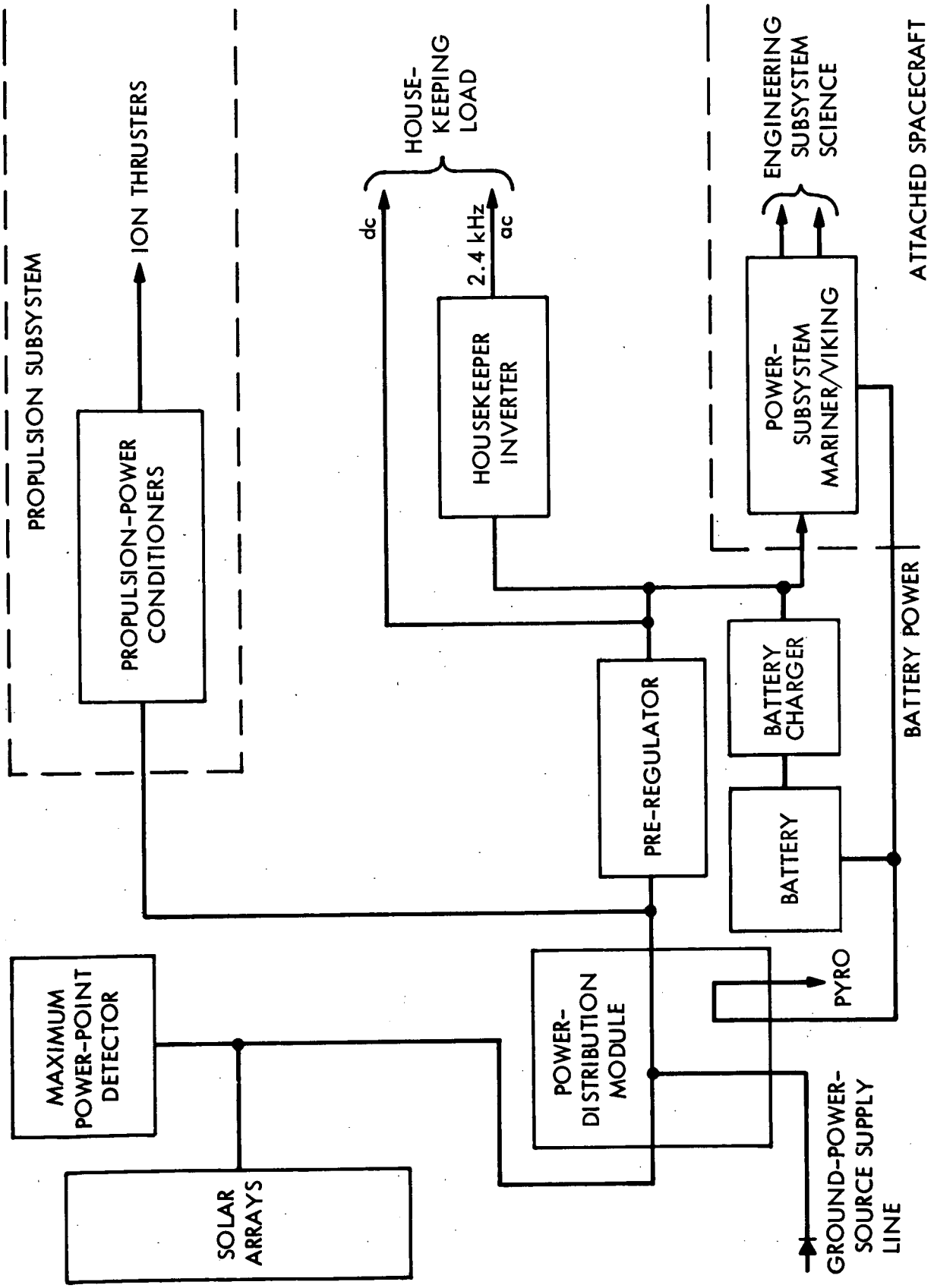

Fig. IV-D-1. SEP Module Power Subsystem with Mariner/Viking Spacecraft

Table IV-D-1. Solar-array Size, Weight and Power Estimates

Solar Panel Power		Launch Acceleration, 9 g									Launch Acceleration, 4.5 g								
		2.5 kW			5.0 kW			10.0 kW			2.5 kW			5.0 kW			10.0 kW		
Solar Panel Voltage	Volts	50	100	200	50	100	200	50	100	200	50	100	200	50	100	200	50	100	200
Panel Area	m^2	24.447	24.193	23.943	48.895	48.385	47.887	97.789	96.771	95.773									
Panel Length	m	10.283	10.176	10.072	14.072	13.925	13.782	24.801	24.542	24.289									
Boom Diameter	cm	2.497	2.471	2.469	3.797	3.772	3.688	7.013	6.944	6.883									
Substrate Tension	kg/blanket	0.280	0.278	0.280	0.788	0.779	0.730	2.673	2.634	2.600									
Natural Frequency	Hz	0.040	0.040	0.040	0.040	0.040	0.040	0.040	0.040	0.040									
Actuator Width	m	0.112	0.111	0.111	0.170	0.169	0.165	0.314	0.312	0.308									
Panel Width	m	2.489	2.488	2.488	3.645	3.643	3.640	4.257	4.254	4.251									
Storage Drum Weight	kg	5.345	5.311	5.278	17.308	17.203	17.100	33.757	33.550	33.347	3.175	3.154	3.133	9.967	9.903	9.840	19.475	19.349	19.226
End Cap Weight	kg	1.576	1.556	1.537	5.300	5.235	5.172	13.791	13.623	13.459	0.556	0.549	0.541	1.755	1.733	1.711	4.585	4.527	4.469
Support Shaft Weight	kg	1.203	1.195	1.188	3.968	3.944	3.920	7.859	7.811	7.764	0.688	0.684	0.679	2.203	2.188	2.174	4.331	4.303	4.276
Bearing Weight	kg	0.615	0.611	0.608	1.406	1.397	1.389	2.456	2.441	4.240	0.353	0.351	0.349	0.771	0.766	0.761	1.336	1.327	1.318
Leading Edge Beam Weight	kg	0.386	0.384	0.385	1.880	1.871	1.825	4.771	4.734	4.702	0.267	0.266	0.267	1.134	1.127	1.088	3.105	3.075	3.049
End Support Weight	kg	2.764	2.729	2.694	8.442	8.340	8.240	21.389	21.129	20.875	1.230	1.213	1.197	3.363	3.319	3.277	8.485	8.374	8.266
Center Support Weight	kg	1.207	1.188	1.175	3.757	3.704	3.623	11.547	11.358	11.180	0.629	0.619	0.612	1.786	1.760	1.720	5.428	5.337	5.251
Non-Structural Weight	kg	0.965	0.955	0.945	1.930	1.910	1.890	3.859	3.819	3.779	0.965	0.955	0.945	1.930	1.910	1.890	3.859	3.819	3.779
Negator Weight	kg	0.327	0.326	0.327	0.548	0.545	0.527	1.010	1.002	0.996	0.327	0.326	0.327	0.548	0.545	0.527	1.010	1.002	0.996
Boom Weight	kg	1.507	1.464	1.446	4.777	4.658	4.407	28.693	27.849	27.069	1.507	1.464	1.446	4.777	4.658	4.407	28.693	27.849	27.069
Actuator Weight	kg	1.216	1.180	1.166	3.852	3.756	3.554	23.138	22.457	21.828	0.789	0.766	0.756	2.504	2.442	2.311	15.028	14.586	14.178
Blanket Weight	kg	20.292	20.081	19.874	40.584	40.161	39.748	81.169	80.323	79.495	20.292	20.081	19.874	40.584	40.161	39.748	81.169	80.323	79.495
Total Panel Weight	kg	37.404	36.980	36.621	93.752	92.725	91.396	233.437	230.096	226.919	30.779	30.426	30.126	71.322	70.512	69.455	176.503	173.871	171.373
Watts Per kg/*	W/kg	13.751	13.909	14.046	10.973	11.094	11.256	8.813	8.942	9.067	16.711	16.905	17.074	14.423	14.589	14.811	11.657	11.833	12.003

*The above data are based on natural frequency 0.040 Hz, a conservative value. With natural frequency of 0.020 Hz and launch acceleration levels less than 4.5 g anticipated, a 10-kW array with specific power greater than 66 W/kg (30 W/lb) would be postulated.

The study also determined the feasibility of providing isolated power for spacecraft housekeeping and for the thrusters. This isolation may be required to prevent transients originating within the thrust subsystem from affecting the performance of the other engineering subsystems. To accomplish this isolation, each substrate of the solar array was designed with several independent circuits terminating at the spacecraft/array interface. Each circuit was sized to deliver a relatively uniform, minimum power level of 600 W for housekeeping.

From this study, it can be concluded that:

(1) A roll-out solar-array with a voltage output between 50 to 200 V at 1 AU and power levels up to 10 kW can be designed and built using conventional techniques, provided that additional development effort solves problems associated with array substrate fabrication, substrate stiffness and bending, and solar-cell module assembly techniques.

(2) Array designs having output voltages of 50 to 400 V are relatively free from the effects of space plasma in planetary missions and are substantially below the voltages that are believed to be affected by the most dense regions of the ionosphere. Additional study is required.

(3) Calculations of the solar-array design based on the General Electric Company solar array (2.5-kW model) have shown that the specific power density, W/kg, is greater at the highest voltage design of 200 to 400 V for all power levels. The data obtained are shown in Table IV-D-2.

(4) A solar-array design utilizing switching to maintain two electrically isolated array sections looks feasible. However, more detailed analysis in the number and type of switching circuits and interwiring should be performed before the approach can be recommended.

Table IV-D-2. Specific Power Density, 2.5-kW Solar Array

Power Output kW/panel	Launch Acceleration g	Voltage at 1 AU		
		50 V	100	200
		Power Density W/kg (W/lb)	Power Density W/kg/(W/lb)	Power Density W/kg (W/lb)
2.5	9.0	13.75 (30.32)	13.91 (30.66)	14.04 (30.96)
2.5	4.5	16.71 (36.84)	16.91 (37.27)	17.07 (37.64)
5.0	9.0	10.97 (24.19)	11.09 (24.46)	11.25 (24.81)
5.0	4.5	14.42 (31.80)	14.59 (32.16)	14.81 (32.65)
10.0	9.0	8.81 (19.43)	8.94 (19.71)	9.07 (19.99)
10.0	4.5	11.66 (25.70)	11.83 (26.09)	12.01 (26.47)

c. Power Distribution Study

The power distribution is divided into four areas, as shown in Fig. IV-D-2:

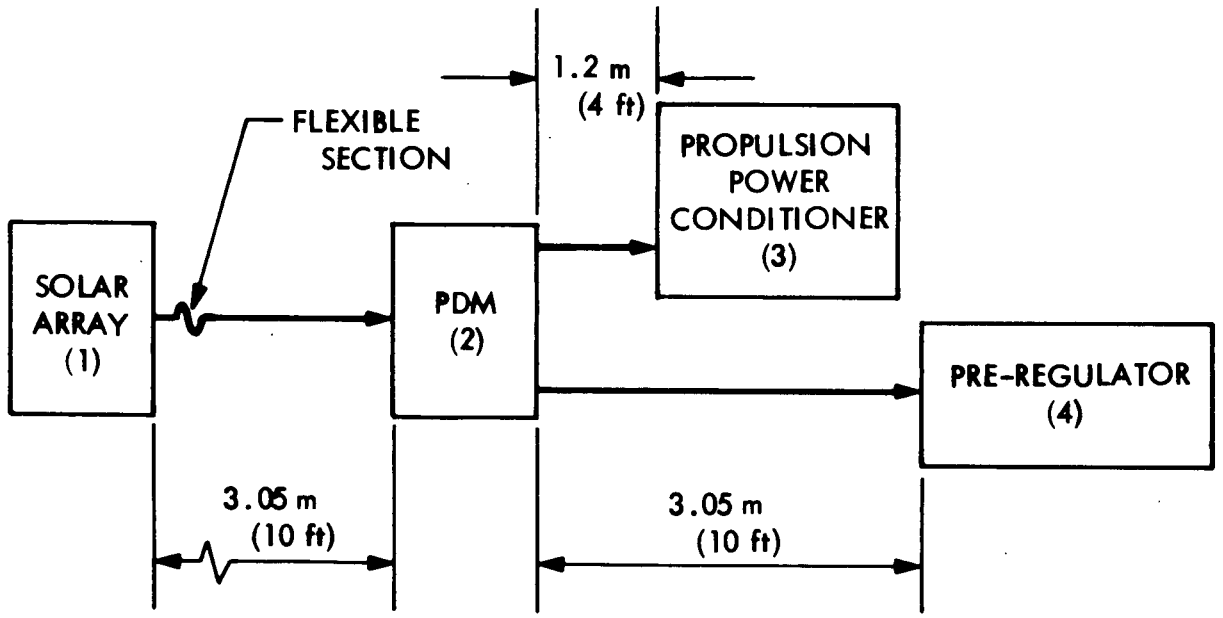

Fig. IV-D-2. Power Distribution Subsystem

(1) The cables from the solar array to the power distribution module (PDM).
(2) The PDM.
(3) The cables from the PDM to the thrust-subsystem PCs.
(4) The cable from the PDM to the pre-regulator.

Each of the two solar arrays contain two substrates. Each substrate is divided into four sections, which provide 600, 800, 1200 and 2400 W, respectively. Each section is connected to the PDM by a single cable 3.05 m (10 ft) long, resulting in a total of 16 cables.

It is assumed that the worst-case peak-input power requirements for each of the five PCs for the 30-cm thrusters are 4000 W; actually, the expected peak-input power is 3100 W. A central location for the PDM was assumed to provide equal minimum cable lengths 1.2 m (4 ft) between the PDM and each PC.

The pre-regulator power requirements are about 700 W. This cable was therefore assumed to be identical in length to the 600-W cable between the solar array and the PDM, i.e., 3.05 m (10 ft).

Calculations of the cable losses and lengths were made for two competing design goals: the least weight, and the least power dissipation. For the least weight, the cable weight was minimized at the expense of power dissipation. For the least power loss, the minimum power loss was sought at the expense of weight. A number of design constraints were used in the study, e.g., current limitation on wire gages, current capacity of connectors, 2% maximum permissible voltage drop per cable of the voltage delivered, and a cable-temperature rise not greater than 45°C above spacecraft frame in vacuum operation. The calculation provided a matrix of data as shown in Table IV-D-3.

From the power distribution analysis, it was determined that the least power loss and least weight are obtained within the design voltage range of 200 to 400 V. Table IV-D-4 summarizes the data.

Table IV-D-3. Power Loss and Cable Weights at Three Operating Voltage Ranges

Subsystem Element*	Design Point**	Voltage Range					
		50 to 100 V dc		100 to 200 V dc		200 to 400 V dc	
		Power Loss W	Weight kg (lb)	Power Loss W	Weight kg (lb)	Power Loss W	Weight kg (lb)
Solar-array Cable	LP	377	7.8 (17.3)	221	4.3 (9.5)	63	3.6 (8.0)
	LW	405	6.7 (14.8)	370	2.3 (5.0)	164	1.4 (3.0)
PDM (Estimate)	LP	72	5.4 (12)	28	4.9 (11)	20	4.5 (10)
	LW	52	4.9 (11)	18	4.5 (10)	14	4.5 (10)
Pre-regulator Cable	LP	10	0.3 (0.6)	3	0.2 (0.5)	1	0.2 (0.5)
	LW	12	0.2 (0.5)	10	0.09 (0.2)	5	0.09 (0.2)
PC Cables	LP	276	2.7 (5.9)	107	0.8 (1.7)	64	0.51 (1.0)
	LW	405	1.4 (3.0)	157	0.7 (1.5)	110	0.4 (0.8)
Totals	LP	735	16.2 (35.8)	349	10.28 (22.7)	143	8.8 (19.5)
	LW	874	13.3 (29.3)	555	7.56 (16.7)	293	6.4 (14.0)

*See Fig. IV-A-1.

**LP = Least-power design point.
LW = Least-weight design point.

Table IV-D-4. Least Weight and Power Loss

Voltage Range, V	Power Generated/ Distributed	Least-weight Design		Least-power-loss Design	
		Weight, kg (lb)	Losses, W	Weight, kg (lb)	Losses, W
50 to 100	20 kW/16 kW	13.29 (29.3)	874.0	16.24 (35.8)	735.0
100 to 200	↓	7.57 (16.7)	555.2	10.30 (22.7)	349.0
200 to 400		6.35 (14.0)	293	8.85 (19.5)	143.0

d. Pre-regulator and Power Conditioning for SEP Module Housekeeping Study

The design data for the pre-regulator and the SEP module power inverter are shown in Table IV-D-5. It can be seen that only the pre-regulator is affected by the choice of the array voltage.

Table IV-D-5. Design Data for Pre-regulator and Propulsion Housekeeping Inverter

Power Conditioner	Input Voltage: Source/Range	Output Power (W)	Output Voltage (V)
Pre-regulator	Array: 1. 50-100 2. 100-200 3. 200-400	540 (Mariner) 775 (Viking)	45 V dc 50 V 50 V
Propulsion Housekeeping Power Inverter	Pre-regulator: 40-50 V dc	90	50 V rms

A pre-regulator designed to supply between 40 and 50 V will satisfy both the Mariner and the Viking power-subsystem input requirements. Since the output voltage of the pre-regulator is always greater than the solar-array voltage, a down-switching regulator is used. A pre-regulator designed for both Viking and Mariner and a design for Mariner only were analyzed. The calculated efficiencies for the pre-regulator design and the power inverter are given in Table IV-D-6.

Table IV-D-6. Summary of Efficiency Calculations for Pre-regulator

Spacecraft	Input, V	Pre-regulator Efficiency, %	Housekeeping Inverter Efficiency, %
Viking and MVM 73	50 to 100	92.1	94.4
MVM 73	50 to 100	93.5	94.4
Viking and MVM 73	100 to 200	93.2	94.6
MVM 73	100 to 200	93.9	94.6
Viking and MVM 73	200 to 400	91.8	94.6
MVM 73	200 to 400	92.5	94.6

Conclusions derived from the pre-regulator and SEP module housekeeping-power inverter study are:

(1) The pre-regulator efficiency calculations show that efficiency is somewhat higher within the input range of 100 to 200 V. However, the power processed by the pre-regulator is less than 4% of the total solar-array power generated and processed and has little overall design impact.

(2) The pre-regulator and inverter designs are considered to be essentially state of the art over the entire range of 50 to 400 V. The study assumed that high voltage transistors are available, but these devices must be

procured and tested before acceptance. A breadboard PC, utilizing the high voltage transistor, is required to evaluate alternate designs and to verify performance characteristics with the Mariner (or Viking) power subsystem.

e. Conclusion and Recommendation

Based on the results summarized above, the 200-to 400-V range provides design advantages for the solar array and the power distribution system. The pre-regulator and propulsion housekeeping PC designs have the highest efficiency within the 100-to 200-V input voltage range. The loss in efficiency at the 200-to 400-V input voltage range is approximately 2%. Considering that the power handled by the pre-regulator and propulsion housekeeping PC is approximately less than 4% of the power generated by the solar array and distributed by the power subsystem, the power losses incurred by operating the housekeeping PCs at 200 to 400 V are negligible. For these reasons, it is recommended that 200 to 400 V be selected for the unregulated bus voltage of the SEP module power subsystem.

2. Solar Array Studies

a. Dynamic Interactions With Attitude Control

A tradeoff study was initiated to evaluate a best solar array for an electric propulsion Encke mission from an attitude control point of view. The study was intended to examine, in detail, the flexible solar array/attitude control interaction problem for both the thrust vector control (TVC) and the reaction control system (RCS) modes of operation. The effects of attitude control system non-linearities were also to be evaluated.

At this time, the linear TVC model is complete and has been subjected to exhaustive stability analysis. A digital computer simulation program was constructed for the model and shows the time history of control. It

was decided that inclusion of the non-linearities in the TVC model not only was not feasible, but that, because of earlier simulation work, was not necessary.

Work is continuing on the RCS model and results are expected shortly. However, it is felt that the basic conclusions for the TVC model will be applicable to the RCS model. The remainder of this study is concerned with the TVC model.

The stability study is parametric in nature. The parameters are solar-array aspect ratio, first natural frequency, and solar-array rotation angle (about the yaw axis). In addition, the celestial sensor gain factors were also varied in the study. First natural frequencies varied from approximately 0.014 to 0.06 Hz. Actually, the first six modes of solar array vibration were included. Aspect ratios of 7.38, 5.40, and 4.11 were considered. Solar-array rotation angles of 0, 30, and 60 deg were allowed.

Such anomalous behavior as unequal tension in solar array blankets was not considered in this study. The effects of this as well as of those higher than the sixth mode of vibration should be determined in later studies. Frequency sensitivity studies are also recommended to indicate how accurately natural frequencies need to be known.

The stability analysis takes the form of an eigenvalue analysis; i.e., for a given spacecraft (the aspect ratio, natural frequency, rotation angle, spacecraft inertia properties, etc.), the roots of the characteristic equation for the configuration were determined. For six modes of vibration, the number of roots is 30. The appearance of any root with a positive real part implies instability. The presence of all distinct roots each with a negative real part guarantees attitude stability. The response character of a given configuration was then ascertained with a digital computer simulation program for the system's equations of motion. Results of some of these simulations are included in this report.

The four major conclusions reached are:

(1) That solar arrays with large aspect ratio are more attractive than those with small aspect ratio.
(2) That solar arrays with higher natural frequencies are more likely to be stable than those with lower natural frequencies.
(3) That lowest array frequency is not always the criterion for stability.
(4) That array tip deflections are sufficiently small so that large stresses at the base of the arrays do not develop.

The second of these statements was expected. However, the conclusion (1) seems somewhat surprising at first. Intuition would probably lead one to suspect that a small aspect ratio (a short solar array) would be more stable because an array with small aspect ratio will be stiffer in the roll and pitch axes. However, from the dynamics analysis, it is the yaw axis which is most sensitive to solar-array flexibility, and large aspect ratio has the effect of stiffening in the yaw axis.

At this point in the study of the solar-array attitude-control interaction problem, the 3.657-or 4.267-m (12-or 14-ft) wide array should be recommended for the Encke rendezvous mission. This is in keeping with the concept of the 4.267-m (14-ft) wide array currently being designed, which has an aspect ratio of 5.57, slightly larger than the 5.40 value adhered to in the interaction study. Conceivably, an array with lowest natural frequency of 0.015 Hz could be used. However, additional analysis is required to confirm this.

The study points out vividly the necessity and usefulness of a design tool such as the computer program, SEWART. This coupled three-axis eigenvalue program can determine, in microseconds, if a configuration is likely to be stable. The term "likely" is appropriate in that the SEWART program examines the linear equations, which only approximate the actual

spacecraft configuration. However, such linear models generally tell a good deal about the actual model. The alternatives to using an eigenvalue problem are the root locus analysis, which can not evaluate coupled three-axis stability criteria, or the simulation analysis. However, simulation analysis can often lead to erroneous results (see Fig. IV-D-3). Clearly, for the flexible configuration, a simulation of 1000 sec in real time would indicate a stable configuration. Only after 1500 sec does the instability make itself apparent.

Comparisons of the results for rigid models with those for flexible models show the need for including the flexible characteristics of the arrays in the design of the attitude control system. In many instances, the rigid models are stable whereas the flexible ones are not (see Figs. IV-D-3 and 4). In rare instances, the opposite is true.

b. Structural Interface With SEP Module

A rollout solar array, developed by the General Electric Company for JPL, was selected for the Encke mission. Each of the two panels is 4.3-m wide by 23.8-m long. The ease and manner with which these large panels integrate with the spacecraft structure can have a significant impact on spacecraft configuration and total mass. For this reason, a study was undertaken to identify and explore the requirements of the structural integration of the solar array with the spacecraft structure. The interaction between array and spacecraft during large-displacement, low-frequency, spacecraft launch-vibration modes was of particular interest.

Because the solar array is essentially an add-on subsystem, the spacecraft structural interface design is primarily based on meeting the structural support requirements of the panels. Although the support stiffness and relative motion requirements, discussed in Volume III, are not too difficult to meet for the 2.5-m (8-ft) wide General Electric prototype panel, they become more significant as the width of the panel increases. Meeting the requirements for the 4.3-m (14-ft) wide baseline solar panel could significantly affect the spacecraft configuration and mass.

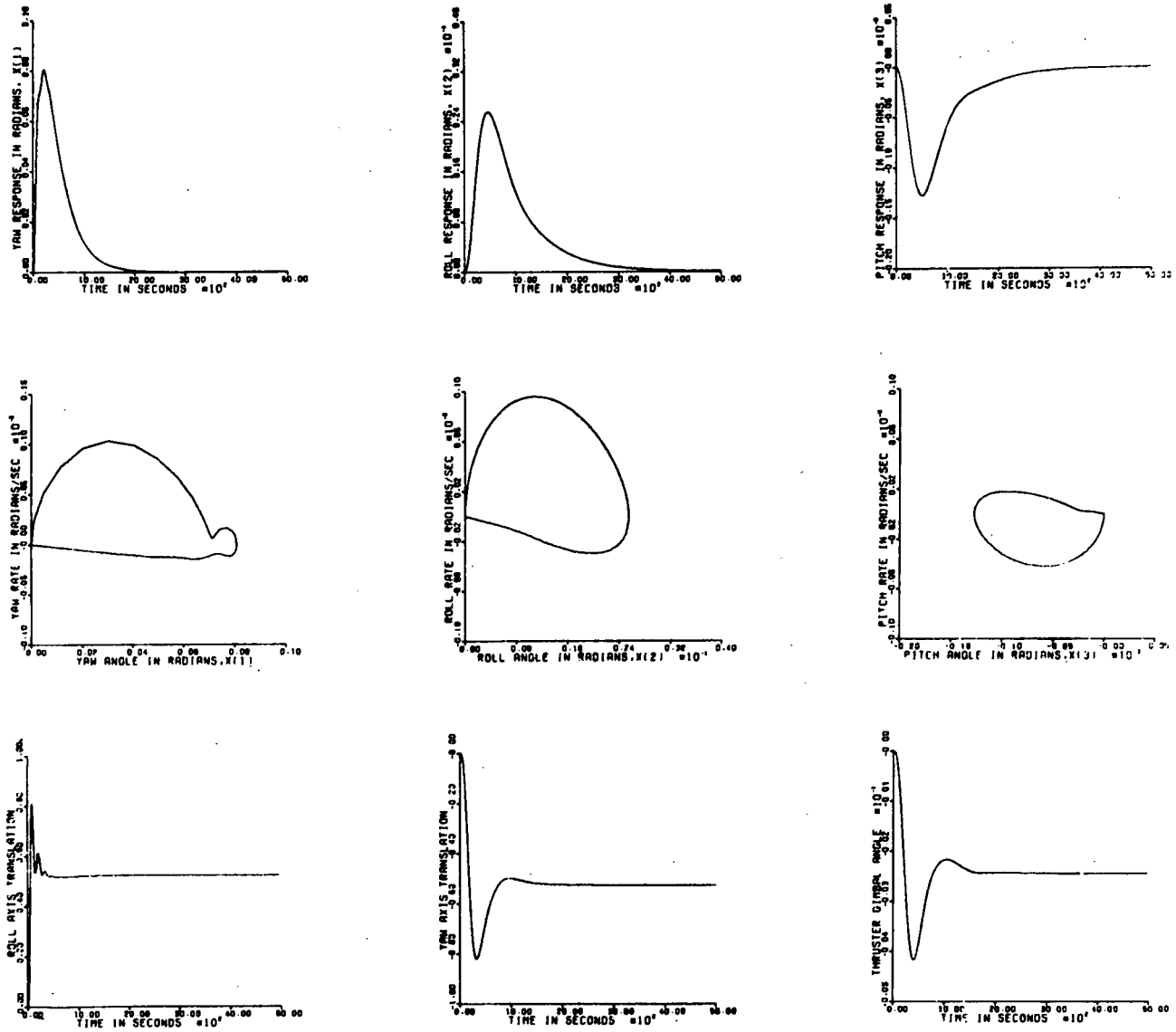

Stable Rigid Model, K_{si} = 300, 250, 295 V/rad,
Rotation Angle = 0°, Aspect Ratio = 7.38

Fig. IV-D-3. Simulation Analysis, Case a

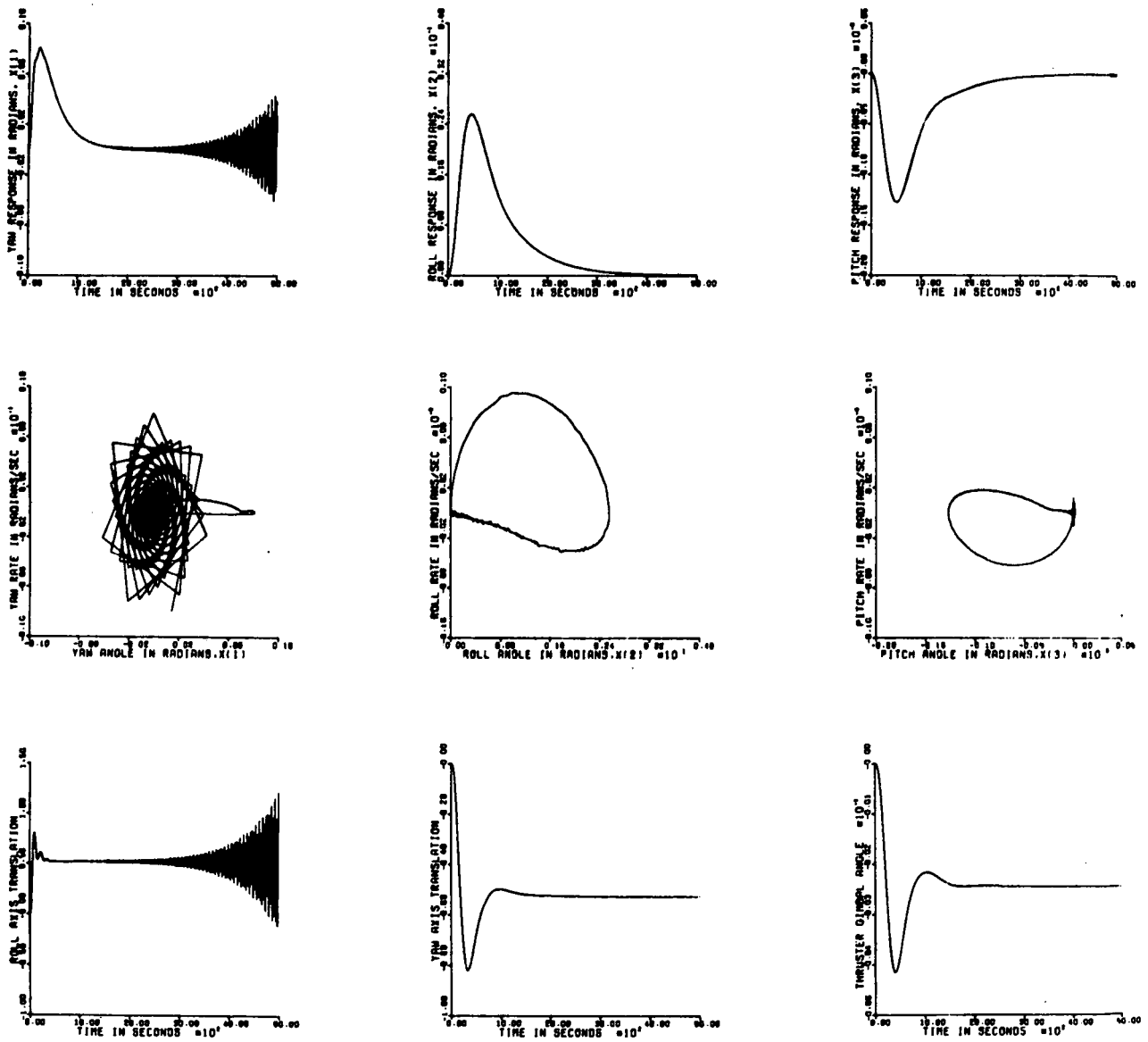

Unstable Flexible Model, K_{si} = 300, 250, 295 V/rad,
σ_1 = 0.01366 Hz, σ_2 = 0.01461 Hz, σ_3 = 0.02111 Hz,
σ_4 = 0.02262 Hz, σ_5 = 0.02798 Hz, σ_6 = 0.02798 Hz,
Rotation Angle = 0°, Aspect Ratio = 7.38

Fig. IV-D-4. Simulation Analysis, Case b

To evaluate the impact of the solar-array support requirements on the spacecraft design, a dynamic analysis of the combined solar array/spacecraft structural system was undertaken. Figures IV-D-5 and 6 show the structural models which were used. Accurate representation of the solar-array support stiffness and calculation of low-frequency spacecraft deflections required a reasonably detailed analytical model of the entire spacecraft, including the solar array. Because the solar-panel interface forces and deflections were of primary interest, the dynamic properties of the solar array had to be accurately modeled. In particular, previous dynamic studies of the stowed solar panel determined that the solar-cell blankets must be treated as separate spring-mass systems with a high degree of damping.

After the structural model was completed, the first 20 natural frequencies and vibration modes were calculated for the cantilevered spacecraft with and without solar-array outboard-end supports. The rigid-elastic coupling terms, which indicate the degree of coupling between the spacecraft modes and the launch vehicle interface motions, were also calculated. Subsequently, each mode was scaled to indicate its expected launch vibration level based on its effective mass and degree of coupling to the launch-vehicle excitation. After the modes were appropriately scaled, the modal deflections were used to calculate the critical stresses in the solar-array drum-bearing assemblies.

During the course of the study, analyses were made using various solar-cell blanket natural frequencies, and solar-array drum-bearing assembly and support member stiffnesses. Each case was analyzed using three spacecraft configurations: (1) all outboard-end supports present, (2) upper outboard-end supports removed, and (3) both upper and lower supports removed.

The results of the study indicate that none of the solar-array configurations is in danger of failing, when all outboard-end supports are used. However, the prototype array is sensitive to large-displacement, low-frequency, spacecraft motion. A sensitive area pointed up by the study is the relative motion observed between the tips of the solar-array drums and the outboard end-support attachments at the spacecraft. The outboard-end supports must be

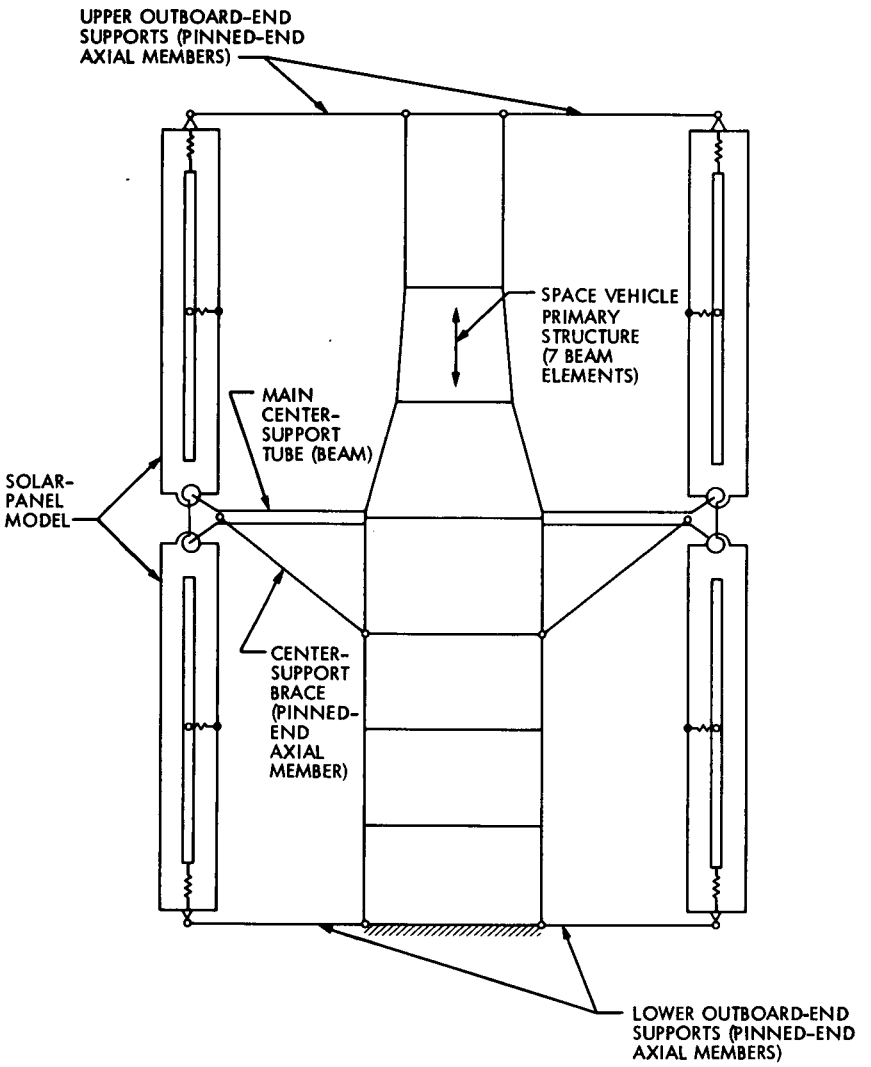

Fig. IV-D-5. Spacecraft Structural Model

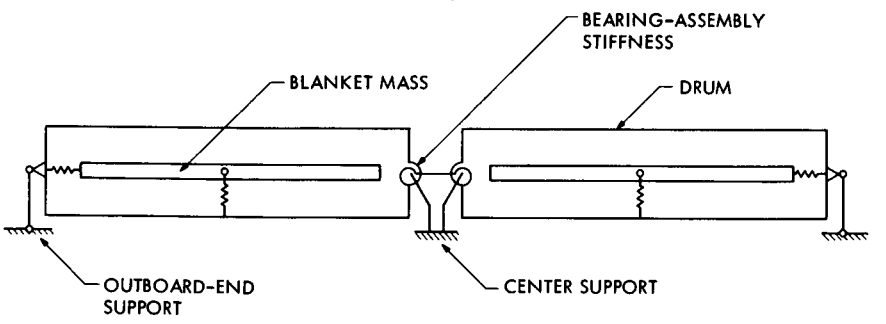

Fig. IV-D-6. Rollup Solar-array Structural Model

capable of accommodating this relative motion. Although the pinned members used in the model have this capability, the prototype design is supported by tapered plugs, which would disengage during such motion. Some minor reconfiguration of the outboard-end-support attachment to the drum is therefore suggested.

The results also indicate that one or both of the outboard-end supports can be removed, providing the solar-panel drum-bearing assembly is sufficiently stiffened. With the current bearing assembly design, the first mode of the cantilevered drum occurs at about 4 Hz and couples extensively with the first mode of the spacecraft. At this low frequency, the solar-cell blanket and drum move in unison and with very low damping. This leads to unacceptably high stresses at the root of the drum assembly.

When the cantilevered drum resonance is increased to about 20 Hz, the drum structure uncouples from the solar-cell blanket to some degree, and the relative motion between the blanket and the drum leads to considerable damping. At this frequency, the drum resonance is uncoupled from the spacecraft first mode and is coupled instead to the much diminished spacecraft second mode. Thus, although an alternate method of locking the drums and leading edge member during launch is required, the elimination of the outboard-end supports appears feasible.

c. Thermal Analyses

Ordinarily, it is desirable to maintain perpendicularity between the cells of the solar array and the incident solar rays to maximize the electrical output of the array. However, another factor must be considered. As the space-vehicle heliocentric distance decreases, the solar-array temperature increases correspondingly. A temperature limit of 140°C is placed on the array when soft-solder connections are used in its construction. A thermal analysis of a perfectly flat array has shown that 140°C will be reached at 0.635 AU, well past the point of Encke rendezvous (which occurs at about 1 AU) but before perihelion (0.34 AU). The present temperature-control scheme is

to rotate the array about its longitudinal axis by an appropriate angle, when necessary, to limit the array temperature to 140°C. The required rotation angle and the array temperature is shown in Fig. IV-D-7 as a function of heliocentric distance.

When the cell blankets are not perfectly flat, unavoidable differences in temperature will exist over the blanket area. The degree of non-flatness is characterized by a parameter called the edge-curl angle (Fig. IV-D-8). Fig. IV-D-9 illustrates the maximum temperature difference, which could occur on a blanket as a function of both edge-curl angle and heliocentric distances less than 0.635 AU. At larger distances, edge-curl temperature effects are negligible.

On the basis of the figures presented, it can be concluded that rotation of the solar array can be used successfully to achieve temperature control, provided the blankets can be kept fairly flat or can be made to withstand large temperature deviations. It should be emphasized that edge-curl effects only become a problem well beyond the point of Encke rendezvous.

3. Maximum Power Point Detector Survey

The objective of this study was to evaluate concepts developed for determining and obtaining the maximum power of a solar array as an energy source, compare the adaptability of the concepts to the requirements of a SEP spacecraft, and recommend the most promising concept for development.

A number of techniques have been proposed for determining the maximum power of a solar array and the maximum utilization of that power. The techniques selected for development were low-power systems, in open-or closed-loop modes. In the open-loop mode, the maximum power is determined by direct or indirect measurements of the solar array. In the closed-loop mode, the maximum power is determined and utilized by operating the power subsystem at the maximum power point of the solar array energy.

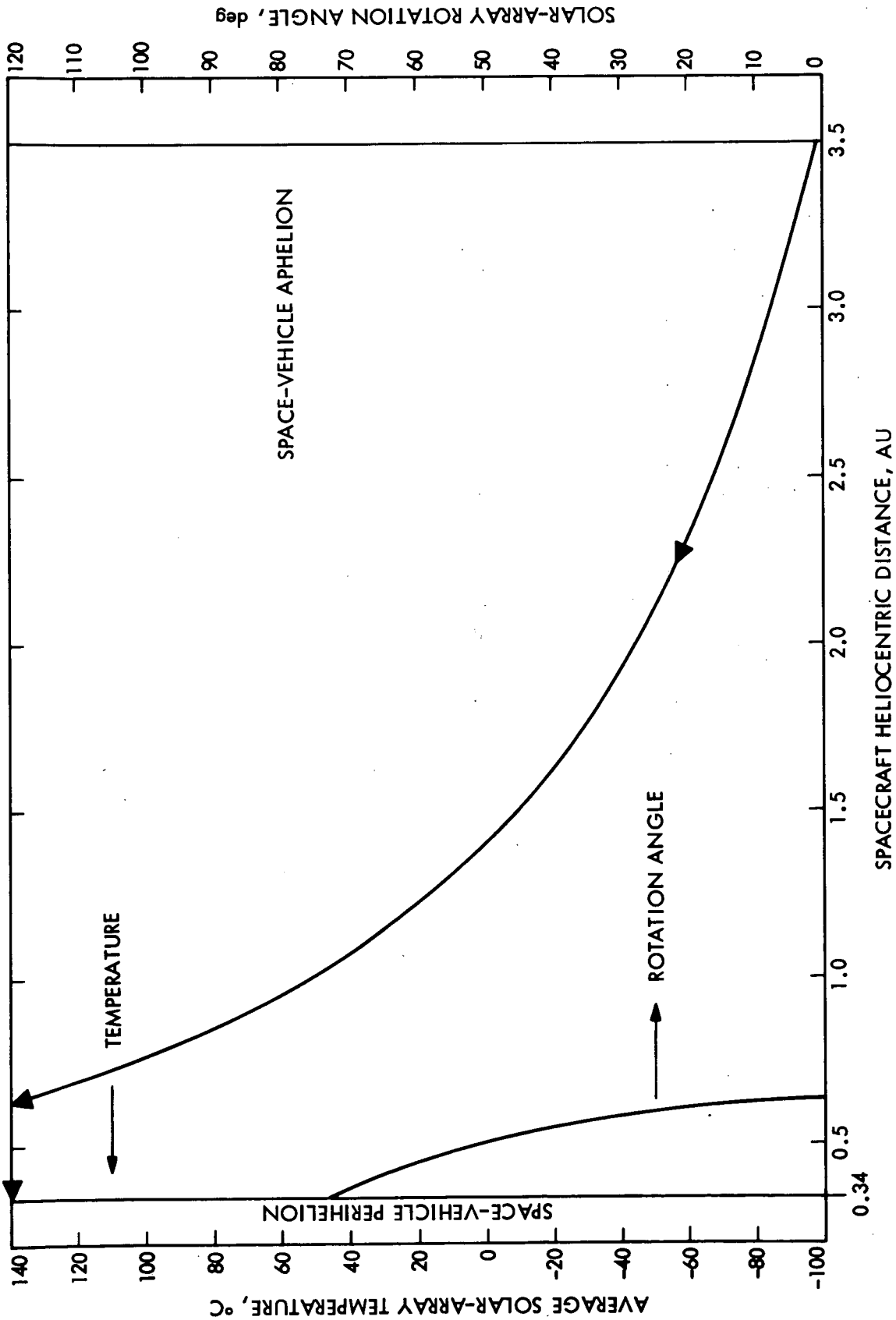

Fig. IV-D-7. Solar-array Sensitivity to Heliocentric Distance

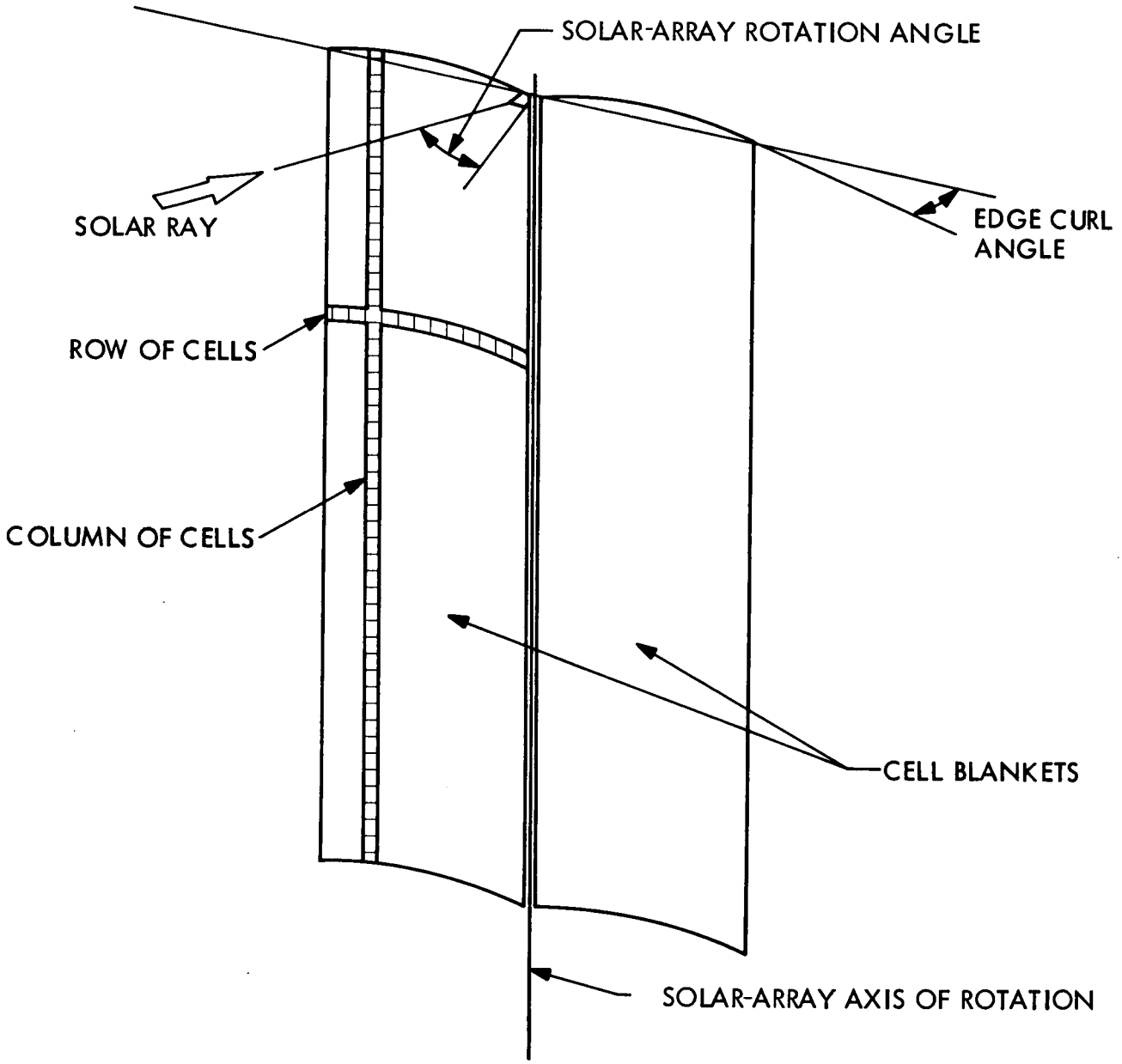

Fig. IV-D-8. Thermal Model of Solar Array

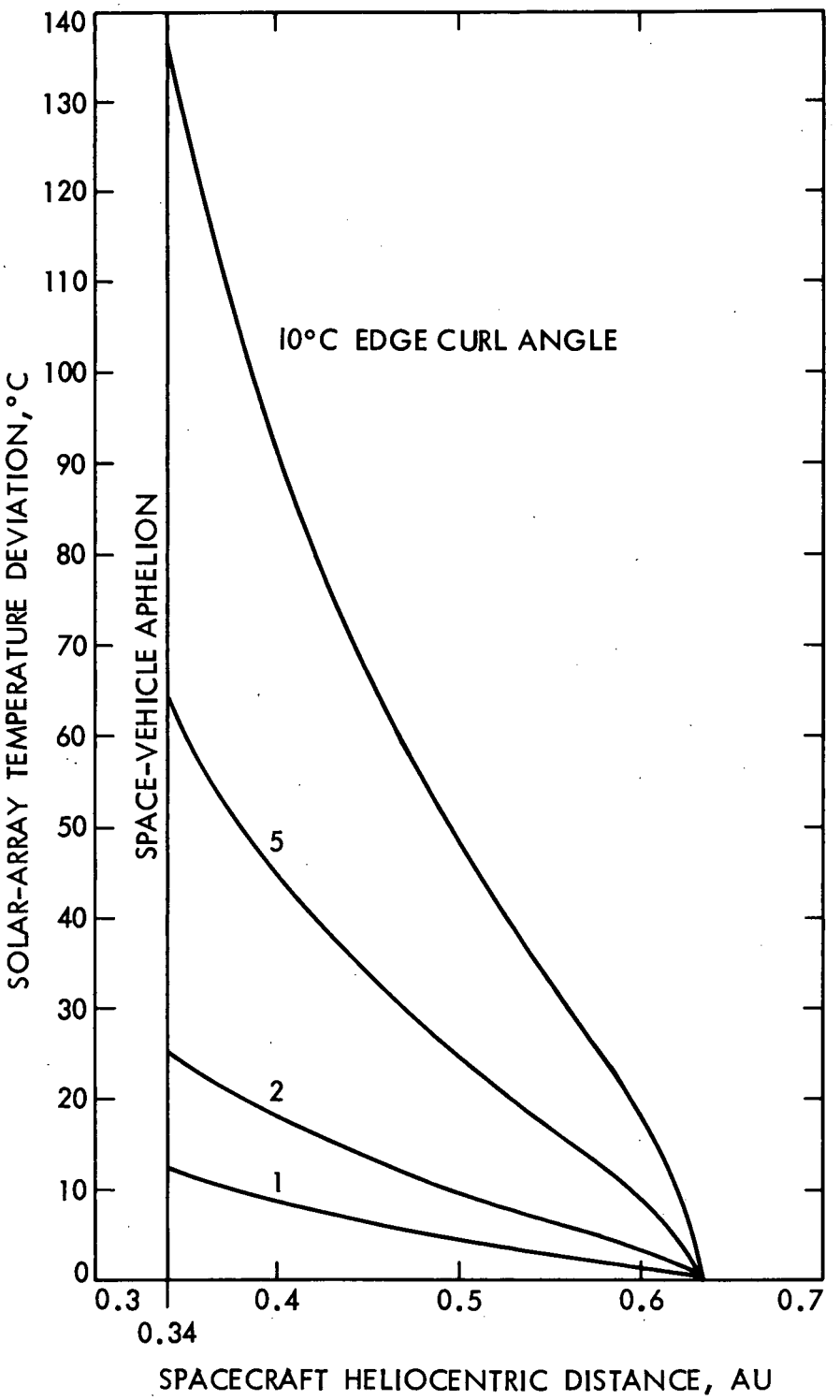

Fig. IV-D-9. Effect of Edge Curl on Solar-array Temperature

The maximum power point tracker is a type of regulator, which searches for the position of the controlled parameter (maximum power point of the array) and maintains the power subsystem at that point, regardless of any variations. There are two trackers that can be considered for this application: (a) a series tracker, and (b) a parallel tracker.

The series tracker controls the total power delivered by the array. The most desirable feature of the series tracker is operating-point stability. In the series tracker, power detecting problems are reduced since system noise is isolated from the power detecting transducer by the series configuration. Also, since the total system power is controlled by the series tracker, the maximum power point can always be recovered after load transients, assuming that the variable load power remains greater than zero.

The parallel tracker controls only the power margin (the difference between the maximum array power and the power consumed by the spacecraft). It is susceptible to noise and power transients, and the system response must be fast to prevent instability under all load transients.

A summary of the open-and closed-loop systems is given in Table IV-D-7.

It was concluded from the survey that not one method presently conceived can meet the requirements of the SEP spacecraft. It is recommended that more detailed study and analysis of the characteristics of the reference array, impedance comparison, and parallel tracker system, as applied to the unique requirements of the SEP spacecraft, be made before a concept can be recommended for development.

Table IV-D-7. Summary of Open-loop and Closed-loop Systems

Method	Type	Advantages	Disadvantages
Series Tracker	Closed loop	Continuous accurate tracking of the maximum power point	Thermal problem and excessive power losses require dummy load and complex circuitry
Parallel Tracker	Closed loop	Continuous accurate tracking of the maximum power point	Requires complex circuitry, dummy load, and has operating point stability problem
Reference Array	Open loop	Simplicity and light weight	Accuracy is difficult to determine
Impedance Comparison	Open loop	Provides power mismatch index	Accuracy is difficult to determine; may have component problems
Direct Array Measurement	Open loop	Provides actual array measurement	Power reduction is required, circuitry is complex, and array section temperatures must be the same

E. SEP MODULE SUPPORT SUBSYSTEM STUDIES

1. Data Handling

The data subsystem is the communications and processing center for the thrust subsystem; it provides the means for monitoring performance and for the generation and distribution of sequencing and control commands. The two objectives of the data subsystem studies were:

(a) To determine the command, control, and sequencing requirements of a SEP thrust subsystem, including the response times required, parameters to be measured, failures to be handled (both transient and permanent), parameters to be controlled, data storage, and data transmission.

(b) To evaluate the various hardware implementations in relation to: complexity, cost effectiveness in satisfying the requirements, reliability, noise tolerance (EMI) and radio frequency interference (RFI), and weight; and, from the evaluation, to arrive at a preferred data system configuration.

In its present state of development, electric propulsion hardware requires constant monitoring and control. Thrust-element measurements and control parameters interact far too rapidly to allow control from earth-based stations during distant missions. Further, the long mission lifetime would unduly restrict earth-based monitoring and command-team scheduling. Adaptive engineering telemetry for ground analysis of thrust-subsystem performance and an adaptive control system are needed.

The data subsystem must not only provide monitoring, analysis, command, and sequencing for the thrusters, PCs, and switchgear assemblies but must interact with other elements of the SEP vehicle to perform the following functions:

(a) Control the power subsystem.

(b) Control the thermal control subsystem.

(c) Control the thrust vector control.
(d) Collect data from the power subsystem.
(e) Collect data from the thermal control subsystem.
(f) Collect data from the thrust vector control.
(g) Condition and format collected data for telemetry.
(h) Receive and execute commands from the earth control station.
(i) Communicate with the main spacecraft.

A tradeoff study was made to define the data subsystem architecture which would best satisfy the needs of the SEP thrust subsystem. Software requirements of the thrust subsystem were examined to a level of detail sufficient to provide confidence in the capability of each configuration to meet system performance requirements or to eliminate it from further consideration. Hardware-software tradeoffs were made; subsystem configurations were established; and cost, weight, functional effectiveness, noise tolerance, and reliability estimates were made. From these activities, it was concluded that a Viking computer command subsystem (CCS) with a modified flight data subsystem (module FDS) was the preferred implementation in the SEP module, when it is desirable to keep the effect of the SEP module on the spacecraft to a minimum. The preferred configuration is shown in Fig. IV-E-1.

The data subsystem has three basic elements:

(a) The CCS.
(b) The master flight data subsystem (MFDS).
(c) A complement of interface control units called flight data-system slaves.

The CCS is the logical, computational, control and data-evaluation center. The Viking CCS can provide the required functions. This unit is part of the spacecraft and communicates with the MFDS via data and command buses.

The MFDS is the center of communications and data distribution within the SEP module. The MFDS controls the measurement-gathering

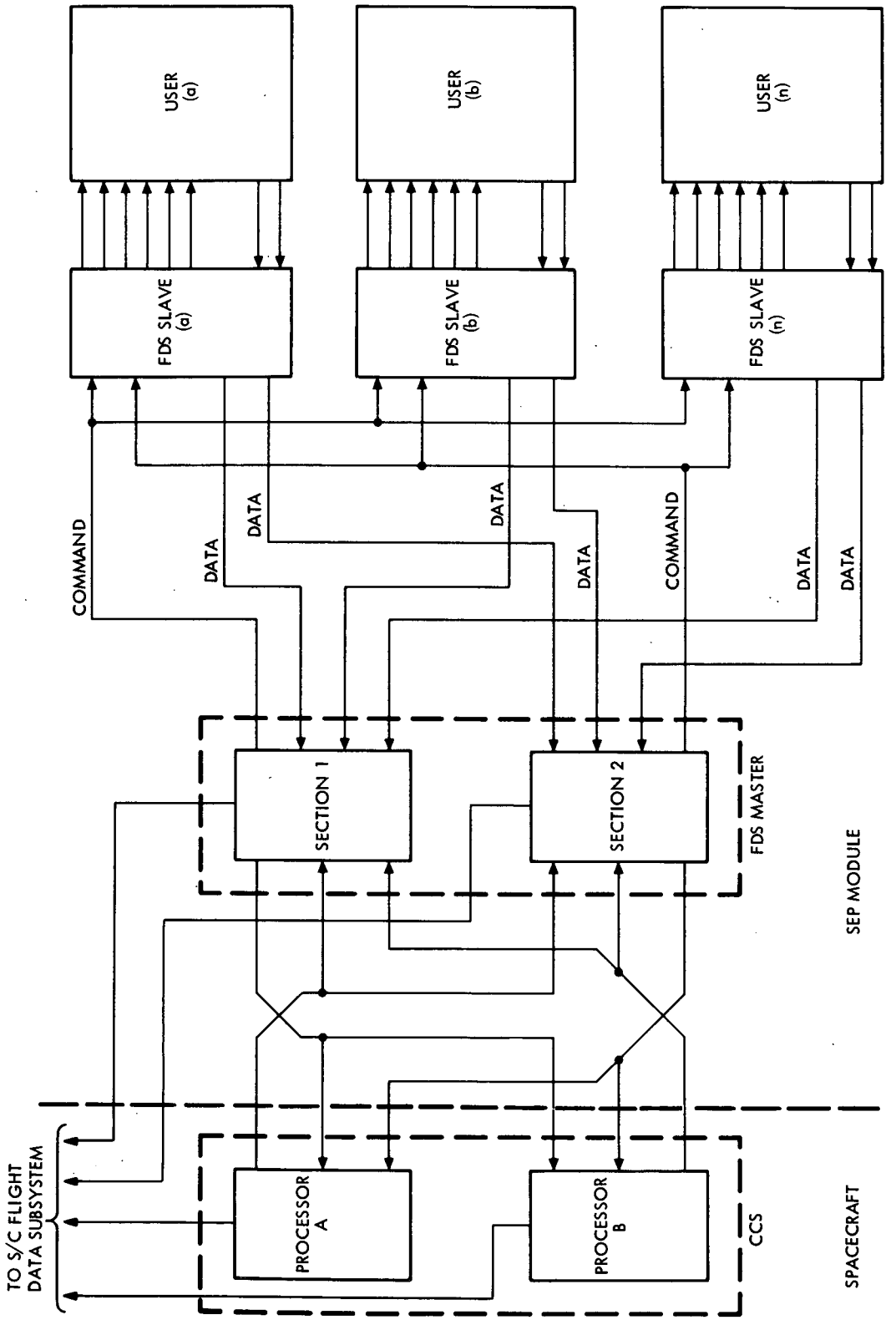

Fig. IV-E-1. Preferred Data Subsystem

process. The MFDS also provides limit checking and interrupt-signal processing, which indicate potential or impending problems. Communications between the CCS and the MFDS supply the data required for problem analysis and the command channel for performance control and fault correction.

The communication between the MFDS and the other elements of the SEP module is accomplished by the FDS slaves. The MFDS communicates with the slave on a command bus. This communication path provides both control and measurement data and their interrupt signals to the MFDS on separate data lines. A dedicated line from each slave is used for elimination of multiple transmitter-bus pollution and for interrupt signaling. There are separate slave units for each element of the thrust subsystem. Isolation digital interfaces are provided between the MFDS and the slave units.

2. Telecommunication - SEP Integration Studies

a. Spacecraft Ion Beam Noise Effects

An examination of the magnitude of the noise interference in an uplink signal reception caused by operation of an ion thruster on board a spacecraft has been made. The summary herein is limited to noise generated by the exhaust beam as a result of ion-electron collisions, or "Bremsstrahlung radiation." Degradation is estimated in terms of the uplink received signal-to-noise ratio and the increase in antenna-noise temperature. This activity represents one phase of the overall study to determine the interaction of a SEP subsystem with other spacecraft subsystems.

Under ideal conditions, the spacecraft antenna is pointing away from the ion-beam axis; thus, there is little chance for ion-noise interference. If the antenna is steerable, however, there is a possibility that the antenna might point into the exhaust beam during certain portions of its mission. For this study, a worst-case spacecraft antenna/ion-beam configuration was assumed in which the antenna is located in the exit plane of the ion engine exhaust, at a distance R_a from the beam axis, and pointing in the direction

$\phi = \pi/2, \theta = \psi$ (see Fig. IV-E-2). R_0 is the beam exit radius, and α is the

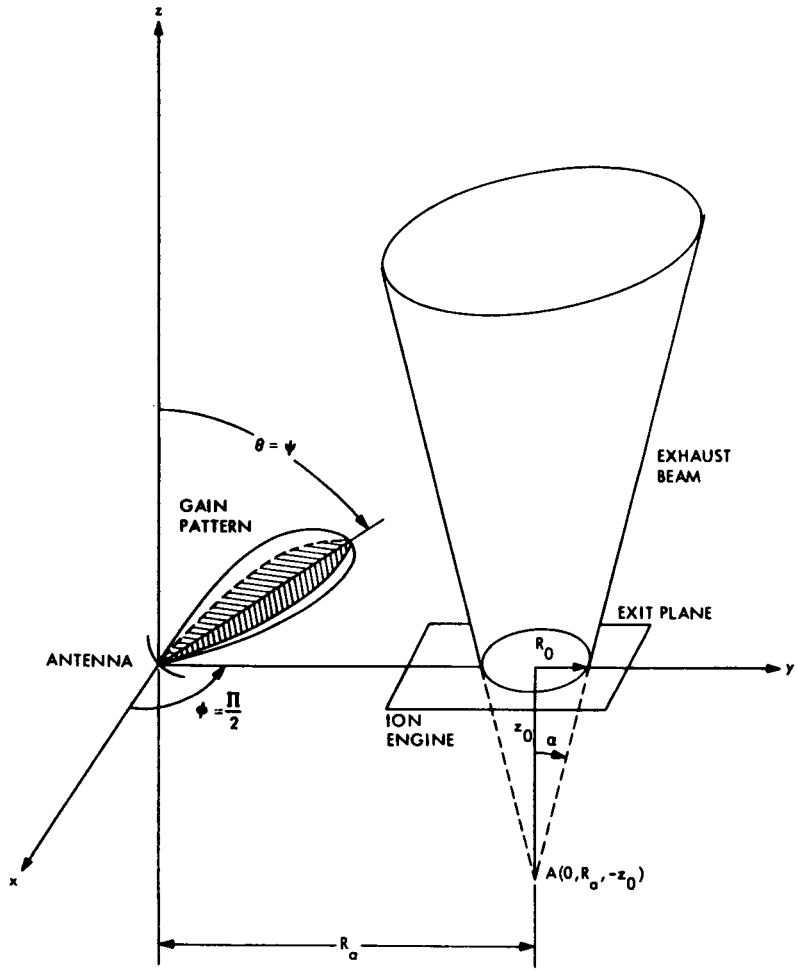

Fig. IV-E-2. Spacecraft Antenna/Exhaust Beam Configuration

beam divergence angle. The geometry of this worst-case configuration simplifies the mathematics and provides an upper limit to other, perhaps more realistic, cases.

The incident noise power to the antenna from the ion beam is obtained by integrating the Bremsstrahlung radiation, weighted by the antenna-gain pattern, over the volume of the exhaust plume. This power may be conveniently related to an antenna noise temperature.

The antenna gain-pattern, $G(\theta, \phi)$, is assumed in this treatment to be symmetric and pointing in the $\theta = \psi, \phi = \pi/2$ direction. For simplicity, the pattern is assumed to have no side lobes. The shape of the pattern is taken to be a simple cosine distribution with a half-power beamwidth of θ_3.

Two effects of ion-beam-induced noise may be calculated: (1) the increase in antenna noise temperature caused by the exhaust beam, and (2) the uplink signal-to-noise ratio, when all other noise contributions are zero.

The expression for the antenna noise temperature was evaluated on the UNIVAC 1108 computer. A peak antenna-noise temperature of about 0.2 K (about -200 dBm/Hz) was found. A spacecraft receiver might typically have a noise temperature of 500 K (or -170 dBm/Hz), a margin of 30 dB above the ion noise.

The ion-beam noise was compared to a typical uplink ranging-signal transmitted by a 26-m diameter antenna (52-dB gain) at 10 kW with 12-dB ranging suppression, at 2 GHz with a 1-MHz bandwidth. Rather than obtaining the S/N at various distances, a critical distance R_{cr} (in AU), at which the uplink signal equals the exhaust beam noise, was determined.

The critical range for a low-gain antenna, under the assumed worst-case conditions, was found to be 4 AU. Thus, it may be concluded that operating an ion thruster ordinarily introduces much less degradation than receiver noise.

b. Effects of Dispersive Media on Coherent Communications

In the proposed SEP mission to Encke, the communication channel at times is not the usual additive white Gaussian noise channel. In two cases, one mission-dependent and one mission-independent, the signal itself is randomly disturbed in both amplitide and phase by its passage through a plasma. In one case, the plasma is the solar corona, which occults the spacecraft twice during the mission, causing a communications blackout. In the

other case, the plasma interference may be the ion beam of the SEP thrusters. This interference, if it exists, must be completely understood to ensure that communications will not be adversely affected by the ion beam.

It was not the purpose of the study to model the specific communication channels, but rather to postulate a general model covering a broad class of channels of interest and to proceed with the communications analysis. When the specific channel models, such as the ion-beam and solar-corona channels, are completed, the parameters of these models can then be applied to the results of this study.

Presently, the configuration used for deep-space communication uses the phase-locked loop (PLL) receivers for carrier tracking and coherent demodulation. The performance of the tracking loop affects all communication subsystem functions. For example, one-and two-way doppler measurements and ranging, which are required for navigation and orbit determination, are highly dependent on the PLL performance. Similarly, the phase jitter of the tracking PLL degrades the telemetry and command performance because of imperfect coherent demodulation. For these reasons, the first step in predicting coherent communications performance through dispersive media must be a thorough analysis of the PLL.

This study, therefore, developed various techniques for obtaining the probability density function, $p(\phi)$, for the phase error, ϕ, in a phase-locked loop when the loop input signal was corrupted by a dispersive channel. In particular, the Rician fading channel was analyzed extensively for the first order PLL. These results and analytical techniques can be extended to second order loops, which are of more practical interest but are more complicated to analyze. Also, the techniques outlined in the study can be used to model and analyze other channels.

Although the general purpose of this study was to develop analysis techniques for a general channel model, some results of the Rician

channel study are noteworthy. The degradation in the PLL performance was shown to depend on the bandwidth of the fading signal compared to the PLL bandwidth. As expected, the degradation increased with an increase in the variance of the dispersive components. For the slow fading case, only a modest amount of PLL degradation was noted for the Rician channel.

SECTION V

SEP THRUST-SUBSYSTEM FUNCTIONAL DESCRIPTION SUMMARY

A SEP thrust-subsystem description document has been prepared which reflects JPL's selection of a thrust-subsystem design point. The document describes the functions of each subsystem element, defines the interfaces of the elements with other SEP module subsystems, and specifies thrust-subsystem performance, physical characteristics, and constraints. The detailed description is contained in Volume II of this study. A summary of the description follows.

The function of the thrust subsystem is to provide the directed impulse required to accomplish a rendezvous with Encke ($\sim 1.5 \times 10^7$ N/sec), and, while operating, to provide control torques for vehicle three-axis attitude stabilization. To provide this impulse, the thrust-subsystem must convert electrical energy from the solar array into the directed kinetic energy of ejected propellant for a period of approximately 950 days. During this period, the power available for conversion to thrust will vary by about an order of magnitude.

The elements comprising the thrust subsystem are the thrusters, PCs, switching matrix, thrust vector control (TVC), propellant tankage and distribution, cabling, and structure. The functional relationships of these elements are shown in Fig. V-1.

The thruster element (seven thrusters, which include excess thrust capacity) produces thrust according to a preset sequencing schedule and delivers the needed total impulse of 1.5×10^7 N/sec at a specific impulse of 3000 sec. Each thruster is 30 cm in diameter and has an expected overall efficiency of not less than 71% at the full operating power of 2630 W. Vaporizers located near each thruster change the liquid-mercury propellant to the vapor required for thruster operation.

The function of the PC element is to convert unregulated solar-array power to the various ac and dc powers required to operate the thrusters and

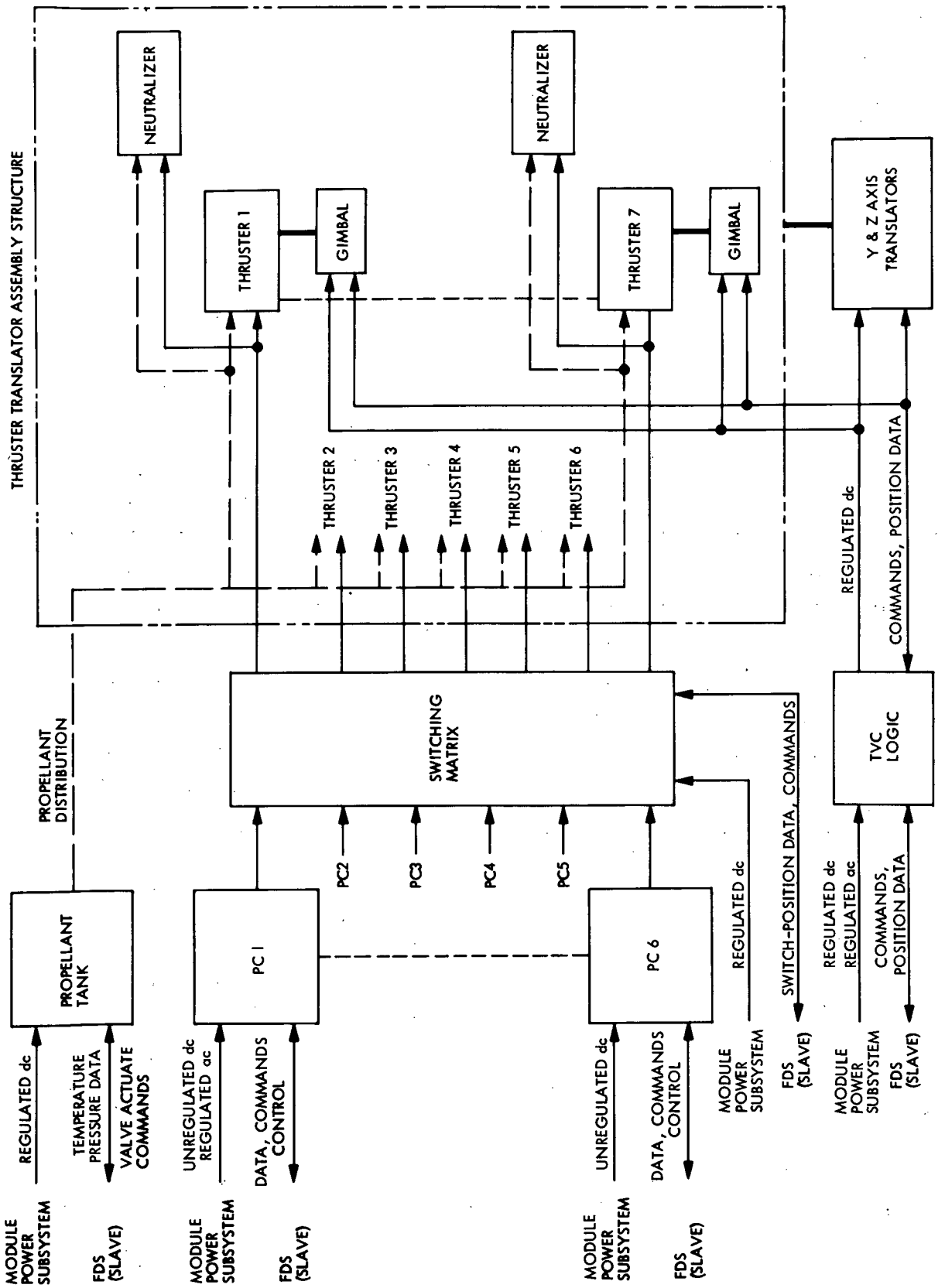

Fig. V-1. Thrust Subsystem Functional Block Diagram

to provide thruster operation control. The operating power level of each of the six PCs required is 2860 W at an input voltage varying between 200 and 400 V. The six PCs are expected to have an efficiency of 92% and a total weight of no more than 81.6 kg.

Outputs of each PC are connected to each of the seven thrusters in the switching matrix. The switching matrix contains six switches (one for each PC) and a connection matrix. The total weight is about 15 kg.

The TVC, utilizing thrust from the thrusters, provides control torques about the three primary spacecraft axis. The TVC performs this function by translating the average thrust vector of all thrusters parallel to two axes through the spacecraft center of mass to provide pitch-and yaw-axis control, and by gimballing individual thrusters to provide a couple about the third axis. During the mission, the TVC operates at all times when thrusting is taking place except during those periods when the deadband limits are exceeded. At these times, the spacecraft reaction control system (RCS) is activated.

The required 480 kg of mercury propellant is stored in a single spherical tank, 0.4 m in diameter. A latching solenoid valve is located at the propellant outlet to prevent spillage during launch, and to serve as an exit when the propellant is expelled from the tank to the thrusters, as required during startup. Propellant expulsion is accomplished by the vapor pressure of Freon TF acting on an expulsion bladder.

The thrust-subsystem cabling provides electrical connections to the various components and independently mounted units. The cabling includes:

(1) A PC-ring harness for connecting the PCs to the switching matrix assembly and to the power subsystem and for incorporating the connector and cable interfacing with the propellant tank and the additional SEP module electronics.
(2) A PC assembly harness connecting the PC to the PC-ring harness.

(3) A thruster-array harness for connecting the electronics equipment mounted on the thruster translator-assembly structure and the interface to the switching matrix assembly.

(4) The pyrotechnic harness for actuation of electro-explosive devices and solenoid valves.

The thrust-subsystem structure includes the support for the thrusters, the PCs, the thrust translator assembly, and the propellant tank support. The thruster structure provides mounting and alignment for the thrusters and their associated gimbal actuators. The PC structure is primarily in the form of module plates which package the PC components and also serve as shearplates for the spacecraft structure. The thruster translator assembly is composed of seven thrusters, the TVC components (less the TVC logic), cable troughs for carrying propellant feedlines and cabling across articulating interfaces, feedlines and cables, any required thermal-control components, and the associated structure. The assembly structure integrates the assembly with the spacecraft and includes latches for adequately securing the assembly to the spacecraft during launch. The propellant tank support structure integrates the tank and the spacecraft.

The thrust subsystem interfaces primarily with six other spacecraft subsystems: power, structure, flight data, attitude control, thermal control, and cabling. The interface requirements are discussed in the detailed description in Volume II.

Thrust subsystem efficiency, defined as the ratio of the square of the thrust delivered to twice the product of the propellant-mass flow rate and power consumed, must not be less than 63% at an input power of 16 kW and a specific impulse of 3000 sec. The calculated reliability of the thrust subsystem must be greater than 0.96, and the total dry mass should not exceed 234.4 kg.